LAND USE AND LAND COVER CHANGE DETECTION IN ISFAHAN, IRAN USING REMOTE SENSING TECHNIQUES

Niloofar Alavi

Thesis submitted to the Faculty of Graduate and Postdoctoral Studies,
In Partial fulfillment of the requirements for the degree of
Master of Science in Geography

Table of Contents

Abstract (English)

Rapid urban growth and unprecedented rural to urban transition, along with a huge population growth are new phenomena for both high and low income countries, which started in the mid-20th century. However, urban growth rates and patterns are different in developed countries and developing ones. In less developed countries, urbanization and rural to urban transition usually takes place in an unmanaged way and they are associated with a series of socioeconomical and environmental issues and problems. Identification of the city growth trends in past decades can help urban planners and managers to minimize these negative impacts. In this research, urban growth in the city of Isfahan, Iran, is the subject of study. Isfahan the third largest city in Iran has experienced a huge urban growth and population boom during the last three decades. This transition led to the destruction of natural and agricultural lands and environmental pollutions.

Historical and recent remotely sensed data, along with different remote sensing techniques and methods have been used by researchers for urban land use and land cover change detection. In this study three Landsat TM and ETM+ images of the study site, acquired in 1985, 2000 and 2009 are used. Before starting processing, radiometric normalization is done to minimize the atmospheric effects. Then, processing methods including principal component analysis (PCA), vegetation indices and supervised classification are implemented on the images. Accuracy assessment of the PCA method showed that the first PC was responsible for more than 81% of the total variance, and therefore used for analysis of PCA differencing. $\Delta PC1_{t1-t2}$ shows the amount of changes in land use and land cover during the period of study. In this study ten vegetation indices were selected to be applied to the 1985 image. Accuracy assessments showed that Transformed Differencing Vegetation Index (TDVI) is the most sensitive and accurate index for mapping vegetation in arid and semi-arid urban areas. Hence, TDVI was applied to the 2000 and 2009 images. $\Delta TDVI_{t1-t2}$ showed the changes in land use and land cover especially the land use transformation from vegetation cover into the urban class. Supervised classification is the last method applied to the images. Training sites were assigned for the selected classes and accuracy was monitored during the process of training site selection. The results of classification show the expansion of urban class and diminishment in natural and agricultural lands.

Abstract (French)

Depuis le milieu du 20e siècle, la croissance urbaine rapide et la transition en milieu rural à urbaine sans précédent, ainsi qu'une croissance énorme de population pays industrialisés et pays en voie de développement. Toutefois, les taux de croissance urbaine et les modèles sont différents entre les pays développés et ceux en voie de développement. Dans les pays moins développés, l'urbanisation et la transition en milieu rural à urbaine ont généralement lieu de manière non gérés et ils sont associés à une série de questions et problèmes d'ordre socio-économiques et environnementaux. L'identification de la tendances de croissance d'une ville dans les décennies passées peuvent aider les planificateurs urbains et les gestionnaires à minimiser ces impacts négatifs. Cette recherche, la croissance urbaine dans la ville d'Isfahan, en Iran. Isfahan, la troisième plus grande ville d'Iran a connu une importante croissance urbaine et explosion démographique au cours des trois dernières décennies. Cette transition a mené à la destruction des terres agricoles et naturelles et les pollutions environnementales.

L'historique et les récentes données de télédétection, ainsi que différentes techniques de télédétection et méthodes ont été utilisées par des chercheurs pour l'utilisation des sols urbaines et la détection des changements de la couverture terrestre. Dans cette étude, trois images de Landsat TM et ETM + du site d'étude, acquises en 1985, 2000 et 2009 ont été utilisées. Avant le début du processus, la normalisation radiométrique est faite pour minimiser les effets atmosphériques. Ensuite, des méthodes de transformation, y compris l'analyse en composantes principales (ACP), les indices de végétation et de classification supervisée ont été effectuées sur les images. L'évaluation de l'exactitude de la méthode ACP a montré que le premier CP a été la cause de plus de 81% de la variance totale, et a donc été utilisée pour l'analyse de la différenciation ACP. $\Delta CP1_{t1-t2}$ montre la quantité de changements dans l'utilisation des terres et la couverture des terres durant la période de l'étude. Dans cette étude, dix indices de végétation ont été sélectionnés pour être appliqués à l'image de 1985. Des évaluations d'exactitude ont montré que le «Transformed Differencing Vegetation Index » (TDVI) est l'indice le plus sensible et précis pour cartographier la végétation dans les zones arides et semi-arides des régions urbaines. Ainsi, le TDVI a été appliqué aux images de 2000 et 2009. $\Delta TDVI_{t1-t2}$ a montré des changements dans l'utilisation des sols et la couverture des terres en particulier la transformation de l'utilisation

des sols à partir de la couverture végétale dans la classe urbaine. La classification supervisée est la dernière méthode appliquée aux images. Les sites de formation ont été assignés pour les classes sélectionnées et la précision a été surveillée pendant le processus de sélection du site de formation. Les résultats de la classification montrent l'expansion de la classe urbaine et la diminution des terres naturelles et agricoles.

Acknowledgment

I would like to express my sincere gratitude to my thesis supervisor Professor Abdou Bannari for his continuous academic help and immense knowledge, guidance and patience, which enabled me to improve an understanding of my thesis subject.

I owe my deepest gratitude to my thesis committee Dr. Andre Viau and Dr. Kenza Benali, for their valuable comments and kind guidance from the initial to the final level of this study.

I would like to thank Dr. Brian Ray, Graduate Students Advisor at the Department of Geography, University of Ottawa, for all his great personality and his kind help, guidance and support during my master degree.

I would like to thank the Department of Geography at the University of Ottawa, for their financial support and providing me numerous teacher assistantship opportunities.

It is a pleasure for me to thank Ms. Sylvie Theriault and Ms. Chantale Arcand for their great helps in many different respects during my studying at the Department of Geography, University of Ottawa.

I am indebted to my friends and colleagues at the Department of Geography, Koreen Millard, Doug Stiff, Eugenio Landeiro Reyes, Alisha Lagasi, Roberto Carlos Tapia Opazo, Paula Aguayo, Mostafa Kamal Mosleh, and Khaled Hazaymeh, for their academic helps and comments and personal supports during my Master's degree and especially in this thesis.

I would also like to express my personal thanks to:

My mother Zari, and my brother Dr. Saman Alavi, for their endless love, care and support, without which I would have gave up long ago.

Miss Dorothy Uy for precise French translation of the abstract.

My Sister Sepideh and my brother Ali, and my adorable friends who supported me emotionally and encouraged me during the hard time and gave me faith for my path and myself, Maryam Yazdi, Negar Havazadeh, Hoda Mirsafian, Saeedeh Esmaili, Shirin Alikhani, Golrokh Niazi, Payam Sadeghi, and last but not least Katayoon Memarmontazerin.

List of Tables

List of Figures

List of Abbreviations

ANN	Artificial Neural Network
ASAR	Advanced Synthetic Aperture Radar
AVI	Agricultural Vegetation Index
BRDF	Bidirectional Reflectance Distribution Function
CASI	Compact Airborne Spectrographic Imager
CVM	Change Vector Analysis
DEM	Digital Elevation Model
DN	Digital Number
DVI	Difference Vegetation Index
ETM	Enhanced Thematic Mapper
GIS	Geographic Information System
MSAVI	Modified Soil Adjusted Vegetation Index
MSS	Multi Spectral Scanner
m	Meter
NASA	National Aeronautics and Space Administration
NDGI	Normalized Differentiating Greenness Index
NDVI	Normalized Difference Vegetation Index
NIR	Near Infra-Red
PC	Principal Component
PCA	Principal Component Analysis
PIF	pseudo-invariant features
PVI	Perpendicular Vegetation Index
RGB	Red, Green, Blue
RS	Remote Sensing

RVI	Ratio Vegetation Index
SARVI	Soil Adjusted Ration Vegetation Index
SPOT	Système Pour l'Observation de la Terre
SAVI	Soil adjusted Vegetation Index
SVM	Support Vector Machine
t	Time
TDVI	Transferred Different Vegetation Index
TM	Thematic Mapper
TSAVI	Transformed Soil Adjusted Vegetation Index
UN	United Nations
UNESCO	United Nations Educational, Scientific and Cultural Organization
USGS	United States Geological Survey
UTM	Universal Transverse Mercator
VI	Vegetation Index
VIN	Vegetation Index Number
VC	Coefficient of variation

Chapter 1: Introduction

In the mid-20th century the world began to transform to a tremendously different place than it was before. The post-World War II technological progress, population boom, political transition, and economic changes were important factors that caused important changes in the world's atmosphere and dynamic. Rapid urbanization and unprecedented population growth were amongst significant world changes that took place by the end of the 20th century. These transitions were along with human's manipulation in the world natural environment (Miller and Small, 2003). Demographic studies demonstrated that in just over 40 years from 1940 to 1980, the number of people living in large cities rose from one in every eight people to one in every three (World Commission on Environment and Development, 1987). Furthermore, in 2007, for the first time in human history, the total population of the world's cities exceeded the rural population (Griffiths *et al.,* 2009). Demographers and human geographers predict that this growth in urban population will be continued in a way that by 2025, large cities and urban agglomerations will accommodate a vast majority of the world's population (O'Meara, 1999; United Nations, 1999). They also believe that most of this increase in urban population will occur in low and middle income countries (Griffiths *et al.,* 2009). According to the United Nations (UN) (2003), the increase in the world's urban population is not only due to the natural causes (the birth rate surpassing the death rate), but also caused by huge rural to urban migration.

The world's urban agglomerations occupy a very small area of the planet's terrestrial surface (approximately 3%). However, natural ecosystems and environments are highly affected by the presence of urban areas. The negative impacts of urbanization and increase in urban population disturb global biogeochemical cycles, accelerate climate change, and affect hydrologic regimes (Foley *et al.*, 2005, Grimm *et al*., 2008). Natural ecosystems such as forests, rangelands, and other forms of natural vegetation covers, as well as manmade ecosystems such as agricultural lands are examples of environments that are highly affected by recent rapid urbanization. Shortage of affordable housing

especially in big cities reinforces the destruction of adjacent natural and agricultural lands and their conversion into built up areas (Mason, 2006).

Furthermore, land use and land cover changes over time, due to urbanization, is an important urban issue, which should be take into consideration in urban research projects. Humans have always lived as a part of nature and have a close relationship with the environment. However, humans' interference and manipulation of their environment is greater than that of any other creature. Humans have changed their environment to the favor of their own progress, safety and short-term welfare. These modifications and manipulations increased the stress on nature and other organisms and resulted in land use and land cover change over time (Jaiswal *et al.*, 1999). In addition, extensive changes in land use and land cover reinforced global environmental changes (Turner *et al.*, 1994). Different biological, economic, social, and physical factors are involved in the modification of an environment or landscape (Turner, 1987). To trace, explain, and quantify these changes, land use and land cover change detection techniques are developed and applied in scientific applications (Hong *et al.*, 2009).

In this research, the case study is the city of Isfahan, Iran. Isfahan is a secondary city and the third largest in Iran. With thousands of years of history, this city has transformed in recent decades into an important industrial and economic hub. During the past 30 years, Isfahan has also experienced an enormous population boom, due to both natural increase and rural to urban migration. These transformations have both changed people's life style and created a series of environmental and socioeconomic issues associated with urban development. Unmanaged city growth, a shortage of affordable housing, high unemployment rates, high crime rates, heavy traffic, air pollution and environmental degradation, health problems (increasing cancer, M.S, lung and heart diseases) are some of the major issues that Isfahan face today. These issues make Isfahan a suitable case study for investigating land use and land cover change detection over time, especially in the past three decades.

1.1. Thesis Structure

Chapter 1 presents the introduction and problem description of the thesis. Objectives and hypothesis are also defined in this chapter. Chapter 2 starts with a review of urban expansion in the 20th century in different parts of the world, with more emphasis on urban growth patterns in developing countries and especially Middle East. Remote sensing land use and land cover change detection techniques in different ecosystems and environments are also presented in the second chapter. The materials and methods used for remote sensing land use and land cover change detection are outlined in chapter 3. In this chapter, pre-processing, as well as processing methods including principal component analysis, vegetation indices, and classification are described in detail. Results are presented in details in chapter 4, and finally conclusions and recommendations are described in chapter 5.

1.2. Objectives

The main goal of this thesis is urban land use and land cover change detection for the city of Isfahan, Iran, over a period of 25 years, using multitemporal Landsat Thematic mapper (TM) and Enhanced Thematic Mapper (ETM+) data acquired in 1985, 2000, and 2009. The objectives are stated as follows:

1. To examine the accuracy of different principal components in mapping land use classes in arid and semi-arid environments, and to use $\Delta PC_{i\ t1\ -\ t2}$ to identify the change in land use classes.

2. To find out the best and most sensitive vegetation index, among ten selected indices, for mapping vegetation in urban areas, and to use $\Delta VI_{t1\ -\ t2}$ to identify changes in land use classes.

3. To map land use and land cover classes using training sites and maximum likelihood classifier to identify and quantify the changes in each class size during the period of study.

1.3. Hypotheses

The following are the main hypotheses of this study.

1. Principal components analyses is a good indicator of land use and land cover change detection, and PC1 is responsible for most of the variances.

2. Vegetation indices are a good indicator of vegetation state and ground biomass and, consequently, most sensitive to spatial distribution of vegetation cover in urban environments.

3. As an improved vegetation index, TDVI is the most accurate and sensitive index for mapping vegetation in urban environments.

4. Maximum likelihood supervised classification is the most accurate classification method for mapping land use and land cover changes in complex and heterogeneous urban areas.

5. Urban expansion and city growth over time led to destruction of natural vegetation and agricultural lands in the study site.

Chapter 2: Problem description

2.1. Introduction

This chapter will provide a brief literature review of two themes. The first theme is the urban growth in the 20th century, with more emphasis on the urban growth patterns in the developing countries, especially in the Middle-East. Examples of developing cities which have experienced huge urban expansion are reviewed in more detail, and the same issue in the study site is presented briefly. The second theme is the application of satellite images and remote sensing techniques in land use and land cover change detection. The considered techniques are principal component analysis, vegetation indices, and classification.

2.2. Urban growth in 20th century

Over a hundred years ago, the actual number of cities in the world with at least a million people was only 16. The vast majority of these cities were located in high income countries. The current number of the cities with a population of one million and more has increased to 400 cities around the world, 75% of which are in low- and middle-income countries (Cohen *et al*., 2004). The number of cities of this type is expected to reach up to 564, in 2015 (United Nations, 2007). Cities in both developed and developing counties are experiencing huge urban and population overgrowth and rural to urban transition. Urban growth is defined as change in traditional physical texture and function of a rural landscape into an urban form (Thapa *et al*., 2010). However, the city growth pattern is different in developing countries compared to that in the developed world. The patterns of city growth in developed countries are compact and dispersed models. Dispersed expansion is mostly seen in developed countries in the form of city sprawl. City sprawl is known as a key urban process in Western cities and a sign of the "economic maturity" of the city (Bruegmann, 2005). City sprawl is defined as spatial and physical expansion of the city borders in a faster pace than its population, and a form of low density development (Lorinc, 2006; Peiser 1989). Sprawled cities are not continuously expanded. In other words, in the city sprawl

pattern, there are un-urbanized areas interposed among urbanized subdivisions (Peiser, 1989). City sprawl is the urban growth pattern in all Western industrial cities. In these cities the population is distributed from the compact center to the dispersed peripheries, namely "suburbs" (Catalan *et al*., 2008). The suburbanization phenomenon started in the West after World War II in the 1950s and 1960s (Schmidt, 2011) when people were looking for peaceful urban settlements for their families and big gardens and green spaces to raise their children. Suburbanization is known as the North American pattern of growth and as "an idealized artificial system" (Dunay *et al*., 2000). In suburban areas, blocks and residential units are usually separated from each other by huge lawns, gardens and green areas. Dependency on motor vehicles is the most important feature of North American suburban areas. The general design of the space, wider streets, fewer blocks and numerous parking lots all encourage a car dependent life style in the suburbs (Lorinc, 2006). Despite all concerns about the negative impacts of suburbanization, this growth pattern is not limited to American cities. Many European and even Canadian cities, which were always known as examples of good urban planning experienced the same city growth model (Bruegmann, 2005). Toronto (Chiotti, 2004) and Los Angeles (Ewing, 1997) are two examples of North American cities with high level of urban sprawl, which are suffering from various environmental problems. Different parts of Europe also experienced the North American pattern of suburbanization (Schmidt, 2011). Eastern European countries and even some of the cities which considered as parts of former Soviet bloc are following the North American Pattern of growth. Sofia, the capital city of Bulgaria is an example of these cities (Hirt, 2007). Mediterranean Europe is experiencing the same growth pattern. The pace of urban growth in Mediterranean Europe exceeds its population growth (Chaline, 2003). Porto, Marseilles, Milan, Bologna, Venice, and Athens, are all cities which exemplify this phenomenon (Catalan, 2008). The same trend can be seen in eastern Germany. From 1995 to 2005, this region experienced a 12% increase in the total built up area, whereas the population declined by 5.1% (Schmidt, 2011). Also in Barcelona, from 1993 to 2000, built up areas increased by 27.7%. 32% of this

new urban area ranked as low density or dispersed residential area (Catalan, 2008).

On the other hand, the rural to urban transition in developing countries is taking place in a different manner than that of Europe and North America (Brockerhoff, 2000). Cohen (2004) describes the main features of urban growth trends in developing countries. He explains that the low and middle income countries are experiencing a rapid increase in the absolute number of large cities and the existing cities are reaching an unprecedented size. According to the United Nation report, *World Urbanization Prospect* (2011), in 1950 low and middle income countries contained no cities with populations of 10 million or more This number increased to 3 and 12 cities in 1975 and 2000 respectively, and is predicted to reach 17 cities in 2015 (United Nations, 2011). The same trend can be seen for the number of cities with the population of 5 to 10 million. For low and middle income countries this number tripled during the period between 1950 to 1975 and doubled from 1975 to 2000. It is also predicted to triple from 2000 to 2015. However, high income countries show a more sustainable trend. Three main processes accelerate the global rapid urbanization: high natural birth rate and excess of birth over death, rural to urban migration, and annexation of neighboring areas and satellite towns (Cohen, 2004). Education, job opportunities and easier access to primary services and infrastructures make the urban areas more attractive for rural immigrants. However, the principal driving factor in population growth in urban areas is natural increase and not rural to urban migration. Although the fertility rate in big cities is often lower than that of small villages, the number of women in reproductive age is usually more in big cities than rural areas (Cohen, 2004). Furthermore, urban growth in both the main city core and neighboring towns causes the peripheries to amalgamate to the center. The population living in the peripheries increasingly occupies new jobs in the main city core and gives up their traditional jobs and life style.

According to the United Nations (2011) the number of people living in megacities in low and middle income countries rose from 32 million in 1975 to 158 million in 2000. In the first half of 20th century urbanization was mainly limited to high

income countries; however, rapid urbanization and population growth is now taking place in a much faster pace in low and middle income countries. Demographically, some developing megacities such as Dhaka, Mumbai, and Mexico City quickly passed European cities like London and Paris (Cohen 2004).

Another important factor stimulating rapid urbanization is the globalization of the world economy, and consequently the decrease in the need for spatial proximity in the economic activities. The recent international policy climate is also facilitating the globalization of the world economy. International trades, investments, labor division and a number of other factors also contribute to the globalization of the world economy (Yeung, 2000; Sassen, 2000). The combination of these factors has led to economic flourish of the developing cities and radically increased their economic production and prosperity (Yeung, 2000). Seoul, Taipei, Hong Kong, Manila, Bangkok, Jakarta, etc. are examples of cities that have flourished over the past 20 years, and changed into industrial hubs with huge populations.

Although urban growth in developing cities demonstrates levels of similarities, the patterns of urbanization are enormously different. The level and spend of urbanization which each individual city experiences also varies tremendously. For instance the level of urbanization in Latin America is now 75%, which is comparable to those of North America, and means this region is predominantly urban and the urbanization rate in this region is quite slow (Aguilar, 1999; Cohen, 2004). Huge urbanization and industrialization took place in South American cities before 1950 and during 1950 to 1975 (World Bank, 2002). Sao Paulo, Brazil, for instance, is a chief industrial hub and urban agglomeration in Latin America Coffee cultivation was an important factor in economic flourishing of the city. Establishment of manufacture in 1900s was also a stimulating economic element. These elements transformed the city from a commercial center in 1880s with population of only 65,000 to a chief manufacturing center and an immigration destination for labor workers from various parts of Europe. Sao Paulo is now responsible for more than half of Brazil's total industrial production (Cohen, 2004). Mexico City is another metropolitan city in Latin America, which experienced a huge population increase in the mid-1990s. The population of this

city increased from 16.5 million in 1995 to 25 million by the end of the 20th century (Aguilar, 1999). This increase in population caused a dramatic shift in the pattern of urban settlement in this city. The average annual economic growth rate in Mexico City was as high as 7.8% during the 1940s and the 1970s. This economic flourishing was due to import substitution, industrialization and development of manufacturing in this city (Reynolds, 1970). During the same period of time, the population growth rate was 3.1%. The natural population growth was accompanied by rural to urban migration. Both natural increase and immigration led to the concentration of population in Mexico City in a way that by 1970, 19% of the total population of the country was residing in Mexico City and this city was six time larger than the next city in terms of population size. Furthermore, this city accounts for 46% of the national industrial products (Aguilar, 1999).

Urbanization in Asia is also taking place in relatively different manner. In 2010, Asia contained 4.1 billion people or approximately three fifth of the world's total population, and almost half of the world's urban population (United Nations, 2011). However, it is impossible to generalize about the population and urban growth situation in Asia, due to the cultural and physical heterogeneity of this region (Cohen, 2004). Many cities in South Asia experienced dramatic economic growth. Hong Kong, Singapore, Seoul and Taipei are examples of South Asian cities that enjoyed an economic growth rate of more than 10% in the 1970s and early 1980s (Cohen, 2004). An example of a South Asian developing city, with a high rate of population growth is Kathmandu. The Kathmandu metropolitan region, capital of Nepal and major tourist gateway, has been facing rapid urbanization over the last three decades. Kathmandu's population in 1960 was 119,000 people, while this number has increased to over a million inhabitants in 2010 (United Nations, 2010) with an annual growth rate of 5.2% (Thapa & Murayama, 2010). Historically, Kathmandu was the center of political and economic power, but in 1960s, a modern transportation infrastructures brought easy access to the city, and changed its predominantly agricultural landscape into an urban one (Thapa, 2010). Analysis shows that from 1978-1991, more than

32,000 km^2 of natural and agricultural lands, were transformed into built up area, while from 1991-2000 this area reached more than 57,000 km^2 (Thapa, 2010).

North African and Middle Eastern cities have experienced the same process of change during last few decades. Some of the world's oldest cities are located in the North Africa and Middle East regions. Arid and semi-arid climate, poor vegetation cover, long periods of drought, low levels of annual precipitation, and water shortages are some of the most important natural features of this region, the same features which led the earliest human settlements in the region to be established near rivers and bodies of water. "These regions are endowed with an extraordinary cultural heritage of great significance for the countries and humanity at large, including 76 sites on the United Nations Educational, Scientific and Cultural Organization (UNESCO's) World Heritage List (19 of which are cities or urban districts)" (The World Bank, 2011, para. 4). This region has also always been the site for many political and religious conflicts and controversies. Alexandria, Baghdad, and Damascus are example of ancient cities with thousands of years of history. However, until the past 50 years, their population was predominantly rural. Most of the urban development in this region started with the development of the oil industry. The emersion of huge oil companies and international labor migration to oil-rich cities resulted in the economic flourishing of the Persian Gulf States, and hence the development of urbanization in this region (Cohen, 2004) According to the United Nations (2011) only 27% of their total population lived in urban areas in 1950, while this proportion grew to 57% by 2010. These changes over the past 50 years made the Middle East and North Africa some of the most urbanized regions amongst the developing countries (Stewart, 2002). For instance, the level of urbanization in oil-rich countries including Libya, Bahrain, Kuwait, United Arab Emirates, Lebanon, Yemen, Saudi Arabia, Iran and Qatar, have already reached more than 85% (Cohen, 2004). However, in this region the rural to urban transition took place at a faster pace from the 1960s to the 1980s, than form the 1980s to the 1990s. The urban growth rate was 4.6% between 1965 and 1980, whereas this rate dropped to 4.4% between 1980 and 1990 (Gilbert, 1993).

Regardless of rapid population and urban growth in the Middle East region, the average growth per capita in 1985-2000 was 0.9%, which indicates a poor economic performance (The World Bank, 2011). The economy of these countries is highly oil-dependent and non-diversified. For most of these countries, the non-oil exports account for only around 6% of the total exports. However, the sharp rise in oil prices could not improve the economic situation of most of these countries, due to the geopolitical conflicts. The Israeli-Palestinian conflict, Lebanon War, the Gulf War, political tensions resulting from the Iran and Iraq War are examples of the geopolitical conflicts in this sensitive region. These issues caused increase in regional political instability and insecurity. Another crucial challenge in this region is the high unemployment rate of up to 15%, especially among youth (The World Bank, 2011). At the same time, the investment climate was stopped from developing by both an unproductive public sector and a non-dynamic private sector. In addition, strong centralization weakened local governments' capacity to finance, deliver and manage urban facilities and services. Poverty is another fact that cities in this region are struggling with. According to the World Bank (2011), in 2001, 23.2% of the population in the Middle East and North African cities lived on less than $2 per day. On the other hand, the poor public land management caused an unprecedented increase in the cost of land and housing, which led to the proliferation of slums and informal settlements in the periphery of the cities throughout the region (The World Bank, 2011). These issues increase concerns about the population living in this region which has also had to struggles with frequent conflicts, wars and natural disasters, as well as shortages of the major natural resources, including water. This phenomenon in the Middle East and North Africa was defined by the World Bank as the "Urbanization of poverty". The purpose is to add enormous pressures on cities' managers and administrations to provide sufficient urban infrastructure, services and affordable housing and to create job opportunities to comply with the demands and needs of the poor urban population (The World Bank, 2011).

Istanbul is an example of a developing cities in Middle East region, which is predicted to be the 20th largest city in the world by 2015. Istanbul's population has

more than doubled in two decades from 4.7 million in 1980 to 10.58 million in 2000 (The World Bank, 2011), due to mass immigration from rural areas to the city. Urban expansion and increases in the total built up area have caused significant decreases in the amount of green areas and hence sped up environmental degradation in this city (Geymen and Baz, 2008). Istanbul is also facing other socioeconomical and environmental issues such as legal and illegal constructions, destruction of vast area of agricultural lands, heavy traffic and a population boom (Maktav and Erbek, 2005).

Cairo also exemplifies environmental and social issues and challenges of typical North African and Middle Eastern cities. Cairo, known as a mirror of Egyptian society, is an important political and cultural center of the Arab world. This city best demonstrates the urban growth features and pattern of this region. Cairo experienced a tremendously concentrated population mass with a population increase of more than 10 million people over 60 years (1950-2010) (United Nations, 2011). Cairo's early establishment is in the Nile river basin. After World War II, different urban infrastructures, including roads, bridges, water, and a sanitation system were developed in the city as a result of economic flourishing. Before this transition, the economy was mostly agriculture-based, but soon a heavy rural to urban migration started and caused a severe housing shortage (Omran & Roudi, 1993). The shortage of affordable housing led to the formation of some informal settlements in agriculturally suitable areas in the west bank of the Nile, or in new industrial zones. Cairo is now suffering from a number of socioeconomical problems, including high unemployment rate, development of slums and a wide rich/poor gap. This city also faces environmental degradation and pollutions, and heavy traffic as examples of other problems associated with unsustainable management plan.

Geopolitically, Iran is an important country in the Middle East, and is a strategic gateway, which connects the three continents of Asia, Europe, and Africa, and is also a chief oil producer. In addition to thousands of years of history, Iran is a diverse country in terms of culture and ethnicity, biology, climate, and habitat. The largest area of the country is desert with an arid and semi-arid climate, which increased the value of water for the original inhabitants, which were mostly

farmers, and led to early human settlements being established adjacent to rivers and other sources of fresh water. In the mid-20th century, Iran, like other parts of the world experienced dramatic changes in terms of population growth, rapid urbanization, and rural to urban transition. Development of oil industry, and establishment of huge steel companies and other industrial mega units, accelerated the industrialization and urbanization trends in the country. In 1970, 45% of the population was living in urban areas, while in 2011 this population increased to 69%.

More than 23% of Iran's rapidly growing urban population is concentrated in the three large cities of Tehran, Mashhad, and Isfahan (The World Bank, 2011). These cities have experienced radical industrial, economic, demographic, environmental and social changes, during the past decades. Tehran, the capital, with a population of over 12 million in 2010, is a huge mega city and the second largest and most populous city in the Middle East, after Istanbul. Isfahan, the third largest city and the target city in this study, is a secondary city, which experienced significant urban expansion during the past 30 years. With more than three thousand years of history, Isfahan is one of the early settlements established in Iran Plateau adjacent to Zayande Rood River, and has experienced different epochs and undergone dramatic changes, especially in the recent decades when this city became an economic hub in the country. Isfahan experienced large industrialization, along with huge population increase and a high rate of rural to urban migration, which makes it a suitable case to study urban expansion. Isfahan's population increased from 306,000, persons in 1960, to 1,743,000 persons in 2010 (United Nations, 2011). This population growth was due primarily to natural population growth (especially in 1980s), as well as rural to urban migration. Furthermore, the "New Town Strategy", encouraged by the government of Iran, led to the construction of new satellite towns on the periphery of this city (Atash and Shirazi, 2004). These towns were built close to industrial mega units and at large distances from the major urban core, without any dependence on it. Zarrin-shahr, adjacent to the Mobarake Steal Company in the south, Fouland-Shahr adjacent to the Isfahan Steal Company in the southwest, and Shahin-shahr adjacent to the Isfahan Oil Refinery in the north, are all examples of

satellite towns constructed in the last five decades for the purpose of accommodating populations working in those industrial units. The most recent urban development type started in 1994. This type of development was not really supported by a master plan or following financial, managerial, or legal standards. In this type of development new residential neighbourhoods were constructed within a definite distance to the main city core. However, in some cases these new residential areas amalgamated to the major core, due to the huge city expansion (Ziari, 2008). The main purpose of these new neighborhoods was to provide affordable housing for the population that worked in the main city core. Malekshahr and Khane-Isfahan are examples of these settlements in the northwest of the city of Isfahan.

Along with urban growth in the city of Isfahan, natural and agricultural lands are highly affected by the urban expansion and population growth, in different ways. Many gardens and fertile farmlands were destroyed and clear cut, due to the development of new towns and the expansion of built-up areas. Many others lost their quality, due to soil and water exploitation. Reduction of the total cultivated area, along with an increase in population also increased the pressure on the existing agricultural lands for more crop production. Soil over-use leads to depletion of soil nutrients, especially nitrogen and phosphorous. As a consequence of soil depletion, more chemical fertilizers are used, which leads to air, soil and water pollution. Especially the contamination of underground water resources as a result of fertilizer over-use is a problematic challenge in arid and semi-arid lands, due to high dependency of these areas on underground water resource as a source of drinking water. Soil erosion and depletion of fresh water resources are other consequences of land over-use. As a result of environmental degradation, low quality agricultural lands were discarded by the farmers, who were in turn obliged to migrate to the adjacent urban areas. The cost of living is usually lower in the new towns than the main city hub, and that's why the rural to urban immigrants usually prefer to settle in these new built-up areas. Unemployment, high crime rate, heavy traffic, environmental pollutions and degradation are amongst the various social and cultural contradictions that these towns suffer from (Ziari, 2008). Mapping land use and land cover change during

the time helps urban planners to identify urban growth patterns and trends, and to prevent negative impacts on people and environment. Section 2.3 describes the land use and land cover change detection techniques, used for mapping land uses in different environments.

2.3. Land Use and Land Cover Change Detection

In section 2.2, the urban expansion, its problems and its consequences are explained in detail. Urban expansion and other human activities are one of the main causes of dramatic changes in land use and land cover over time. In many contexts "land use" and "land cover" might have been used interchangeably, however, these terms are distinct. "Land use" indicates the type of human activity taking place in a certain area, whereas "Land cover" denotes the natural and physical feature on the ground surface. Land use and land cover change detection is the identification of a natural or manmade transformation of an object or a phenomenon on the ground surface over a time period. Aerial photos and satellite data have been used in change detection studies to record and quantify the land use and land cover transitions. Change in spectral response of a ground feature in time could be identified using remotely sensed data. In these studies at least two period data sets are necessary (Jenson, 1986).

Land use and land cover change detection has different applications in environment, agriculture, forestry, water resources, etc. One of the most important applications of change detection studies is in urban management and identification of city growth patterns. As mentioned in the section 2.2, the majority of the world's population now resides in urban environment. In order for city planners and managers and administrative bodies to improve the standards of living in big cities, identification and understanding of internal composition and dynamics of these environments are essential (Phinn *et al.*, 2002; Jenson and Jungho, 2005). They require new and reliable sources of data and information to assess the consequences and overcome the challenges of world rapid urban growth (Miller and Small, 2003). New sources of data are used along with new analytical approaches to ensure a sustainable functioning of megacities and to

minimize the negative impacts of rapid urbanization. However, the management system and city plan monitoring is different in developed countries versus developing ones. In the developing world the administration is often unable to manage and keep track of growth related processes, and urban expansion takes place in an unplanned manner (Maktav *et al.*, 2005).

Remote sensing has been used as a powerful tool for urban change detection applications. Remote sensing provides cheap and effective multitemporal aerial photos and satellite images. These data along with remote sensing analytical approaches has always been of considerable interest for periodic monitoring of large urban agglomerations and mapping land use and land cover in natural and urban environments (Phinn *et al.*, 2002; Griffiths *et al.*, 2009).

Before the launch of satellites, aerial photos were used for change detection purposes. To be able to use historical aerial photos in urban or natural change detection studies, scanning, digitizing, georeferencing, and resampling spatial resolution were required. The study by Mast *et al.* (1997) is an example of using pre-satellite remotely sensed data in change detection. They used historical aerial photos to quantify vegetation change inside ecosystem boundaries from 1938 to 1990 in the northern Colorado Front Range. They used Digital Elevation Model (DEM) and topographic map to locate the area of interest, and subset images and derived the area of common overlap between images acquired in different times. Statistics, field data collection, analysis of spatial patterns of change and other secondary approaches helped researchers to overcome the technical limitations of historical change detection studies. Ihse (1995) used these techniques to validate his study of agricultural lands in Sweden during a 50-year period. He used aerial photos acquired in the 1940s, 1960s, and 1980s to describe the development pattern of grasslands and pastures. He used the Geographical Information System (GIS) to integrate changes in land use classes and spatial patterns, obtained from comparative map analysis. Similarly, in another change detection study using aerial photos, Williams and Lyon (1996) used GIS to formulate impacts of long-term water level fluctuations on the wetland areas of the St. Marys River, on the US and Canada border. They used seven aerial photos taken over 46 years from

1939 to 1985. Wetland boundaries for each photo were outlined manually using analog stereo plotter then GIS was use to combine the data, classify land cover classes in the wetland area, and prepare a year-to-year analysis of change across the entire study site. This study demonstrated the prominence and higher accuracy of GIS change detection techniques over manual methods.

Furthermore, digital image processing techniques have also been applied to aerial photos in different change detection studies. Grey scale digital image processing techniques were used to detect the vegetation dynamics of a Mediterranean maquis ecosystem from 1960 to 1992 (Kadmon and Harari-Kremer 1999). This study used four images of 1960 and three images of 1992 to make a mosaic of images which cover the whole study area, as well as a vegetation map using maximum likelihood image classification. This study also showed the limitation of using gray scale data, since it requires the analyst validation of gray level values to be adjusted for different data sets.

Aerial photos have also been used in combination with satellite images for historical and comparative change detection purposes. Wang *et al*. (2005) studied orthorectification of historical aerial photos acquired during World War II and Ikonos high resolution satellite images, on five densely populated rural sites selected across environmentally distinct regions of China, shows that these two types of data are geometrically compatible. Palandro (2002) combined two aerial photographs (acquired in 1981 and 1992) and an Ikonos image (acquired in 2000) to detect change in the coral reef communities of the Carysfort Reef in Florida (USA). They used a Mahalanobis Distance classifier, and introduce four classes in the benthic communities. In this study, Ikonos imagery appears to be a relevant source of information when used in conjunction with historic colour aerial photography to show change and fragmentation in an initially compact coral reef community. *In situ* studies approved the results and showed a consistent trend of decline, in the coral reef community.

Willhauck (2000) also used a combination of aerial photos and satellite data to study change detection in the Tierra del Fuego forest in Argentina. He used aerial

photos acquired in 1960, and multispectral SPOT scenes acquired in 1995. He scanned, georectified, and resampled aerial photos to match them with the pixel size of the satellite data. Pixel oriented classification, object oriented classification, and segmentation methods, have been used to identify forest classes for the spot image, as well as for the aerial photo to detect changes over time. Total deforested area from 1960 to 1995, derived overlapping three SPOT images with the aerial photo.

After the launch of first the satellite, urban planners and environment researchers began to use satellite images for urban and environmental planning and change detection studies. The temporal resolution of satellite imageries enabled researchers to estimate the extent of land use and land cover changes in a historical framework. In these studies remote sensing tools have been used along with change detection techniques, to assess the changes in land use and land cover over time. Change detection techniques have been reviewed by many authors. Singh, (1989), Lu *et al*. (2003) and Coppin *et al.* (2004) have reviewed the most important change detection techniques. They listed univariate image differencing, image regression, image rationing, change vector analysis (CVA), background subtraction, principal component analysis (PCA), vegetation indices differencing, Chi-square method, artificial neural network (ANN) and different classification methods, as the most frequently used techniques used by different researchers.

In this study the following three change detection techniques are used:

1. *Principal Component Analysis*
2. *Vegetation Indices Differentiating*
3. *Classification*

2.3.1. Principal Component Analysis (PCA)

PCA is a remote sensing approach used to reduce the number of the most variances in the original multispectral images. The first principal component usually contains the maximum amount of variation. In a raw image the spectral bands are significantly correlated. PCA is an image enhancement method and an

important linear transformation technique (Coppin, 2004) that produces a new set of decorrelated bands. Mathematical techniques and statistical methods are used in PCA algorithm to multiply each spectral band by a weight to decorrelate the data and reduce redundancy (Lillesand and Kiefer, 1994). "This linear transformation rotates the axes of spectral bands along lines of maximum variance" (Joshi, 2006, page 87). Consequently the output bands contain fewer values than input spectral bands.

Image differencing and image regression are applied to the PCs of two or more dates to make a comparison between land uses and land covers over time (Lodwick, 1979). The ΔPCA indicates the gross differences associated with both radiation changes and local changes of land use and land cove (Singh, 1989). In multitemporal researches and comparative studies, principal components can give a general overview about land use and land cover changes over time (Deng *et al*., 2008). Fung and LeDrew (1987) found PCA to be the most appropriate method for detecting land use changes for multi-sensor data. PCA was also shown to help enhance the change information from stacked multi-sensor data in a study by Deng *et al*. (2008) on the Hangzho urban environment in Zhejiang Province (China).

PCA together with other change detection techniques have been independently applied in many researches, to compare the accuracy and suitability of different techniques. Sunar (1998) compared image overlay, image differencing, PCA and post-classification methods for land-cover change detection in the Ikitelli area (Istanbul, Turkey), and found PCA and post-classification the best methods for this purpose. A study by Collins and Woodcock (1996) on mapping forest mortality using Landsat TM data also showed that PCA is the most reliable single indicator of forest change.

Gong (1993) used PCA to study and detect the changes in urban and rural areas in Kitchener (Waterloo, Ontario). He applied PCA on the data acquired from Landsat TM sensor in 1985 and 1986. The results of this study showed that the first and the second components are responsible for 64.9% and 27.1% of the

variance respectively. Hayes and Sader (2001) studied land cover changes in a forest area in Maya Biosphere Reserve, El Peten (Guatemala). They applied PCA to two Landsat TM datasets from 1993 to 1995 and 1995 to 1997 and found 76.02% and 79.15% of the variation of first two PCs for each dataset, respectively. In addition, Byrne *et al.* (1980) used PCA to detect changes in the township of Batemans Bay, the largest town in New South Wales area. They used Landsat Multi Spectral Scanner (MSS) images for the years 1972 and 1975, and made four different component analyses for each image in each year. The first component was very highly correlated with brightness in the infrared channels 3, 4, 7, 8 and was responsible for 91% of the variance. The second component was a measure of brightness in the two visible bands. Component 3 was a measure of difference between the two images and finally component 4 presented differences in the infrared channel reversed. In this study, PCA has introduced an effective way of identifying areas of change within two four-channel MSS images of different dates. However, the authors did not talk about the quantitative accuracy of their method.

PCA has also been used combined with other change detection techniques in order to improve accuracy. Pu *et al.* (2008) took advantage of PCA as an input channel for hybrid classification to monitor change detection for an invasive plant species, Saltcedar, in Near Lovelock (Nevada). PCA has proven to outperform classification in this study and increase the overall accuracy to up to 91.56%. PCA was also used on unite vectors of change vector analysis by Lamhin and Ehrlich (1997) for seasonal changes in the Sub-Sahara desert of Africa. This study showed that PCA performs more precisely for smaller regions than continental scale. Likewise, Deng *et al*. (2008) used a multi-temporal and multi-sensor's data (SPOT-5 and Landsat-7) to detect land use change in an urban environment in Hangzho area, Zhejiang Province (China), using PCA and hybrid classification, methods, for the three dates of 2000, 2001, and 2003. PCA was used to enhance the change information from stacked multi-sensor data, then a combination of both supervised and unsupervised classifiers were used to identify and quantify

land use change. The overall accuracy of the methodology was 89.54% and 0.88 for the Kappa coefficient.

2.3.2. Vegetation indices differencing

Vegetation indices are mathematical indicators based on the relationship between different spectral bands. They are more sensitive to the vegetation spectral response than the individual bands (Asrar *et al*., 1984). Vegetation indices are useful tools in the interpretation of remote sensing images to quantify vegetation parameters such as growth stage, density, health situation, moisture content, etc. Red (630-690 nm) and near infra-red (760-900 nm) bands have the most contributions in the formation of vegetation indices ratios. However, the spectral relations of other spectral bands are also used to create them. Different vegetation covers demonstrate same spectral behavior in relation to other ground features. This fact makes the vegetation cover distinguishable from the background. On a green canopy the red radiation is absorbed by chlorophyll, while the near infrared radiation is strongly reflected by the cellular structures of the leaves (Bannari *et al.,* 1995). The combination of red and near infra-red spectral bands allows image interpreter to discriminate vegetation from soil background and determine vegetation status, density, and other vegetation biomass characters.

More than 50 vegetation indices have been developed by different scientists for different applications. Most of these indices are based on the linear or ratio relationship of the red and the near infra-red reflections of the green leaves (Huet, 1988). In this study 10 vegetation indices are selected to apply on the images used in the research. These indices were applied in urban change detection studies done previously by other scientists and proved to have high accuracy in urban application.

The first vegetation indices developed only based on linear combination (difference or sum) or simple ratios of the raw bands. Other external factors including soil-vegetation interaction was not take into consideration (Bannari *et al.,* 1995). The first vegetation indices which developed in the form of simple ratios of red and near infra-red bands are the Ratio Vegetation Index (RVI)

(equation 2.1), and the Vegetation Index Number (VIN) (equation 2.2). These indices developed by Pearson and Miller (1972) to monitor the vegetation growth and canopy status. These indices help to increase the contrast between the vegetation and soil.

$$RVI = \frac{Red}{NIR} \qquad (2.1)$$

$$VIN = \frac{NIR}{Red} \qquad (2.2)$$

The Differenced vegetation index (DVI), developed by Clevers (1986) is an example of a ratio index based on the linear relationship of red and near infrared bands (equation 2.3).

$$DVI = NIR - Red \qquad (2.3)$$

Ashburn Vegetation Index or Agricultural Vegetation Index (AVI), developed by Ashburn (1978), is another ratio index, suggested as the measure of green growing vegetation (equation 2.4).

$$AVI = 0.2 \times Band7 - Band5 \qquad (2.4)$$

The Normalized Difference Vegetation Index (NDVI) developed by Rouse (1974), is amongst the most popular and most frequently used vegetation indices, which has been in use for many years to measure and monitor plant growth, vegetation cover, and biomass production from multispectral satellite data. NDVI is one of the first vegetation indices developed based on a linear combination (Equation 2.5).

$$NDVI = \frac{NIR-Red}{NIR+Red} \qquad (2.5)$$

NDVI value rages between 0 and +1. A value of zero or close to zero means no or very low density vegetation, whereas a value close to +1 (0.8 - 0.9) indicates the highest possible density of healthy green vegetation. NDVI can be used to study

the vegetation state and density. It can also be used in prediction of agricultural crops, and estimation of the total annual precipitation in semi-arid areas, (Bannari *et al*., 1995)

Scientists have modified NDVI and developed new indices to adjust for different reflectance. In these new indices other important factors in the vegetation measurement such as soil brightness have been taken into consideration, which influence the measurement of vegetation indices. The Perpendicular Vegetation Index (PVI) is one of these indices, which considers the effect of bare soil. This index was developed by Richardson and Weigand (1977), but was then modified by Jackson *et al*. (1980) based on the bare soil line theory. The modified version of PVI is shown in equation 2.6. Where a and b are soil line parameters. a is "the slope of the bare soil line", and b is "the ordinate at the origin of bare soil line" (Bannari, *et al*., 1995)

$$PVI = \frac{NIR - aRed - b}{\sqrt{a^2+1}} \qquad (2.6)$$

Huete (1988) showed that NDVI and PVI indicate some levels of inconsistency in presenting the spectral behavior of vegetation and soil background. To overcome this problem, he added a coefficient (L) to the NDVI formula as the soil adjustment factor and developed the Soil Adjusted Vegetation Index (SAVI), which is a compromise between NDVI and PVI (equation 2.7).

$$SAVI = \frac{NIR - Red}{NIR + Red + L}\ (1 + L) \qquad (2.7)$$

L is a soil adjustment factor. According to Huete (1988) L= 0.5 provides the best adjustment to minimize bare soil reflectance effects.

Another modified version of SAVI is the Transformed Soil Adjusted Vegetation Index (TSAVI) (equation 2.8), developed by Baret (1989). An X value equal to 0.08 is added to minimize the effect of soil brightness on vegetation (Baret and Guyot, 1991). A and b in the equation are the bare soil line parameters (the slope

and the intercept of the bare soil line). The SAVI and the TSAVI are able to present both changes in the vegetative cover and soil background (Bannari *et al.*, 1995).

$$TSAVI = \frac{a(NIR - aRed - b)}{Red + aNIR - ab + X(1 + a^2)} \qquad (2.8)$$

Major *et al.* (1990) took into account the effect of wetness or dryness of the soil and the variation in the solar inclination angle to modified SAVI and develop Soil Adjusted Ratio Vegetation Index (SARVI) (Bannari *et al.*, 1995). SARVI is one of the modified versions of SAVI, based on soil line parameters (a and b in equation 2.9).

$$SARVI = \frac{NIR}{Red + \frac{b}{a}} \qquad (2.9)$$

Qi *et al.* (1993) also modified SAVI to minimize the effect of bare soil on this index, and derived Modified Soil Adjusted Vegetation Index (MSAVI) (equation 2.10).

$$\text{MSAVI} = \frac{2\text{NIR} + 1 - \sqrt{(2\text{NIR} + 1)^2 - 8(\text{NIR} - \text{Red})}}{2} \qquad (2.10)$$

Transformed Difference Vegetation Index (TDVI), developed by Bannari *et al.* (2002), minimizes the limitations of NDVI and SAVI. Compare to NDVI, this new index minimizes "the problem of linearity and saturation". It also minimizes "the effect of optical properties of bare soil on SAVI" (Bannari *et al.*, 2002). Equation 2.11 presents this vegetation index.

$$\text{TDVI} = 1.5 \times \frac{\text{NIR} - \text{Red}}{\sqrt{\text{NIR}^2 + \text{Red} + 0.5}} \qquad (2.11)$$

TDVI have proven to effectively minimize the impact of bright soil, as well as minimizing the impact of darker and wet soil. It has also shown more sensitivity and higher accuracy for mapping vegetation in urban environments, compared to NDVI and SAVI (Ozbakir and Bannari, 2007)

The greenness index or Normalized Difference Green vegetation Index (NDGI) (equation 2.12) is another ratio index developed by Chamard *et al*., (1991). This index is based on the ratio between red and green bands. NDGI is useful for mapping green vegetation and active vegetation growth. It also has been used to detect damages to agricultural lands caused by different factors (Minekawa *et al*., 2005; Hoshino *et al.*, 2005)

$$\mathrm{NDGI} = \frac{\mathrm{Green}-\mathrm{Red}}{\mathrm{Green}+\mathrm{Red}} \qquad (2.12)$$

Vegetation index differencing is an algebraic method that has been vastly used for land use and land cover change detection purposes. In change detection studies the difference of vegetation indices (i.e. (vegetation index t_1) - (vegetation index-t_2)) helps to detect the possible changes in the vegetation cover and the significance of these changes (Singh, 1989). This method highlights the changes in the spectral response of various ground features and minimizes the impacts of topographic effects and illumination. It is also capable of processing any number of spectral bands and to create detailed information about changes in ground features (Lu *et al.*, 2003).

Vegetation index differencing is one of the most accurate and frequently used change detection techniques. NDVI, SAVI, MSAVI, TDVI, DVI, PVI, RVI, SARVI, TSAVI and NDGI, are some of the vegetation indices used in the literature for change detection purposes. Different vegetation indices have been compared to identify the most accurate and suitable one for different land use purposes in different researches. In a comparative study, using Landsat MSS and TM, Lyon *et al*. (1998) used seven vegetation indices (DVI, PVI, RVI, SARVI, NDVI, SAVI and TSAVI), and the spatial distribution pattern of each, for land cover change detection of a forest area in Chiapas (Mexico). They showed that NDVI is the best performing vegetation index for detecting land cover changes in the biologically complex vegetation communities. NDVI has also been used as the most accurate vegetation index by Lunetta *et al*., (2006) on Landsat MSS data of Albemarle–Pamlico estuary system (APES) located in North Carolina and Virginia. Huet *et al*. (1997) also compared NDVI, SAVI, ARVI, SARVI and

SARVI2 for a set of 16 TM images of different ecosystems acquired in different months. Unlike the results of Lyon *et al*. (1998) and Lunetta *et al*. (2006) studies, their results showed that SAVI, SARVI and SARVI2 are extending the range of sensitivity of vegetation indices into both densely vegetated, forested regions, and sparsely vegetated, arid and semiarid regions, while NDVI is saturated in densely vegetated areas due to high sensitivity to the red (chlorophyll) absorption band. Moreover, in a comparison study between NDVI, SAVI and TDVI over Montréal Island, Bannari and Ozbakir (2007) showed that TDVI has higher accuracy than both NDVI and SAVI, and is the most sensitive index for mapping vegetation cover in urban environments.

Vegetation index differentiating has been independently applied together with other change detection techniques in many researches, to compare the accuracy and suitability of each technique. Bakr *et al*. (2010) used hybrid classification, as well as NDVI, to detect changes in Nile Delta (Egypt), using TM and ETM data for five dates from 1984 to 2008. The overall accuracy of NDVI is higher than 94% for the first four dates, and is 77% for the 2008 image, which present a higher accuracy compared to a hybrid classification method. Furthermore, Pu *et al.* (2008) used Multidate Compact Airborne Spectrographic Imager (CASI) hyperspectral dataset, with the spatial resolution of sub-meter to 10 m, to monitor change detection for an invasive plant species, Saltcedar, in Near Lovelock, (Nevada, USA), for three decades. He compared NDVI differencing and supervised classification techniques, and in the classification strategy, a PCA was performed on single date CASI imagery separately in visible bands and near infrared bands. The overall accuracy of these results was 91.56% with a kappa value of 0.618 for the classification method against corresponding values of 93.04% and 0.684 for the NDVI differencing method. It indicates that the NDVI differencing method outperformed the classification method in this particular study.

Vegetation indices have also been used combined with other change detection methods. Hayes and Sader (2001) used NDVI, RGB-NDVI, and PCA, in their study on land cover changes in a forest area in Maya Biosphere Reserve, El Peten

(Guatemala). In this study, these three methods had been compared and the RGB-NDVI method had been shown to have the highest accuracy of 85%. Furthermore, Rastmanesh *et al.* (2010) studied the impact of air pollution on vegetation cover in Sarcheshme Copper Complex, the center of Iran, over 14 years. They combined a statistical method and NDVI on bands 3 and 4 of Landsat TM (1987) and ETM+ (2000) imageries. They used the K-mean cluster classification method as an accurate statistical method. The results are NDVI maps for selected bands which show deterioration in vegetation in the prevailing wind direction. This study is an example of statistical methods that can be used to monitor vegetation cover, even in a region of spare vegetation.

Researchers used different vegetation indices to map vegetation in urban areas. NDVI has been used in many urban change detection studies (Howarth and Boasson, 1983; Rouse 1973) Nicoloyanni (1990) also used NDVI to map the urban growth for Athens, (Greece), using Landsat MSS data for the period of 1975 to 1981. However, Griffith (1988) used NDVI to study the urban growth in south-east England. The results of his study showed that NDVI differencing not only map the real urban growth, but also will include areas of agricultural change in addition to real city expansion. In addition, Masket *et al.* (2000) used NDVI differencing for Landsat MSS and Landsat TM images of Washington DC. to distinguish urban growth in this area. The results also show that the ΔNDVI can present both changes in urban and agricultural lands.

2.3.3. Classification

Any individual pixel is characterized by a digital number for each spectral band. A “spatially grouped sets of pixels” representing same ground feature or class also shows relatively small range of digital numbers for each band monitored by the remote sensor (Short, 2010). The purpose of the classification process is to categorize all these pixels into an identified land use class and the result is a thematic map of the land uses.

Supervised and unsupervised classifications are two commonly used classification methods, which have been followed in many change detection studies.

Supervised classification is much more accurate for mapping classes, but it heavily depends on the skills of the operator. In this method, pixels are clustered based on the training sites selected manually by the operator. The training sites are selected based on the prior knowledge of the operator from the ground features. "They represent each known land cover category that appears fairly homogeneous on the image" (Short, 2010).

Griffiths *et al.* (2009) used supervised classification to map Dhaka, Bangladesh, as a mega city, to observe urban growth during the years 1950 to 2007. They used TM and ETM+ images, and all analysis was based on the bands of the TM and ETM+ sensors, excluding thermal and panchromatic bands. They also used the European Remote Sensing Satellite, as well as Advanced Synthetic Aperture Radar (ASAR) to overcome the limitations of Landsat data in assessing urban versus non-urban features. In their study supervised classification was used to define six land cover classes. These classes characterized major changes in the land use and land cover of Dhaka and its hinterlands. The study obtained an overall accuracy of better than 83% for each image in each year.

Furthermore, Seto *et al.* (2002) used supervised classification to monitor land use changes in the Pearl River delta in China. They used Landsat TM data from 1988 to 1996, and did image segmentation and map editing on the classification results. Map accuracy assessment showed high overall accuracy of the land-use change map (93.5%) and supported the use of change vectors and multidate Landsat TM imagery to monitor land-use change.

The same method applied to the different datasets by Anys *et al*. (2002) to study urban expansion in Beni-mellal (Morocco), in order to assess the impact of urbanisation on agricultural lands in the three decades from the 1970s to 1990s. For this study, SPOT panchromatic data (resolution 10 m) was used to provide good discrimination of land uses, and better accuracy in mapping and calculating the area for each theme. Classification was used to create 8 classes of land uses for different years of the study, and then make a comparison between the classes, in order to identify difference between each year, to help detecting the changes

during the study period. They also used GIS tools to map the total changes which had occurred during study period, as well as increases and decreases in each land use class. Their results showed different urban expansions in hectares and urban dense areas in different decades.

Hybrid classification takes advantage of both supervised and unsupervised classification techniques, to increase overall accuracy (Deng *et al.,* 2008; Pu *et al.,* 2008). Deng *et al*. (2008) used hybrid classification for change detection in an urban environment in Hangzho area, Zhejiang Province (China) for the three dates of 2000, 2001, and 2003. He used a multi-temporal and multi-sensor's data (SPOT-5 and Landsat-7), and he combined both supervised and unsupervised classifiers to identify and quantify land use change. The overall accuracy of their methodology was 89.54% and 0.88 for the Kappa coefficient. In addition, Pu *et al.* (2008), applied hybrid classification to monitor changes for an invasive plant species, Saltcedar, in Near Lovelock (Nevada, USA). Accuracy assessment of hybrid classification in this study showed an overall accuracy of up to 91.56%. Furthermore, Döner (2011) used three Landsat images from 1975, 1984 and 2000 to detect the changes in Gumushane (Turkey). He used a post-classification approach based on the hybrid classification technique, and classified the images into five distinct classes. He used the classification results to quantify the increase and decrease in the total area of each class and concluded that the urban class increased by 2.53%, while the pasture class decreased 3.3%.

Knorn *et al.* (2003) used chain classification of neighbouring Landsat satellite images to map a large area of Carpathian Mountain which is located in the countries of Ukraine, Poland, Romania, hungry and Czech Republic. The chain classification has been used in horizontal chain of six Landsat scenes and 2 vertical chains of the Landsat scene. They used Support Vector Machine (SVM) classifier which obtains an overall accuracy of 92.1% and 98.9% in the results of this study. This study showed high accuracy and low Kappa lost (average of 0.0408) in results for chain classification method, which showed the high reliability of chain classification method.

In many studies, the result of other transformation or rationing techniques, have been used as input for classification, and in most cases algorithms such as PCA and vegetation indices, proven to outperform the classification results and increase the accuracy (Ramirez-Garcia *et al.,* 1997; Pu *et al.,* 2008; Deng *et al.,* 2008). Pu *et al.* (2008) used PCA and NDVI as input channel for the classification of CASI imageries to monitor change detection for an invasive plant species, Saltcedar, in Near Lovelock, (Nevada), for three decades, and the accuracy assessment results indicated that PCA and NDVI increase the overall accuracy. Furthermore, Ramirez-Garcia *et al.* (1997) used TM image acquired in 1993 to assess mangrove vegetation cover in the Santiago River Mouth (Mexico). They applied PCA, and found the first three PCs responsible for 99.06% of the total variances and used as input channels for bands 4/5/3 to make a color composite for supervised classification. The accuracy assessment presents the overall accuracy of 96.7% for this study. Deng *et al.* (2008) applied PCA as an input channel for hybrid classification of SPOT-5 and Landsat-7 imageries to detect the change in an urban environment in Hangzho area, Zhejiang Province (China) for the three dates of 2000, 2001, and 2003. The results showed that the overall accuracy increases to 89.54% by using PCA as an input channel for hybrid classification.

For land use and land cover change detection purposes, different supervised classification methods have been applied. These methods are based on the quality and quantity of training sample data, and they will provide "a matrix of change information" for the mulitemporal images. However, the most challenging and time consuming step in these methods is to select accurate and high quality training site samples in sufficiently large number (Lu *et al.,* 2003).

Different classifiers are using different statistical algorithms to classify pixels based on the training sites. Maximum likelihood, minimum distance, and parallelepiped classifiers are commonly used for land use classification purposes; however, maximum Likelihood is the most powerful and accurate among them, and was selected to use in this study. "This classification method is a statistical decision criterion to assist in the classification of overlapping signatures and

assumes that each class in each band can be described by a normal distribution" (Lillesand and Kiefer, 1994). In the maximum likelihood method, each pixel is assigned to a class based on the highest probability and variance and covariance of the class signature. In the minimum distance classifier, the mean spectral value in each band is used, and in the parallelepiped approach the lowest and highest values in each band are used. Maximum likelihood uses the training sites to create lines of equal likelihood for each class. The highest likelihood for a certain pixel determines the class of that pixel. This method performs most accurately in classification of unknown pixels. Furthermore, it evaluates the variance and correlation of spectral response patterns when classifying an unknown pixel. However, in the minimum distance classifier an unknown pixel is assigned by calculating the distance between the pixel and the average value of that class. Moreover, in the parallelepiped classifier, the lowest and highest digital number values in each band are utilized to draw a box surrounding the training data. Any unknown pixel which falls within a certain box is assigned to that class.

Maximum likelihood has been used in many researches for change detection purposes of different ecosystems and environmental and urban applications. For instance maximum likelihood has been used in mangrove vegetation assessment of Santiago River Mouth (Mexico) over a 30 years period, showing an overall accuracy of higher than 95.8% (Ramirez-Garcia *et al*., 1997). In addition, this method showed overall accuracy of 88.0%, in a study by Bayarsaikhan *et al.* (2009) on land use change detection of Hustai National Park (Mongolia), using Landsat MSS, TM and ETM+. Furthermore, Keuchel *et al*. (2003) studied the land cover analysis of Tenerife, the largest of the Canary Islands. Their results showed that the maximum likelihood classification has the overall accuracy of 90%. Maximum likelihood algorithm was used by Macleod and Congalton (1998) in change detection of eelgrass population in Great Bay (New Hampshire). Abo-el-Ghad *et al.* (2004) also obtained overall accuracy of 87%, using maximum likelihood supervised classification for agricultural land monitoring in the Egyptian Nile Delta, using Landsat TM and ETM+ data.

2.4. Conclusion

Urban growth rate and patterns are different in developing countries than developed ones. In developing countries and especially the Middle East, urban expansion is an unmanaged process and usually is associated with a population boom, rural to urban migration, pollutions and environmental degradation, high unemployment rate and other socioeconomical issues. Urban land use and land cover change detection over time can help urban planners to identify and model the growth patterns to minimize the negative environmental and socioeconomical impacts. Satellite data and remote sensing methods can be used in land use and land cover change detection. Various remote sensing techniques have been used in the literature to detect changes in different environments over time. PCA, vegetation index differencing, and maximum likelihood supervised classification have been discussed for urban application, and selected to be used in this study. The study site, remote sensing data and methodology are presented in the chapter 3.

Chapter 3: Methodology

3.1. Introduction

This chapter presents the methodology used in this study. In the first section, the city of Isfahan is described as the study site. Geographical, historical, and socieconomical aspects of the city are viewed from the perspective of urban and population growth. The next section presents the methodology flowchart. Remote sensing data used in this study are described in the next section. Finally in the last section, the methodology used, including the preprocessing and processing procedures are described

3.2. Study site

The study site is the city of Isfahan, Iran. This country is very important in terms of oil production and political affairs in the Middle East region. The city of Isfahan, capital of Isfahan Province is the third largest city in the country. It is located in the central desert of Iran, at a distance of 420 km of south east of the Capital, Tehran (32°39'N, 51°43'E). The city of Isfahan is an improving city in terms of economy and industry, as well as urban expansion and population growth. Isfahan's demographic, socioeconomic, and industrial growth and urban expansion is discussed in section 2.2. Figure 3.1 shows the geographical location of Iran in Middle East area, Isfahan Province in the country, and the city of Isfahan in the province.

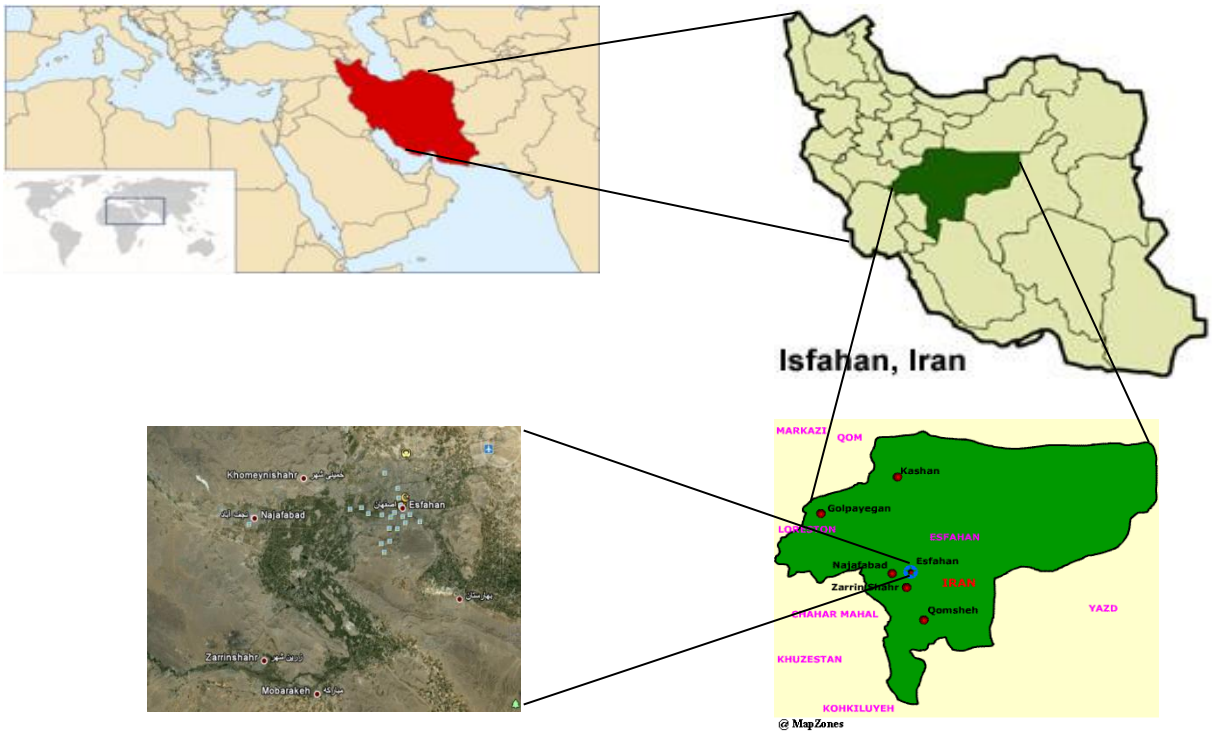

Figure 3. 1. Geographic location of Iran and Isfahan in the region

The City of Isfahan was established over 1000 years ago in the Zayande Rood River basin. Since the first establishment of this city, Isfahan has always been of great importance and had been the capital of the Persian Empire in different historical eras. Old buildings and monuments, presenting Islamic architecture, as well as ancient neighbourhoods and memorials, are the reasons why this city is a famous tourist destination and why it has been selected by UNESCO as a world heritage site.

Isfahan is located in an arid and semi-arid area, where the climate plays an important role in natural and agricultural conditions. The absolute maximum and minimum temperatures in Isfahan are 39.8 °c in July and -7.8 °c in January, respectively. The maximum relative humidity is 78% in February and the minimum is 8% in June. The mean annual precipitation is 122.8 millimeters.

Additionally, the maximum monthly precipitation is 35.5 mm in March, and maximum of freezing days is 26 days in January (Meteorology Administration of Isfahan Province, 2008). The Zayande Rood River watershed, covers a total area of 41,500 km ^{2} and irrigate large areas of agricultural lands in its way to the Gavkhooni Wetland (Natural Resource Administration of Isfahan Province, 2010). Figure 3.2 is the true color TM image acquired in 1985 from the city of Isfahan and the surrounding lands. In this image, the river path and the agricultural lands adjacent to the river are shown.

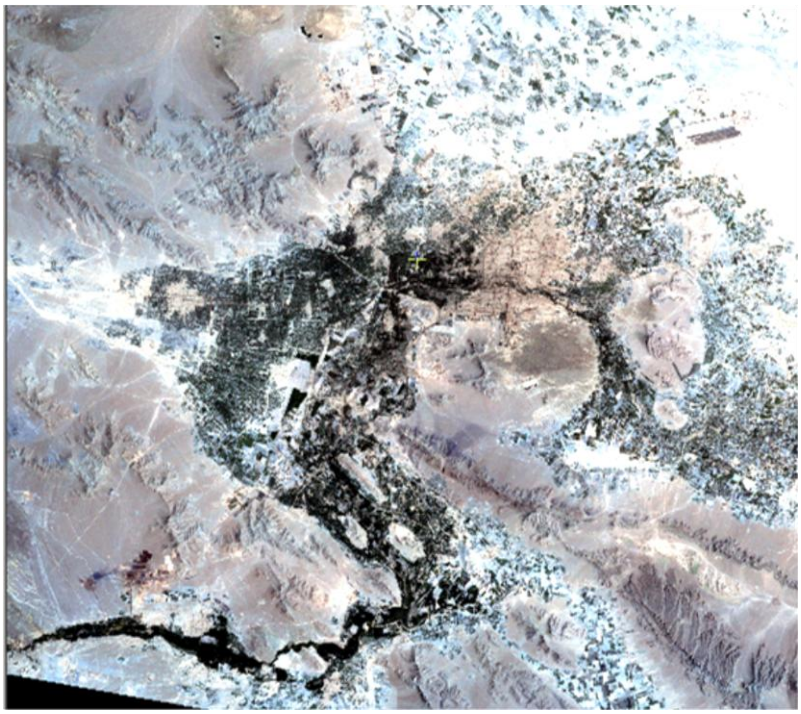

Figure 3. 2. Landsat TM image of Isfahan

In the past centuries, agriculture played an important role in the socioeconomics of the city, while more than half of the city's dwellers were farmers. They cultivated lands in the river basin and used the river's water to irrigate their crops. The river was divided into several branches, so that farmers in satellite towns and villages could use the water for their cultivations. However, in the second half of the 20th century, the traditional socioeconomical life of the people has undergone huge changes. The emergence of huge industrial units in the periphery of the city, mainly adjacent the river and aiming to use the water in the assembly lines,

changed the traditional farming life style of the dwellers. Many farmers lost their fields, and many others decided to migrate to the city in order to work in the factories and industrial units. Natural growth, as well as rural-to-urban migration increased housing demand, led to building new satellite towns and townships, and caused more destruction of the agricultural and natural lands. These problems and consequences are explained in detail in section 2.2.

Demographic statistics during last few decades show large amounts of increase in population as well as immigration from the suburbs and surrounding villages to this city. Table 3.1 shows the population growth in the 3 decades from 1977 to 2007. In 1977 the population was 661,510, while within 30 years, with the population growth rate of 1.45, this number increased to 1,602,110. The population growth trend, within intervals of 10 years, shows approximately the same growth rate in each period.

Table 3. 1. Population growth trend in Isfahan, Iran, within the past 30 years (Iran Statistics Centre, 2008)

Year	1977	1987	1997	2007
Population	661 1510	986 753	1 266 072	1 602 110

Official statistics show a huge increase in the total construction and built up area. During 2007, the Isfahan Municipality gave the authority of construction to both private and public sectors, to an area of 4,469,664 $m^{2.}$ Most of this area was agricultural lands in the bank of the Zayande Rood River, and orchards in the older parts of the city (Iran Statistics Centre, 2008). However, in 2008 the Iran Statistics Centre released that the total agricultural area in Isfahan city is 566367 hectares. In 2008, 8.2% of all agricultural lands of the country were located in Isfahan and 7% of all agricultural products, produced in Isfahan (Government of Iran Portal, 2008). Figure 3.3 shows a perspective of the city in the 16^{th} century, mid-20^{th} century and the present.

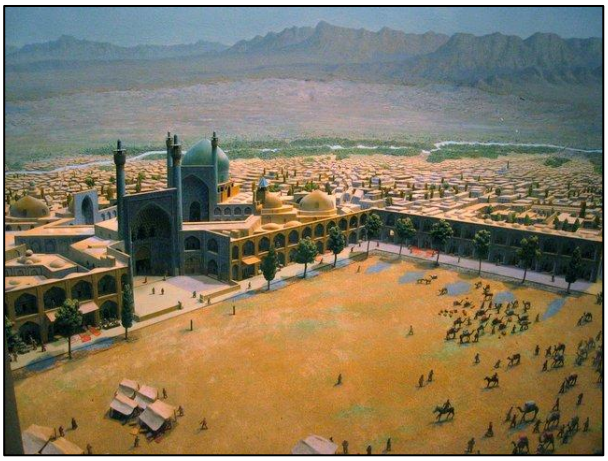

a

b

c

Figure 3. 3. City expansion in Isfahan: a) Isfahan in 16th century; b) Isfahan in mid-20th century; and c) present Isfahan (source: Ali Vaezi, 2008);

3.1. Methods

Figure 3.4 summarizes the methodology steps. The data used in this study, the pre-processing, and processing procedures are shown in this flowchart and are described in detail in the following sections.

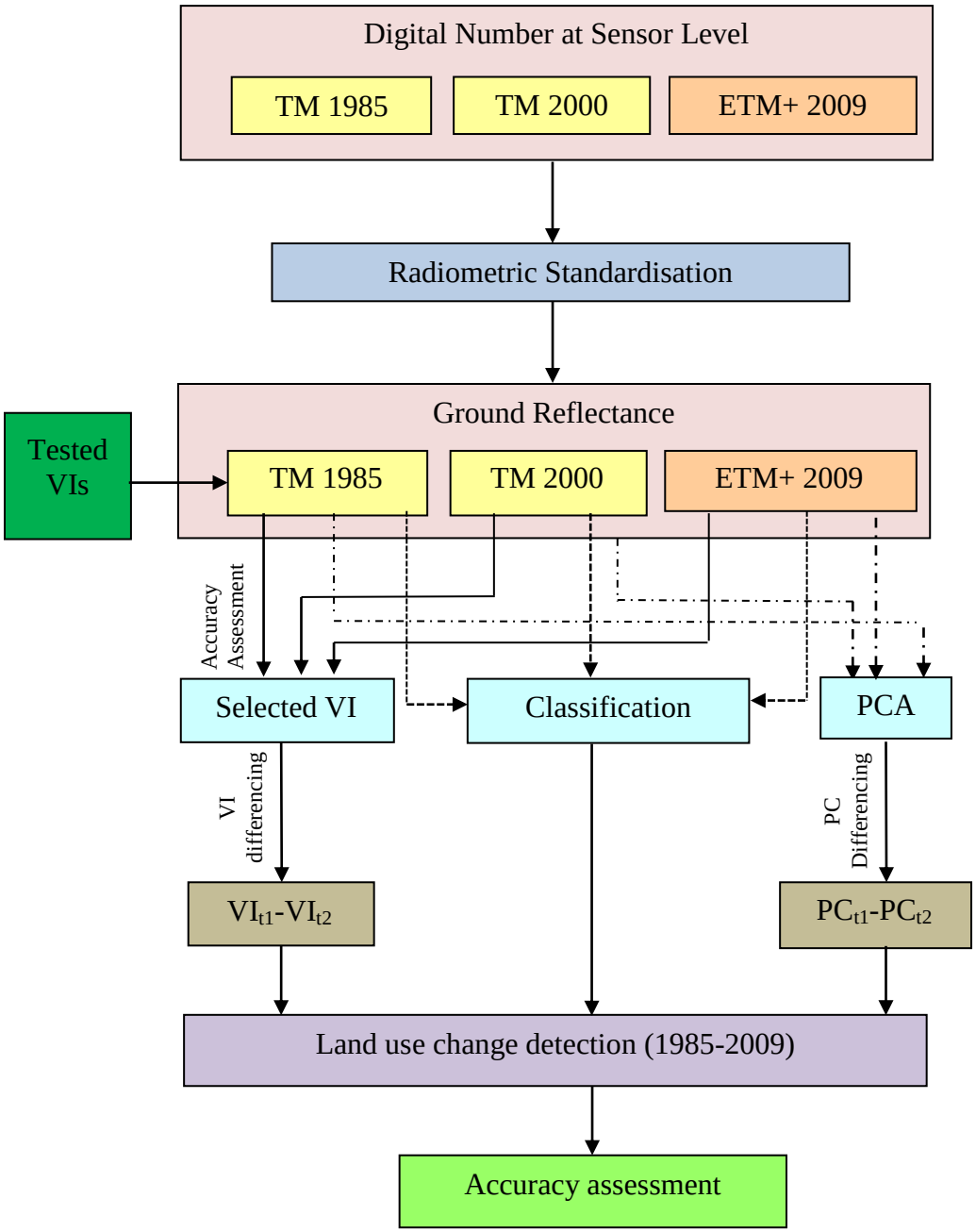

Figure 3. 4. Methodology flowchart

3.3.1. Data Acquisition and Sensor Parameters

In this study three Landsat images of the study site were acquired over a period of 25 years. The first and second images were acquired on August 2, 1985 and July 26, 2000, respectively, with the TM sensor. The third image was acquired on September 5, 2009 with the ETM+. The TM instrument is a second-generation imaging instrument in the Landsat program on Landsat 5, launched by NASA in 1970s. The TM data are sensed in 7 spectral bands with a spectral resolution of 0.45-12.5 µm. Band 6 senses thermal (heat) infrared radiation, and can only be acquired at night (Chander *et al.*, 2009). The TM scene has spatial resolution of 30 meter in bands 1 to 5 and 7, while band 6 has spatial resolution of 120 meters (NASA, 2010). The ETM+ instrument, launched within Landsat 7 in 1999, is an optic-mechanical sensor with eight distinct bands and spatial resolution of 30 meter for multispectral and 15 m for panchromatic bands, as well as a thermal infrared channel with 60 m of spatial resolution (NASA, 2010). Table 3.2 shows the spectral range of each band for Landsat TM and ETM+ (NASA, 2010).

Table 3. 2. Landsat TM and ETM+ bands (NASA, 2010)

	TM		ETM+	
Band Number	Spectral Range (µm)	Resolution (m)	Spectral Range (µm)	Resolution (m)
1	0.45-0.52	30	0.45 to 0.515	30
2	0.52-0.60	30	0.525 o 0.605	30
3	0.63-0.69	30	0.63 to 0.690	30
4	0.76-0.90	30	0.75 to 0.90	30
5	1.55-1.75	30	1.55 to 1.75	30
6*	10.4-12.5	120	10.40 to 12.5	60
7	2.08-2.35	30	2.09 to 2.35	30
Pan*	-	-	0.52 to 0.90	15

* These bands will not be considered in this research

The images used in this study were taken during same growth season, were not highly affected by atmosphere (scattering and absorption), and were clouds free. All three images are geometrically projected using Universal Transformed Mercator (UTM) coordinate system and World Geodetic System 1984 (WGS84) zone 39 (3598500 N, 572000 E).

3.3.2. Pre-processing

Satellite images of an area are affected by numerous atmospheric and radiometric factors. Sensor spectral properties, atmospheric scattering, and change in illumination are examples of parameters that impact the digital number sensed by the instrument. These parameters can cause difficulty in comparing more than one image of the same scene which are taken under different conditions (Schott *et al*., 1988).

A sensor's digital number is not a suitable parameter for measuring the changes in the ground features over time. The sun nadir angle, sensor viewing angle, Earth-sun distance, and atmospheric conditions affect the spectral respond of the ground features and hence modify the sensor's digital numbers (Moran, *et al.*, 2001). These factors can increase or reduce the radiance of the ground features, and differentiate the radiations through the spectrum (Hadjimitsis *et al*., 2009). The purpose of radiometric calibration is to minimize the impacts of these parameters or at least to normalize them. Radiometric calibration applies when the objective of the study is to detect changes in ground features and when more than one image is used in the study in different times.

3.3.2.1. Sensor Radiometric calibration

In the first step of this study, digital number (DN*(λ)), which is measured at the top of the atmosphere with each sensor, is transformed into apparent equivalent radiance (L*(λ)). The appropriate radiometric absolute calibration parameters (gain: G(λ) and offset: O(λ)) are used for this transformation. Gain and offset are calibration constants, delivered by NASA for each sensor. The TM instrument has

only one gain state and the data are quantized in 8 bits, while the ETM+ images are acquired in either a low or a high gain state. "The purpose for using two gain settings is to maximize the sensor's 8 bit radiometric resolution without saturating the detectors" (Chander *et al*., 2009; page 895). The low gain dynamic range, used for high brightness surfaces, is approximately 1.5 times the high gain dynamic range, used for low brightness surfaces. The study site is an arid and semi-arid environment with a high brightness surface; therefore gain and offset constants for the low gain mode are used in equation 3.1 to calibrate the 2009 ETM+ image used in this study.

$$DN^{*}(\lambda) = G(\lambda) \,.\, L^{*}(\lambda) + O(\lambda) \qquad (3.1)$$

In the next step, apparent radiance needs to be transformed into apparent reflectance ($\rho^{*}(\lambda)$). Extra-atmospheric irradiance ($E_s(\lambda)$), solar zenith angle (θ_s) and Earth-sun distance (D, in astronomical units) are used for this transformation using the equation 3.2 (Bannari *et al*., 1999). Without these two operations, the changes caused by artifacts relative to the sensor can be mistakenly attributed to changes in the land use and ground biophysical components. Consequently, errors can propagate in all subsequent steps taken during the image processing such as spectral indices calculations, multi-temporal analysis, classification, etc. (Bannari *et al.*, 1999; Teillet, 1994). Table 3.3 summarizes the gain, the offset and the irradiance values for TM and ETM+ spectral bands (Chander *et al*., 2009). The solar zenith angles (θ_s) for each image are presented in table 3.4.

$$\rho^{*}(\lambda) = \frac{L^{*}(\lambda).\pi \,.\, D^{2}}{Es(\lambda) \,.\, Cos(\theta s)} \qquad (3.2)$$

Table 3. 3. Gain, offset and irradiance values for TM and ETM+ spectral bands (Chander *et al*., 2009).

Bands	Landsat-5 TM			Landsat-7 ETM+		
	Gain(λ)	Offset(λ)	$E(\lambda)_{sun}$	Gain(λ)	Offset(λ)	$E(\lambda)_{sun}$
1	0.671339	-2.19	1985	1.180709	-7.38	1997
2	1.322205	-4.16	1796	1.209843	-7.61	1812
3	1.043976	-2.21	1536	0.942520	-5.94	1533
4	0.876024	-2.39	1031	0.969291	-6.07	1039
5	0.120354	-0.49	220	0.191220	-1.19	230.8
7	0.065551	-0.22	83.44	0.066496	-0.42	84.9

Table 3. 4. $\boldsymbol{\theta_s}$ values for data imageries (Chander *et al*., 2009)

	θ_s	$\cos(\theta s)$
1985	31.5278	0.852
2000	29.2232	0.872
2009	38.7441	0.779

Furthermore, atmospheric effects contribute significantly to the signal received by optical remote sensing satellite systems. When atmospheric parameters measurements are absent, many methods were developed in the literature to remove, or at least to normalize, these impacts from images acquired in different times from a series of satellite sensors using pseudo-invariant targets or ground spectroradiometric measurements (Farrand *et al*., 1994; Schott *et al*., 1988; Freemantle *et al*., 1992). According to Schroeder *et al.* (2006) the most widely used method is the multi-temporal normalization technique; which is based on the normalization of the atmospheric effects in the spectral bands of all the considered images to a standard image which is chosen as a "*reference scene*". This method is correctly applied using pseudo-invariant targets; which are significantly stable over time. In addition, these targets must be large, near Lambertian, have uniform soil color across the target, an absence of vegetation and low variance in reflectance through time (Bannari *et al*., 2005). According to these criteria, asphalt, bright and dark soils are selected as pseudo-invariant targets the cross-

calibration of these images. After the standard image selection as a "*reference scene*", 30 pixels are extracted from each image considering the three pseudo-invariant targets (ten sample pixels from each target: asphalt, bright and dark soils). Then, a linear relationship between apparent reflectance and reference reflectance (considered as a ground reflectance) is established (equation 3.3). This equation is used to normalize atmospheric effects in the considered images to the "*reference scene*".

$$\rho_G(\lambda)_i = a \,.\, \rho^*(\lambda)_i + b \qquad (3.3)$$

Here, $\rho_G(\lambda)_i$ is the standardized (ground) reflectance in each spectral band "i" by reflectance to homologous band "i" in the "*reference scene*", $\rho^*(\lambda)_i$ is the apparent reflectance to be corrected in the band "i", a and b are the slop and the intercept calculated for the atmospheric effects corrections. Figure 3.5 shows the derivation of the prediction equation parameters (a and b) from within image atmospheric calibration targets for the semi-empirical line approach.

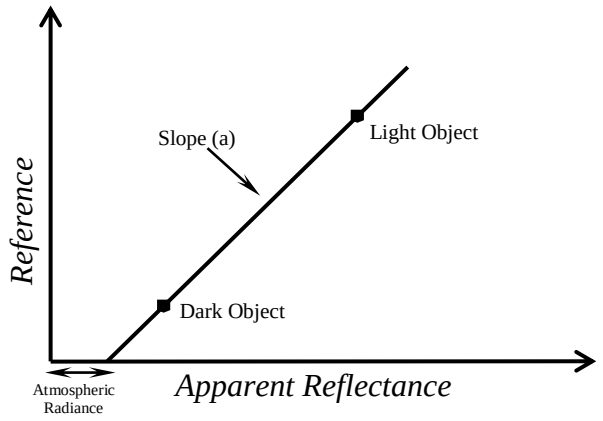

Figure 3. 5 Derivation of the prediction equation from two within image calibration targets for the Empirical line approach (Smith and Milton, 1999)

3.3.3. Processing

In this section, processing methods are presented. As mentioned previously, principal component analysis, vegetation index differencing, and classification are the land use and cover change detection methods that are followed in this study. These techniques are explained here in detail.

3.3.3.1. Principal component analysis (PCA)

As mentioned in section 2.3.1, the main idea of PCA is to reduce the dimensionality of a set of spectral data (bands), which contains numerous interconnected variables. The PCA algorithm transforms those variables into a new set of decorrelated ones. The order of new variables is such that usually only the first few are responsible for most of the variances in the original variables. (Jolliffe, 2002). PCA-based change detection can be done in different ways. In this study, the PCA algorithm is applied to three images, and a PC transformation is done by transforming each image into a new PCA image. Although six components are derived from the original bands, PC1, PC2, and PC3 are proven to be responsible for more than 98% of the total variation for each image. They provide the most information about different land uses. Therefore, new PCA images are made using the first three components. PCA differencing then are done using the image rationing technique, by subtracting the PC1, PC2, and PC3 in the 1985 image, from the PC1, PC2, and PC3 in the 2000 and the 2009 images, respectively. Equation 3.4 shows this function. The EASI Modeling and programing application in PCI Geomatica (PCI, 2011) is used for this purpose.

$$\Delta PC_{i_{t1-t2}} = PC_{i_{t1}} - PC_{i_{t2}} \qquad (3.4)$$

The new vectors are made using $\Delta PC_{1_{t1-t2}}$, $\Delta PC_{2_{t1-t2}}$, and $\Delta PC_{3_{t1-t2}}$ for 1985-2000, 1985-2009, and 2000-2009 to make a new color composite. These new data sets contain the overall amount of change in the ground surface for the assigned periods of time.

3.3.3.2. Vegetation index differencing

Vegetation index differencing is another important method that is followed in this study. Different vegetation indices are developed based on the linear and ratio relationships between red and near infra-red bands or a combination of both methods to regulate vegetation response to spectral bands. More than 50 vegetation indices have been developed and used in different remote sensing applications including land use and land cover change detection of different environments. In the literature, different vegetation indices have been applied and accuracy assessments have indicated the most sensitive and accurate indices for mapping vegetation in different environments.

The response of vegetation differs between forest and natural vegetation cover terrain and agricultural lands and urban landscapes. An urban environment is very complex and heterogeneous. The heterogeneity of urban environments is caused by the presence of different urban features and components, houses, parks and green lands, roads, different roof materials, metallic installations, buildings in variable sizes, and construction areas with variable densities and alignments (Goodchild *et al.,* 1992). Heterogeneity and diversity of the construction materials affects the reflection and make it difficult to analyze and interpret satellite images. These characteristics increase the probability of confusion of the features within a pixel and between pixels and make it difficult to use remote sensing techniques for urban application.

For this study ten vegetation indices are selected, which had been used previously in different urban application, and showed high accuracy and sensitivity for mapping vegetation in urban environment. Table 3.5 shows the list of the selected

vegetation indices. It is the first time that these indices will be examined and compared for land use change detection applications of an urban area over time.

The vegetation indices method is applied in two steps. First, the considered vegetation indices listed in table 3.5 are calculated for the 1985 image. The accuracy and saturation level are examined for each index, and the most accurate and sensitive index for detecting vegetation changes during the time in the urban environment is identified. In the second step, the selected index from the first step is applied to the 2000 and 2009 images, and differencing is implemented using the EASI Modeling and programming application to subtract VI_{1985} from VI_{2000} and VI_{2009}, using equation 3.5. The subtracted maps show the difference in land use and land cover in the defined time intervals.

$$\Delta VI = VI_{t1} - VI_{t2} \qquad (3.5)$$

Table 3. 5. Vegetation indices used for land cover change detection in an urban environment

Vegetation index	*Equation*	*Developed by:*	*Used in urban environment by:*
NDVI	$NDVI = \frac{NIR - RED}{NIR + RED}$	Rouse *et al.* (1974)	Rastmanesh *et al*. (2010), Lunneta (2006), Hayes *et al*. (2003), Lyon *et al*. (1998)
PVI	$PVI = \frac{NIR - aRED - b}{\sqrt{a^2 + 1}}$ (a = 0.96916 and b = 0.084726)	Richardson and Weigand (1977)	Yu *et al*. (2006), Daryaei (2003), Fung (2000), Lyon *et al.* (1998)
DVI	DVI=NIR - RED	Clevers (1986)	Lyon *et al*. (1998)
RVI	RVI= RED / NIR	Pearson and Millar (1972)	Makkeasorn (2009), Wang (2009), Xiuwan (2002), Lyon *et al*. (1998)
SAVI	$SAVI = \frac{(NIR - RED)(1 + L)}{(NIR + RED + L)}$ (L=0.5)	Huete (1988)	Nackaerts *et al*. (2005), Lu *et al*. (2004), Lupo (2001), Lyon *et al*. (1998)
AVI	AVI = (0.2* Band7 – Band5)	Ashburn (1978)	Lyon *et al*. (1998)
SARVI	$SARVI = \frac{NIR}{RED + b/a}$ (a = 0.96916 and b = 0.084726)	Major *et al*. (1990)	Lyon *et al*. (1998)
NDGI	$NDGI = \frac{GREEN - RED}{GREEN + RED}$	Chamard *et al.* (1991)	Hoshino (2005)
TDVI	$TDVI = 1.5 * (\frac{NIR - RED}{\sqrt{NIR^2 + RED + 0.5}})$	Bannari *et al.* (2002)	Ozbakir *et al*. (2001)
MSAVI	$MSAVI = \frac{2 \times NIR - \sqrt{(2 \times NIR + 1)^2 - 8 \times (NIR - RED)}}{2}$	Qi *et al*. (1994)	Rogan and Yool (2001)

3.3.3.3. Classification

The supervised classification method and training site selection are discussed in this section. In the supervised image classification method, training site samples are selected by the operator manually to gain control over the classification procedure. Training site selection aims to collect a set of statistics that best represent the spectral signature of each land use class to be classified within the image. The skill of the image operator and his previous knowledge on the area of interest is important in the quality and accuracy of training sites and the success of the classification process. If the training sites are selected precisely, all ground features will be assigned to a meaningful class. In this study training samples are selected for all classes over entire images, ensuring that they are good representatives of each information class. Furthermore, the on-screen polygonal selection tool is preferred as an effective way of training site selection. The polygon selection tool draws a polygon around the close by multiple pixels of the same class to avoid pointing to them one by one. However, in some land uses such as urban areas, the pixels present a relatively heterogeneous reflection due to variation in building materials (concrete, asphalt, building stones, and different roof coatings). For these cases, point selection is used to minimize confusion between classes. Table 3.6 shows the classes selected for both the TM and ETM+ images.

Table 3. 6. Selected classes for 1985 and 2000 TM and 2009 ETM+ images

Images / Classes	1985 and 2000 TM Images	2009 ETM+ Images
Building	*	*
Roads	*	*
Water	*	*
Vegetation Type 1	*	*
Vegetation Type 2	*	*
Vegetation Type 3	*	*
Vegetation Type 4		*
Soil Type 1	*	*
Soil Type 2	*	*
Soil Type 3	*	*
Soil Type 4		*
Bright Soil	*	*

For the 1985 and 2000 images, training sites are collected from all parts of the scene for 10 land cover classes to be extracted from the multispectral Landsat TM bands. These classes are building, road, water, four vegetation and crop types, which present different growth stages and density of vegetation cover, as well as three soil types, which present different tones and colors of bare soil from very bright to very dark. However, for the 2009 image, due to higher sensitivity of the ETM+ spectral bands, 12 classes are extracted, which are building, road, water, five vegetation and crop types, and four soil types. The selection of the training sets basically depends on visual interpretation. Visual components, including tone, color, texture, pattern, and shape of land cover classes within particular band combinations, as well as classification results obtained from K-mean unsupervised classification method, help to identify the land cover classes.

Sample size and class separability are parameters that are taken into consideration when selecting training samples. Training sites should be sufficiently large to generate accurate statistical parameters used by classifiers, and at the same time, the samples size should be restricted to ensure class separability. The level of confidence for training site selection is 97%. Table 3.7 shows the number of pixels selected as training set for each class.

Table 3. 7. Sample size or the number of pixels selected as training set for each class in each image

Images / Classes	1985 TM Images	2000 TM Images	2009 ETM+ Images
Building	274	366	267
Roads	233	142	330
Water	217	222	263
Vegetation Type 1	141	305	271
Vegetation Type 2	194	161	185
Vegetation Type 3	95	211	208
Vegetation Type 4	-	-	270
Soil Type 1	469	378	277
Soil Type 2	180	172	194
Soil Type 3	339	359	190
Soil Type 4	-	-	137
Bright Soil	225	383	185

Signature separability is calculated as the statistical difference between pairs of spectral signatures, and presents the quality and accuracy of the training sites. Signature separability has a value between zero and two. Zero indicates complete overlap, while 2 indicates a complete separation between the signatures of two classes. Theoretically, signature separability values between 1.9 and 2 presents acceptable accuracy of training sites, while values lower than 1.9 are not acceptable and will increase the confusion between the classes with a close range of reflectance values. Signature separability is carefully monitored during the process of training site selection. However, training site selection for a natural phenomenon is often problematic, and training samples representing an individual subject often cover a part of spectral signature of another feature. The signature separabilities of the training sites selected in this study are presented in chapter 4.

After collecting satisfactory training sites, a maximum likelihood classifier is applied to images. A confusion matrix is a measure for accuracy assessment of the classification. A confusion matrix consists of an equal number of rows and columns, which rows normally represent the classification results from remotely sensed data, while columns represent the reference data. Accuracy values are presented as percentages in the confusion matrices. These values help to obtain the best possible classification results, and to minimize the operator error and training sites confusion. The overall accuracy and kappa coefficient are also derived from applying the maximum likelihood algorithm for each image. These statistical parameters helped to assess a classification procedure's accuracy. However, it is difficult to get the same overall accuracy for all three images due to difference in operator error, vegetation density and the Bidirectional Reflectance Distribution Function (BRDF) problem. In the classification method, the classified maps can be compared directly to detect the changes in the land cover classes during the assigned periods of time. Change in the total area of each selected class displays natural or manmade activities which indicate the expansion or diminishment of that class over time.

3.4. Conclusion

This chapter presents the study site, remote sensing data, radiometric calibration techniques and processing methods used in this study. The Landsat 5 TM images are acquired in 1985 and 2000, and the Landsat 7 ETM+ image is acquired in 2009 over the study site, city of Isfahan, Iran. In the pre-processing step, the specific radiometric calibration parameters for each sensor are applied to each image and the semi-empirical line model and pseudo invariant targets are used for the atmospheric normalization. Three independent techniques are applied as the processing methods. In the first technique, ten vegetation indices are selected and calculated for the 1985 image. Then, the most accurate index is selected and calculated for the 2000 and 2009 images. The 2000 and 2009 vegetation index maps are subtracted from the 1985 vegetation index map to retrieve the overall amount of change in the land use during the 1985-2000 and 2000-2009 periods of time. Principal component analysis is the other remote sensing technique that is applied. PC1, PC2, and PC3, are used to make new color composites for the 1985, 2000 and 2009 images. PC differencing presents the changes in land use and land cover for the period of study. The maximum likelihood supervised classification method is the other method which is applied in this study. The classification maps are the representative of different land use classes. Change in the total area of each class during the assigned periods of time shows the expansion or diminution of that certain land use class over time. Chapter 4 will examine the application of the proposed methodology. Results will be presented and discussed.

Chapter 4: Results

4.1. Introduction

This chapter will examine and discuss the results of applying the methodology on the Landsat TM and ETM+ images. In the first section the results of radiometric calibration of the 1985, 2000 and 2009 images will be presented and discussed. The second step is to show the results of the calculation of principal component analysis. In the third step the vegetation indices presented in table 3.5 will be applied to the 1985 image, and the most sensitive index will be selected. This index then will be applied to the 2000 and 2009 images. Finally the maximum likelihood supervised classification maps will be presented and the accuracy of each map will be analyzed in details.

4.2. Pre-processing results

The first step in pre-processing is the conversion of apparent radiance into apparent reflectance. After this conversion, the histogram of each spectral band in each image is analyzed to retrieve the mean and the standard deviation which are used to compute the coefficient of Variation (VC) for the "*reference scene*" selection. The "*reference scene*" must be characterized as having the lowest contribution of the atmosphere, as well as cloud free and high contrast. Therefore, for the image to be chosen as "*reference scene*", the mean must be high; while the standard deviation should be low and automatically the VC values must be low. Figure 4.1 shows the VC in each spectral band in the three considered images. The 1985 image shows the lowest VC values in the visible bands, similar VC values in bands 4 and 7, and relatively high VC values in band 5 especially between 1985 and 2009. Certainly, this variation values in band 5 is not related to the scattering phenomena which is absent in this waveband region. However, it could be associated with the absorption effects. Consequently, the 1985 image will be considered and used as a "*reference scene*" in this study.

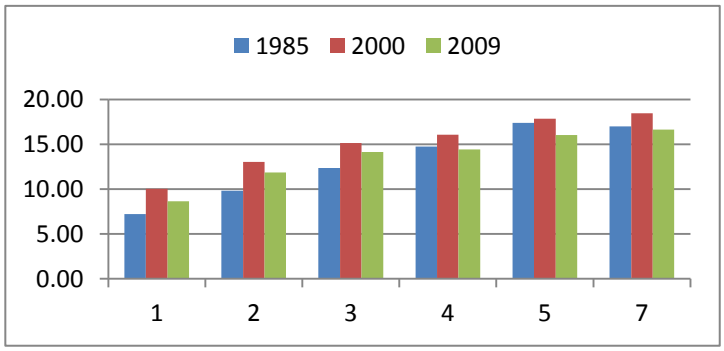

Figure 4. 1. Coefficient of variation calculated from the apparent reflectance in each spectral band for the 1985, 2000 and 2009 images

Furthermore, in the second step, the multi-temporal normalization technique is implemented using three pseudo-invariant targets (ten sample pixels from each target: asphalt, bright and dark soils) to establish a linear regression relating the spectral bands in the "*reference scene*" to their homologous bands in the other images acquired in 2000 and 2009. Table 4.1 summarizes the expected corrections equations between the references band "i" and the homologous band "i" under standardization. The intercepts and the slopes values represent, respectively, the corrections of the additive effects caused by the atmospheric path radiance and the atmospheric attenuation. Then, the equation 3.3 is used to standardize all the spectral bands in the images TM-2000 and ETM+-2009. The corresponding histogram of the linear regression relating the spectral bands in the "*reference scene*" to their homologous bands in the 2000 and 2009 images are presented in appendix A.

Table 4. 1. Standardization equations between the reference image and other images for each spectral band

Bands	Landsat-5 TM		Landsat-7 ETM+	
	Linear equation	R^2	Linear equation	R^2
1	Y = 0.986 x + 6.94	0.93	Y = 0.641 x + 5.39	0.92
2	Y = 1.015 x + 10.82	0.95	Y = 1.300 x + 10.04	0.94
3	Y = 0.839 x + 10.58	0.97	Y = 1.077 x + 11.79	0.96
4	Y = 0.855 x + 11.98	0.97	Y = 0.890 x + 11.31	0.97
5	Y = 0.888 x + 11.89	0.96	Y = 0.557 x + 22.32	0.87
7	Y = 0.868 x + 10.96	0.98	Y = 0.958 x + 12.50	0.96

The analysis of the raw data (DN) of the three images shows the necessity of sensor radiometric calibration and atmospheric corrections for multi-temporal studies using satellite remote sensing data. In fact, figure 4.2 shows the DN variability in all spectral bands for each scene and considering different targets (bright soils, asphalt and dark soils). Significant variations occur particularly for bright soils samples, especially between TM and ETM+ sensors. The recorded DN by TM in 1985 and 2000 show much lower variance comparatively to received DN by ETM+ in 2009, which is due to differences in the sensor's optical characteristics and radiometric sensitivity. Nevertheless, recorded images over a 15 year difference period with the same TM sensor (1985 and 2000) show insignificant differences (less 5%) for all spectral bands. The asphalt target, which is slightly darker but probably contaminated with other material or discolored, shows significant DN variation particularly between the images acquired in 1985 and 2009, respectively, with TM and ETM+. Fortunately, usually it is possible to remove the influence of the sensor artifacts transforming DN to apparent reflectance at the sensor level using the sensors' absolute calibration parameters. Ignoring atmospheric path radiance and attenuation to convert apparent to ground reflectance would result in large error for biophysical and geophysical information extraction. In order to examine the relative accuracy and the effectiveness of the approach used for removing the atmospheric impacts, pseudo-invariant validation pixels were identified considering bright and dark soils and asphalt. Nevertheless, the entire selected pixels for this verification are completely independent from the pixels used in the standardization equations' derivation. The results of this cross-calibration show an excellent agreement between the reflectances in each spectral band for all three images and for each target. Indeed, independently of the considered target (bright and dark soils or asphalt) and the sensors' characteristics, figure 4.2 shows the perfect conformity among the reflectance's in the six spectral bands ($\Delta\rho_G(\lambda) \leq 2\%$). These results demonstrate the potential and the utility of the semi-empirical line approach in a semi-arid environment for atmospheric corrections in multi-temporal studies using optical remote sensing satellite systems.

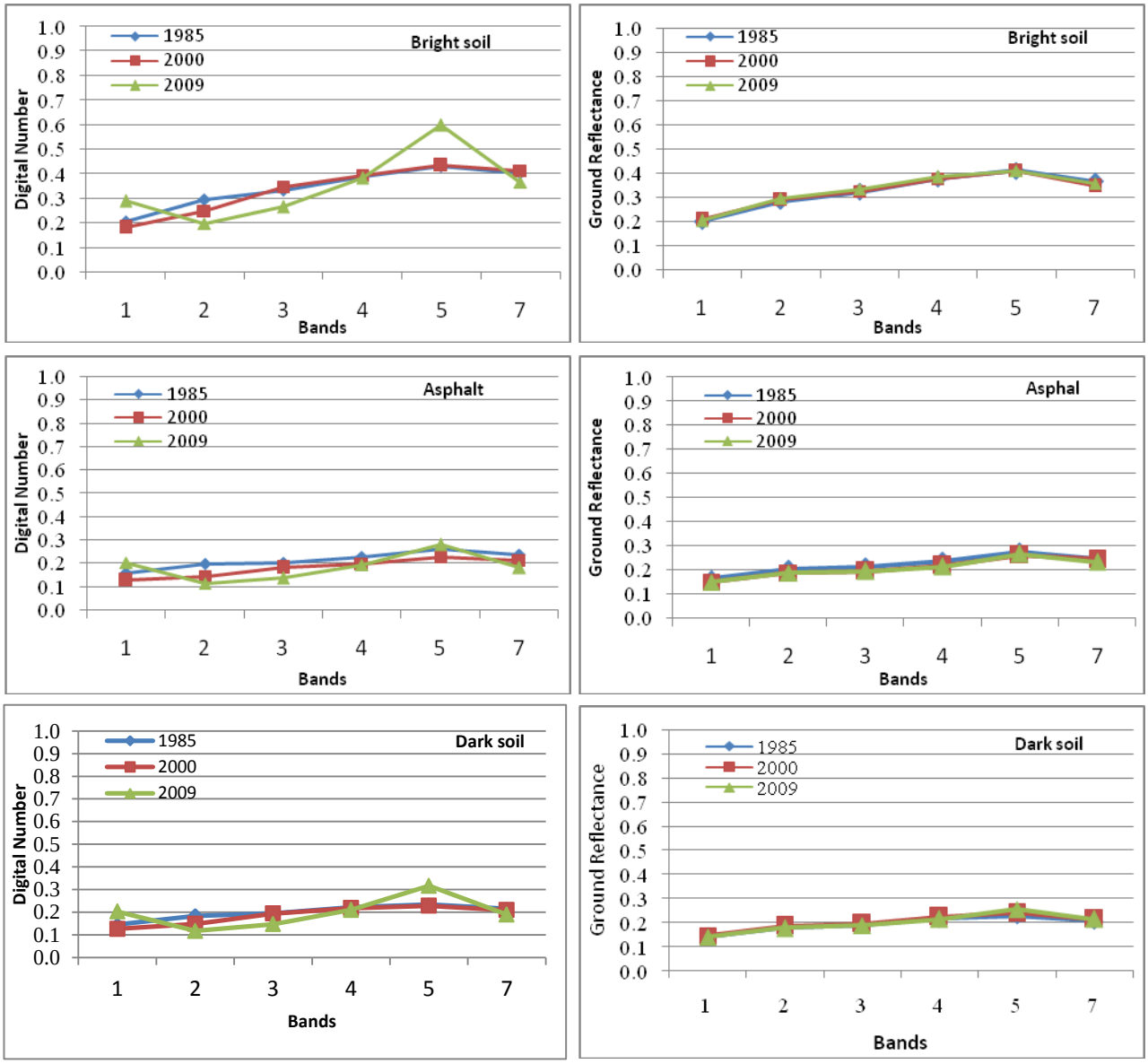

Figure 4. 2. Comparison between raw data and the corrected reflectance in the spectral bands for each scene and considering different targets: bright soils, asphalt and dark soils

4.3. Processing

After radiometric calibration and normalization, processing techniques are applied to the images. As mentioned in the chapter 3, principal component analysis, vegetation indices, and classification techniques are the processing methods applied to the images. Results of these techniques are presented in this section.

4.3.1. Principal component analysis

The PCA algorithm is applied to the images from 1985, 2000 and 2009. Decorrelating correlated data of each band, enable PCs to highlight different features and land uses on the images. PC1 is the index of the spectral signature of each feature on the ground. The PC1 containing the least amount of noise and the most ground information and details, can be used to extract the change information during the period of study. Table 4.2 shows the percentage of variation for each eigenchannel in each image. The first PC shows 83.93%, 81.87% and 84.78% of the total variance for 1985, 2000 and 2009 images, respectively. It suggests that the first PC contains the most ground information and is the most accurate one for mapping land use classes. Grayscale PC1 for the 1985, 2000 and 2009 images are shown in figure 4.3. PC2 is the brightness index and suitable for distinguishing the vegetation cover from bare soil and urban area. This PC has the second largest variance of 12.45%, 10.45% and 10.58% for 1985, 2000 and 2009 images, respectively. Figure 4.4 shows the grayscale PC2 vectors for all three images. The variances of the third component for all three images are even lower and the vectors contain some noise. Table 4.2 shows variances of 2.73%, 5.32% and 3.29% for the PC3 of the 1985, 2000 and 2009 images, respectively. The grayscale PC3 vectors for all three images are shown in figure 4.5. Furthermore, the sum of variances for the PC1, PC2 and PC3 shows that the first three components are responsible for 99.11%, 97.64% and 98.65% of the total variance for the 1985, 2000, and 2009 images, respectively, and contain the most information. The PC4, PC5, and PC6 were not considered in the PCA

analysis in this study due to low variance and high amounts of noise. However, these components are shown in Appendix B in grayscale. In fact, the first three components are used to make new color composites for 1985, 2000 and 2009 (figure 4.6, 4.7 and 4.8, respectively). The new PCA color composite defined a better overview of the area, than the true color composite, and can be used to best distinguish different land uses in the study area, and to compare the change in land uses in different years.

Table 4. 2. Deviation and variance (%) for each eigenchannel for each image

Eigenchannel	1985		2000		2009	
	Deviation	%Variance	Deviation	%Variance	Deviation	%Variance
1	34.8964	83.93%	33.1067	81.87%	32.2724	84.78%
2	13.4394	12.45%	11.8272	10.45%	11.4025	10.58%
3	6.2893	2.73%	8.436	5.32%	6.3552	3.29%
4	2.8549	0.56%	3.9291	1.15%	3.0562	0.76%
5	2.0657	0.29%	3.4523	0.89%	2.3003	0.43%
6	0.7295	0.04%	2.0589	0.32%	1.412	0.16%

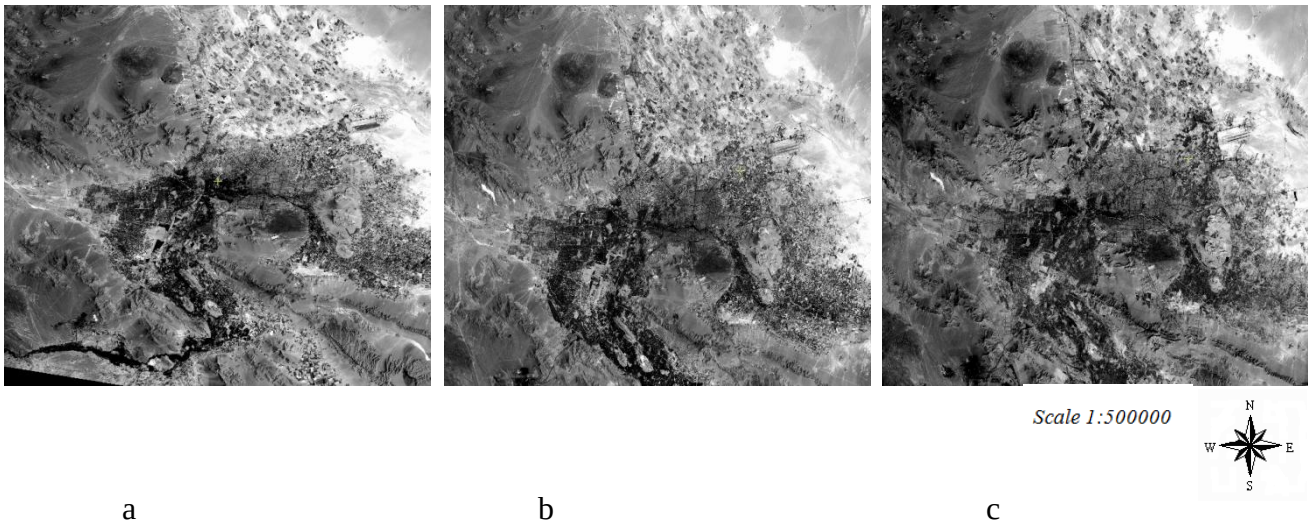

a b c

Figure 4. 3. The PC1 vector of a)1985, b)2000 and c)2009 images of Isfahan

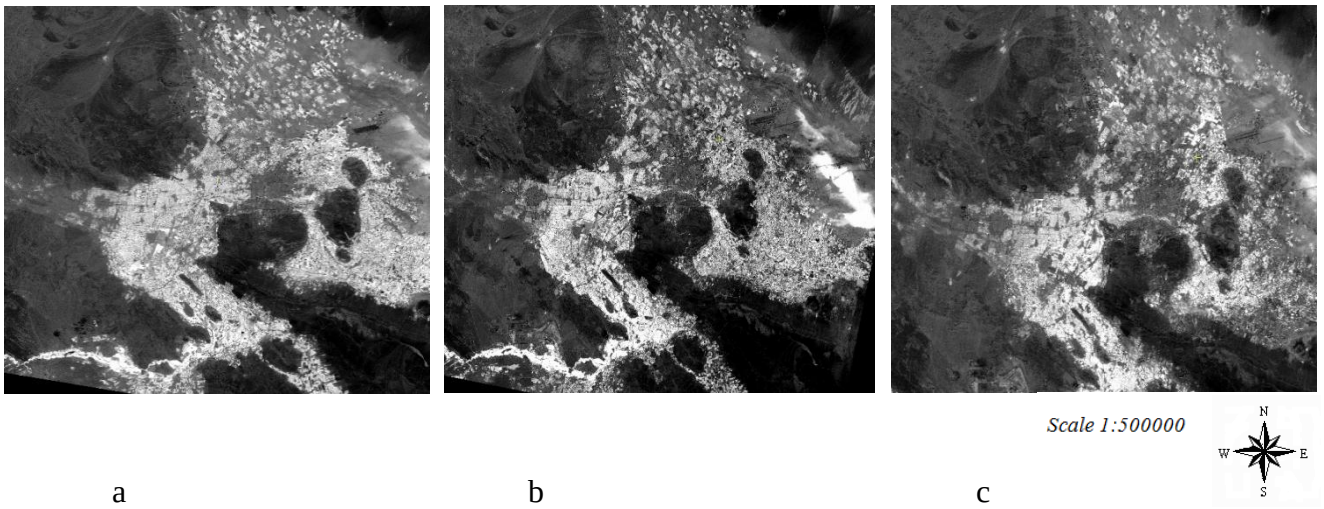

a b c

Figure 4. 4. The PC2 vector of a)1985, b)2000 and c)2009 images of Isfahan

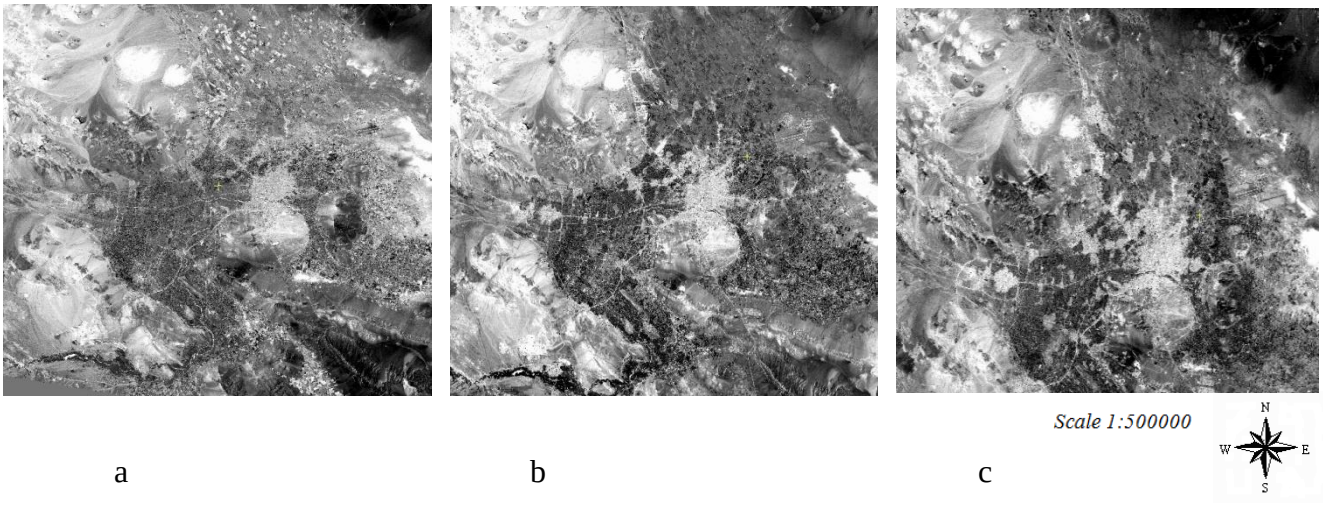

a b c

Figure 4. 5. The PC3 vector of a)1985, b)2000 and c)2009 images of Isfahan

In figure 4.6 the areas shown in green present natural vegetation or cultivated lands. Comparing this figure with figure 4.7 and 4.8 clearly shows the diminishment of the total green area during the 25-year period of study. Creation of new city hubs and expansion in the existing hubs can also be seen over this time. Expansion of the existing urban hubs is showed in the figure 4.9.

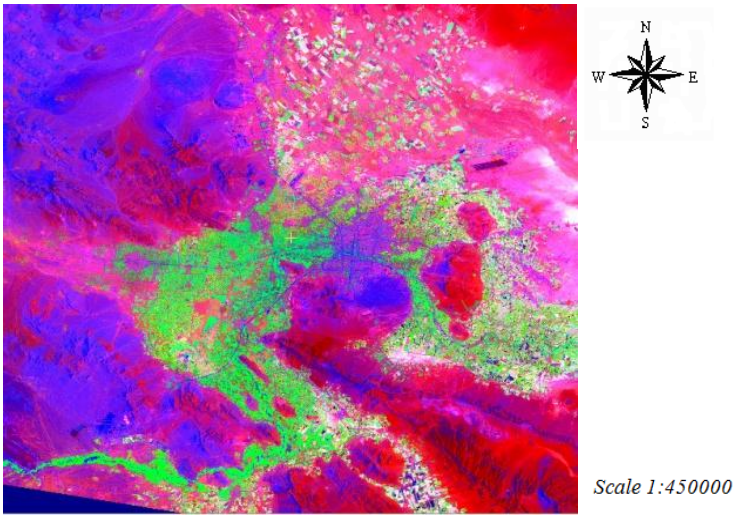

Figure 4. 6. PC1, PC2 and PC3 color composite for 1985 image of Isfahan

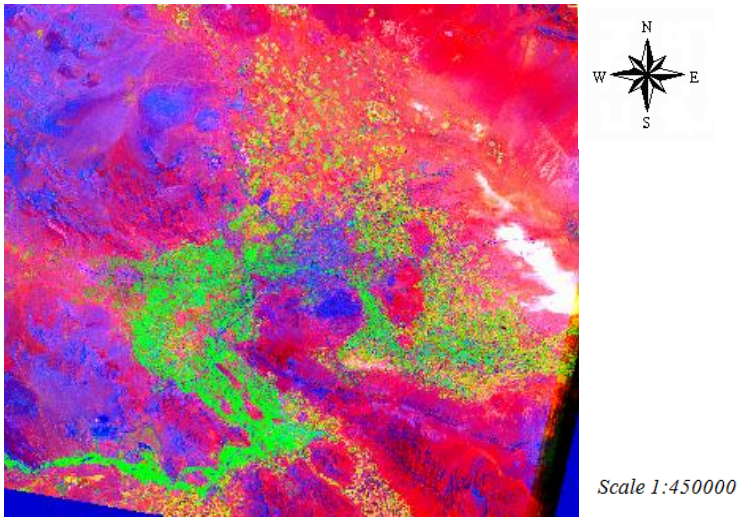

Figure 4. 7. PC1, PC2 and PC3 color composite for 2000 image of Isfahan

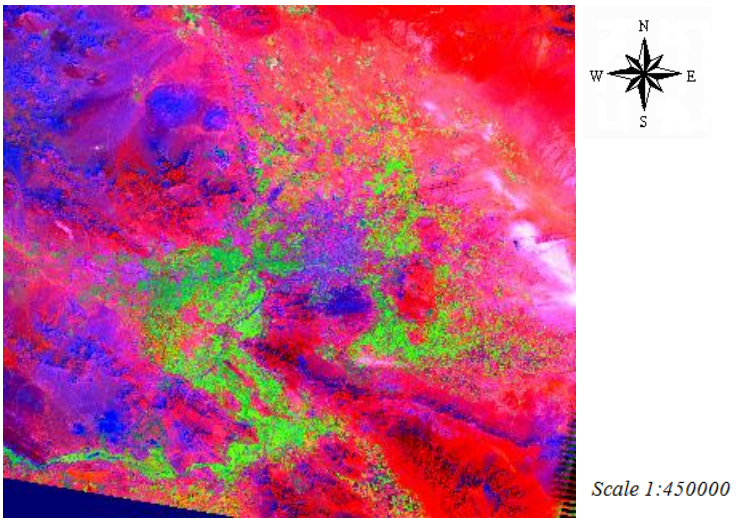

Figure 4. 8. PC1, PC2 and PC3 color composite for 2009 image of Isfahan

More focus on the city core can help provided more accurate visual interpretation. Figures 4.9 gives more focus on the $PCA_{1\text{-}2\text{-}3}$ color composite map of the 1985 images. Black circles on figure 4.9 show small towns that have been expanded during the period of study. Circle number 1 shows the town of Najaf-Abad, which is further away from the main city hub, but shows huge expansion in the 2000 and 2009 maps. More details can be seen in figure 4.10. These maps show that the expansion of built up area in Najaf-Abad in the 1985-2000 period is much more than the 2000-2009 period. Circle 2 is the town of Khomeyni-Shar. In the 1985 map, this town was thoroughly separated from the main city core. However, in 2000 and especially 2009, the expansion of the urban class west of the main urban core, caused this town to be attached to the city. More details about this city can be seen in figure 4.11. Circle 3 is the town of Khorasgan at the east of Isfahan, which was annexed to the main city core during the 1985-2009 period due to the expansion of both the Khorasgan town and the main city core. Figure 4.11 shows more details about the urban expansion in this town. In addition, the main city core shows huge expansion in north, north-east and south-west. These areas are showed in figure 4.13 in more detail.

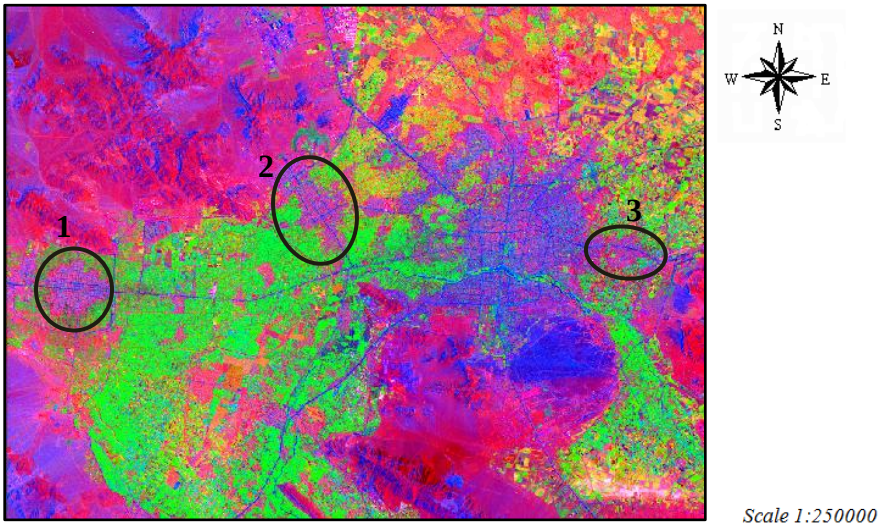

Figure 4. 9. A close up view of the city of Isfahan and adjacent towns on PCA color composite of the 1985 image

a b c

Figure 4. 10. Urban expansion in Najaf-Abad, a)1985, b)2000, and c)2009

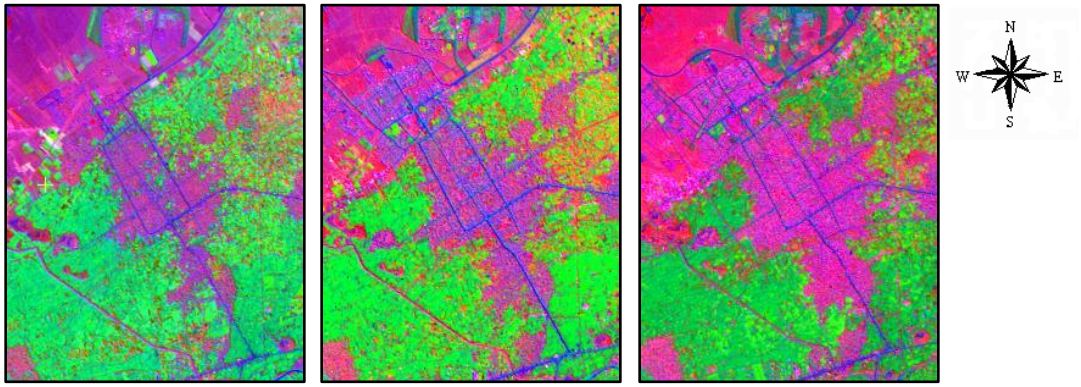

a b c

Figure 4. 11. Urban expansion in Khomeyni-Shahr, a)1985, b)2000, and c)2009

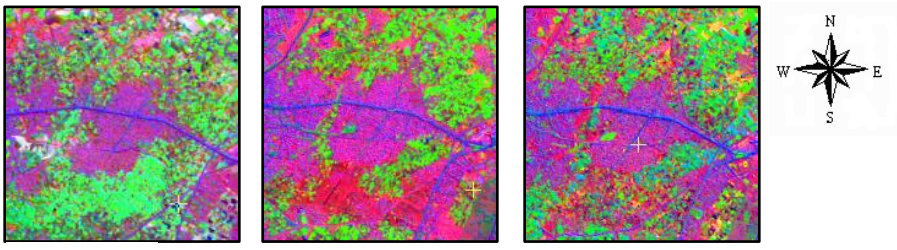

a b c

Figure 4. 12. Urban expansion in Khorasgan, a)1985, b)2000, and c)2009

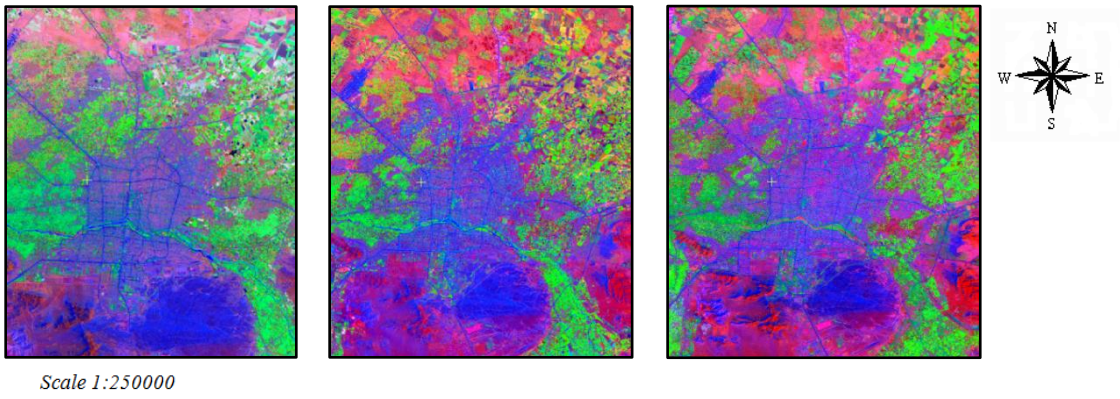

a b c

Figure 4. 13. PC1, PC2 and PC3 color composite of a)1985, b)2000 and c)2009 images, with more focus on the main city core

To get a better overview of changes over time, $\Delta PC_{i\ 1985\text{-}2000}$ and $\Delta PC_{i\ 2000\text{-}2009}$ for PC1, PC2, and PC3 vectors are calculated using PCI Geomatica EASI Modeling tool. Visual interpretation of the subtracted vectors indicates that the ΔPC1 shows the widest dynamic range of the color scheme and is the most informative component containing most of the change information. Consequently, for further analysis only $\Delta PC1_{t1\text{-}t2}$ is used for visual interpretation and pixel analysis. $\Delta PC1_{\ 1985\text{-}2000}$ and $\Delta PC1_{\ 2000\text{-}2009}$ are shown in figure 4.14. $\Delta PC2_{t1\text{-}t2}$ and $\Delta PC3_{t1\text{-}t2}$ are also presented in Appendix C.

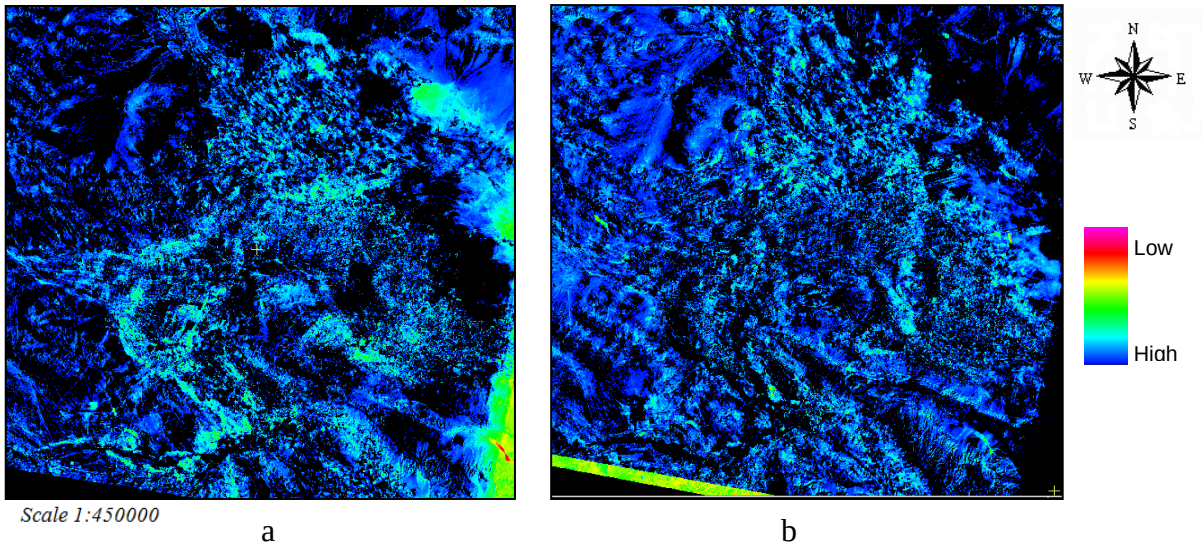

a b

Figure 4. 14. PC1 differencing a) $\Delta PC1_{\ 1985\text{-}2000}$ and b) $\Delta PC1_{\ 2000\text{-}2009}$ of Isfahan

The visual interpretation and pixel analysis of $\Delta PC1_{t1-t2}$ helps to identifying the trends of change in the study period. In the $\Delta PC1_{t1-t2}$ vectors the changed areas are distinguished in brighter colors and show higher values in the dynamic range. Furthermore, black and dark blue pixels are areas with no or least amount of change and show values of 0 or close to 0 in the dynamic range. A pixel analysis is done on the $\Delta PC1_{1985-2000}$ and $\Delta PC1_{2000-2009}$ vectors to quantify the total amount of change in the study site over these periods of time. The pixel analysis of $\Delta PC1_{1985-2000}$ shows that 141,226 pixels out of total of 282240 pixels, i.e. 50.03% of total pixels, present the value of 0, hence the black color. In other words, 50.03% of the total area remained unchanged from 1985 to 2000. For the $\Delta PC1_{2000-2009}$ vector however, 151,023 out of total number of 282,240, or 53.5% of the total pixels show the value of 0 and black color. These results show approximately the equal percentage of unchanged pixels during 1985-2000 and 2000-2009. The unchanged areas are mostly the bare soil and areas with very poor vegetation cover.

The dynamic range of the pixel values in the $\Delta PC1_{1985-2000}$ vector is 0 to 64 (out of 255), or 25.09 % of the color scheme. In other words, the pixels that demonstrate the most changes show the maximum value of 64. For the $\Delta PC1_{2000-2009}$ vector the dynamic range is 0 to 60 (out of 255), or 22.74 % of the color scheme. Maximum value of changed pixels in the 1985-2000 period is larger compared to the 2000-2009 interval.

The visual interpretation and pixel analysis of the maps led to identifying two city growth trends: from 1985 to 2000, new built up areas were constructed, and new towns and townships emerged for the first time, while from 2000 to 2009 the already existing towns and urban hubs continued to expand. These hubs can be observed in the north-east, west, and north-west of the main city. New roads and transit ways also were built and widened within both the 1985 to 2000 and 2000 to 2009 periods. Agricultural lands and vegetated areas are the other ground features that also had undergone changes in the period of study. North and south-east of the city present the areas with most changes in vegetation cover. Change in

vegetation cover can be seen more in the 1985-2000 period. This could be either due to change in the land use and land cover, or due to differences in the total annual precipitation in different years. According to Isfahan Meteorology Centre (2011), the annual precipitation in the 2000 is 88.1 millimetres, whereas in the 1985 and 2009 the annual precipitation is 167.5 and 215.7 millimetres, respectively. The low precipitation might affect the results and create some bias.

Figure 4.15 shows the $\Delta PC1_{1985\text{-}2009}$ and the total amount of change in the period of 25 years. More focus on the city area shows the change in land use classes adjacent to the main city core. 52.21% of the total pixels show a value of 0 and hence black color. The highest value in the dynamic range of this vector is 59, which is presented in light blue and greenish colors and presents the areas with most changes during the time. These areas are located mostly in the agricultural lands in the north of the city, and in some other sparse vegetation sub-classes.

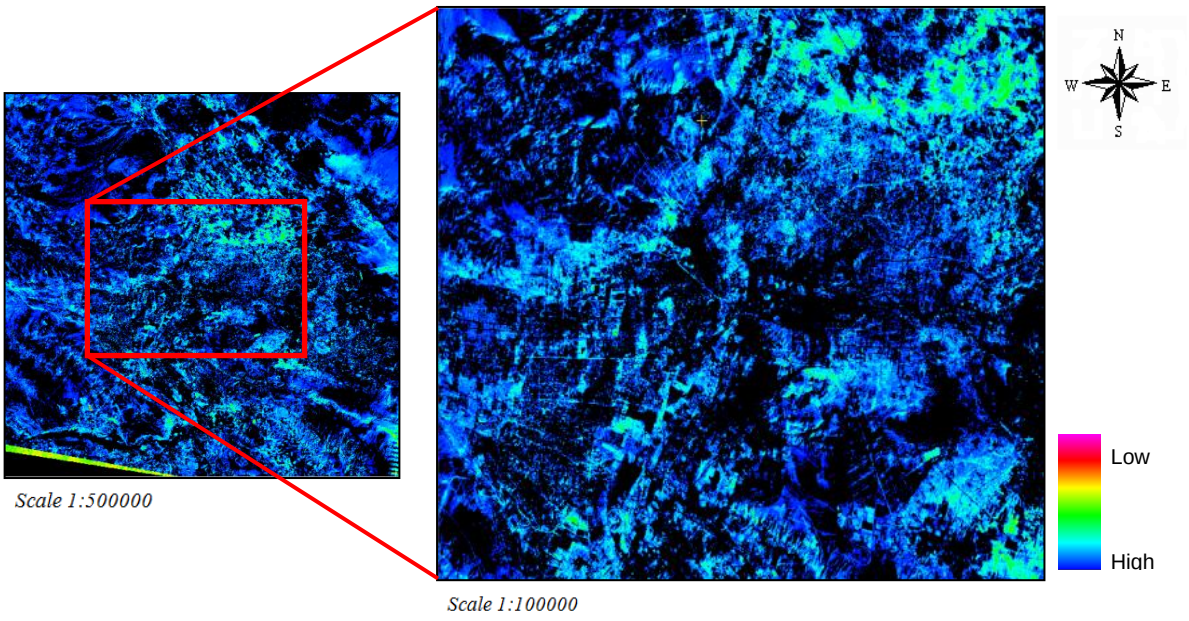

Figure 4. 15. A close up view of the city of Isfahan and adjacent towns on the $\Delta PC1_{1985\text{-}2009}$

4.3.2. Vegetation indices

The 10 vegetation indices listed in table 3.5 are selected to be applied to the 1985 image. The maps of the selected vegetation indices are shown in figures 4.16 to 4.25. Visual interpretation and analysis of different vegetation indices can help to identify the most sensitive and accurate one for mapping vegetation. The analysis of the dynamic range of the color scheme in each map helps to identify and select the most accurate vegetation index. The dynamic range for PVI, DVI and SARVI limited from 0% for bare soil to 43%, 42% and 21% for the completely dense vegetation, respectively, while the corresponding maps do not show more than two distinguishable classes in their dynamic range and it is impossible to discriminate among different sub-classes, especially in dense vegetation cover. RVI and AVI show high levels of saturation and large area of no data for the dynamic range of lower than 35% and 26% respectively. These areas mostly illustrate the area with no or very low density vegetation cover. NDGI is the only index that uses green band in the equation. The NDGI map does not clearly distinguish the sub-classes of both low and high density vegetation cover. Due to high level of saturation, this index is not a good measure to identify land use and land cover classes. The dynamic range of NDGI limits from 10.19% to 51%. NDVI and SAVI maps are visually identical. However, their respective histograms are slightly different and show dynamic ranges between 0% for bare soil, to 70% and 71% for dense vegetation cover, respectively. MASVI shows more sub-classes of vegetation cover and shows higher maximum of 87% in dynamic range. However, this index shows some levels of saturation by demonstrating a minimum of 7.8% and small areas of no data. Finally the results of visual and dynamic range analysis show that the TDVI performs better than the other indices. This index illustrates a very good characterization for the spatial distribution of vegetation cover in many classes and subclasses. The TDVI shows a dynamic range between 0% for bare soil and 90% for a dense cover.

Comparing the TDVI map and the ground truth, it was observed that the general categories for green areas have been sub-categorized into different green vegetation covers which indicate the power of this index. For instance, different

crop types, the urban vegetation cover, dense agricultural lands, natural vegetation cover at the river basin are well discriminated from one another.

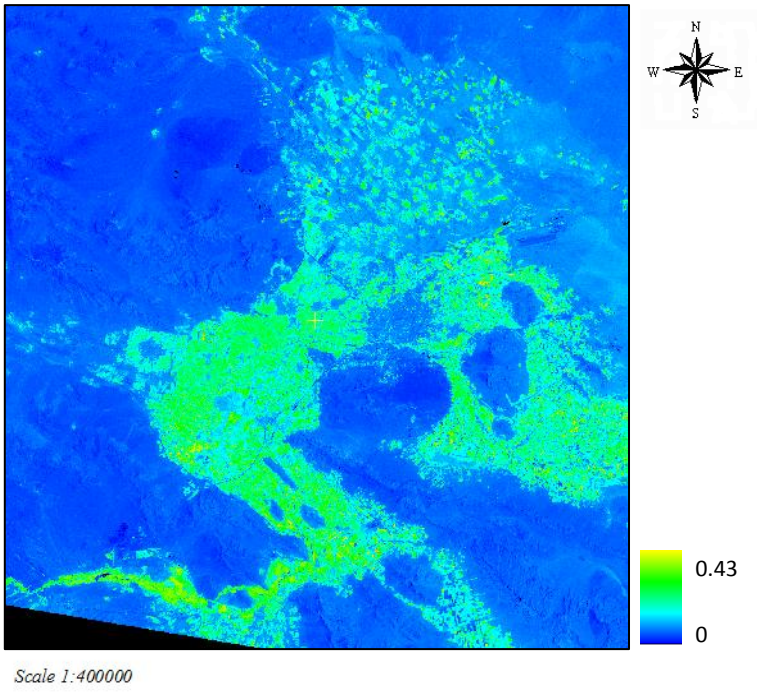

Figure 4. 16. PVI map of the1985 image of Isfahan

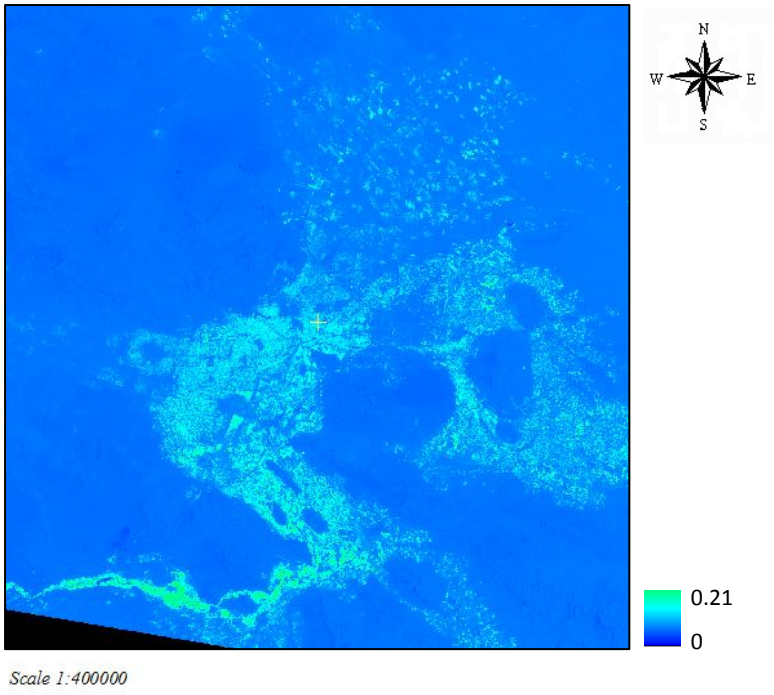

Figure 4. 17. SARVI map of the1985 image of Isfahan

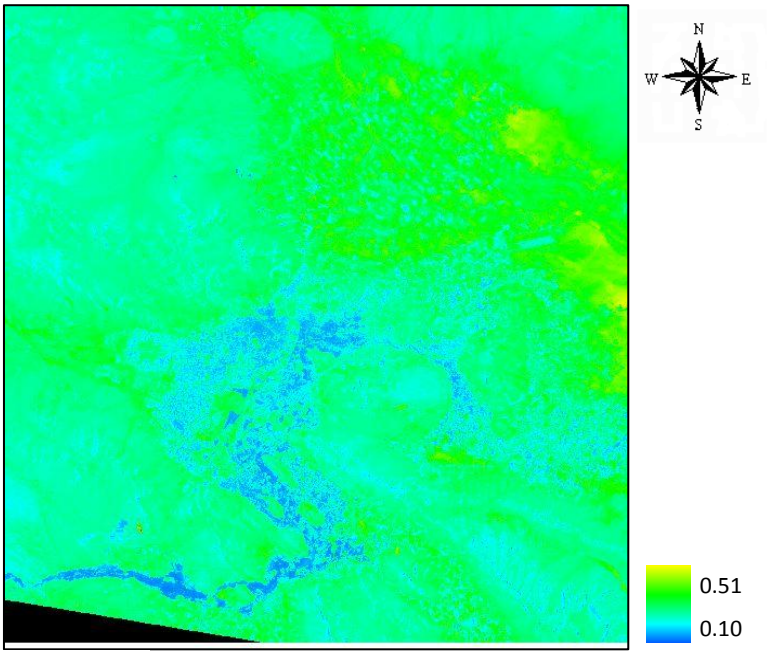

Figure 4. 18. NDGI map of the1985 image of Isfahan

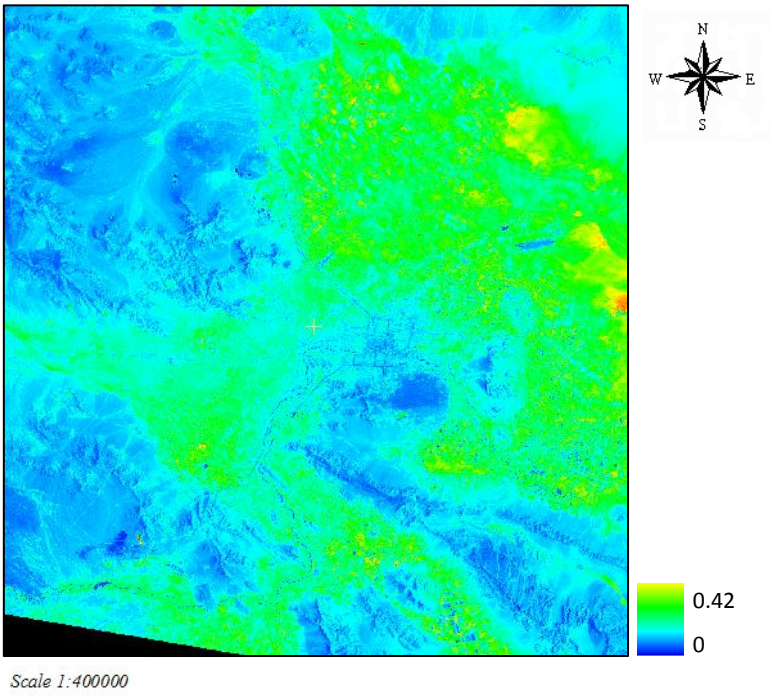

Figure 4. 19. DVI map of the1985 image of Isfahan

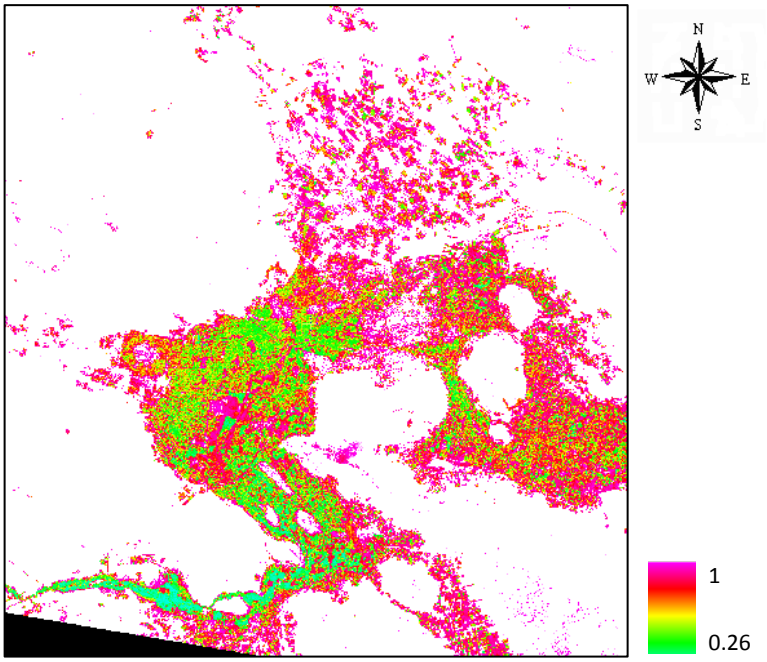

Figure 4. 20. RVI map of the1985 image of Isfahan

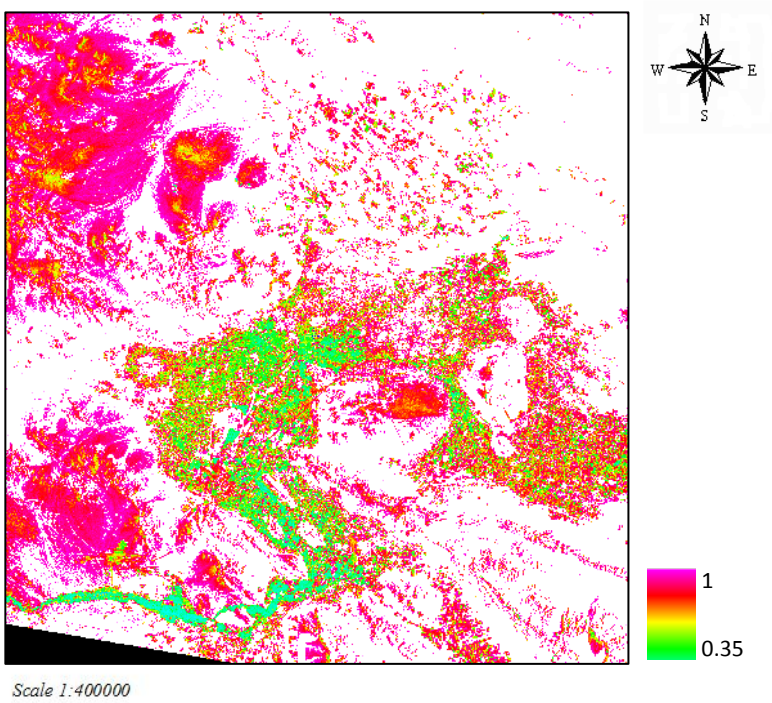

Figure 4. 21. AVI map of the1985 image of Isfahan

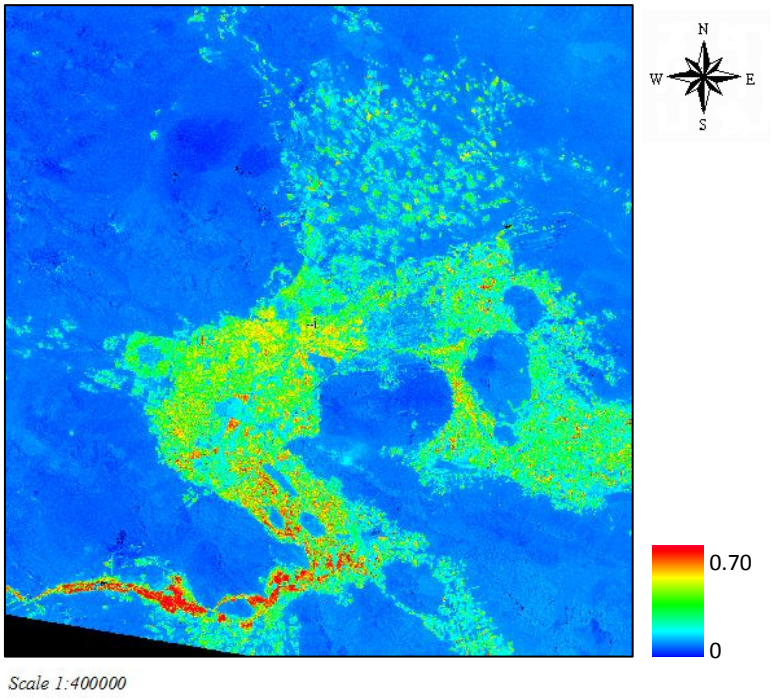

Figure 4. 22. NDVI map of the 1985 image of Isfahan

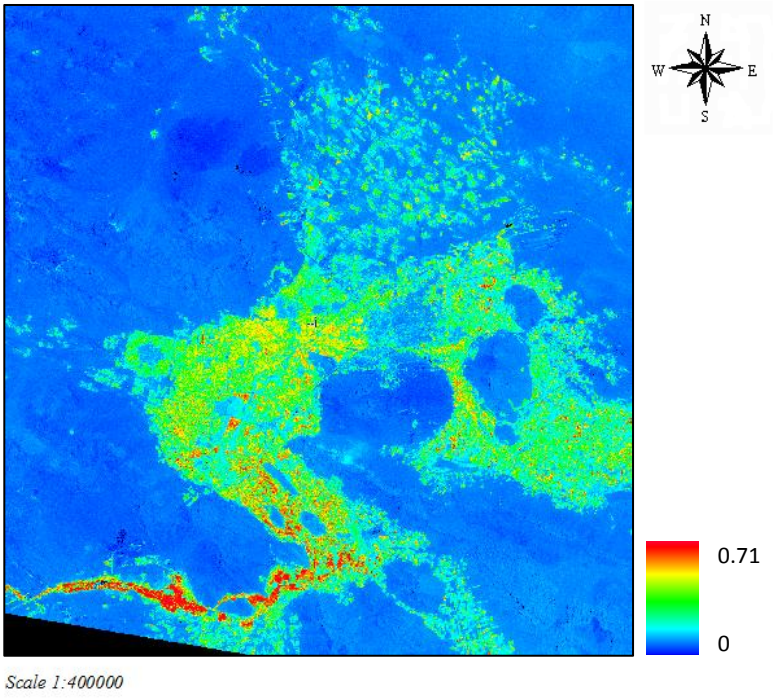

Figure 4. 23. SAVI map of the1985 image of Isfahan

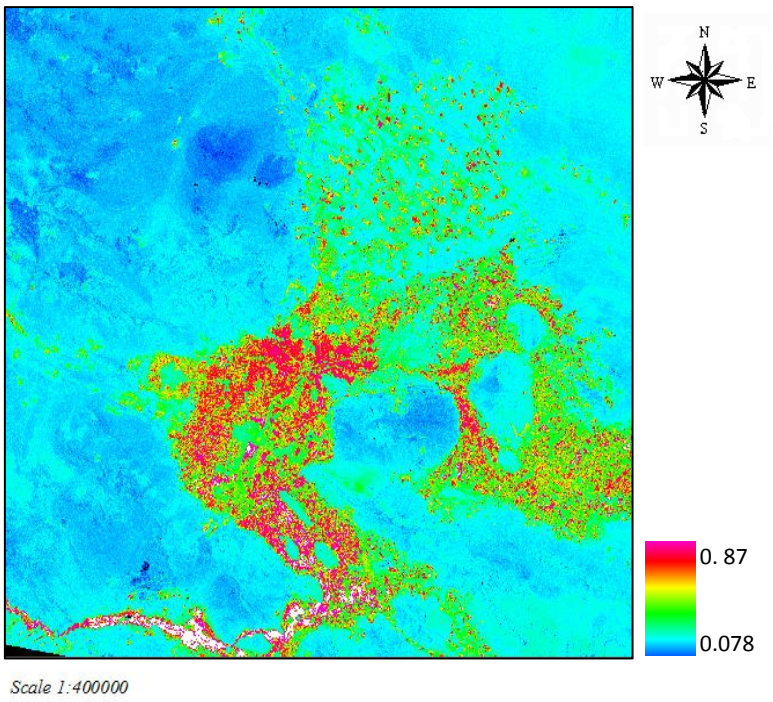

Figure 4. 24. MSAVI map of the1985 image of Isfahan

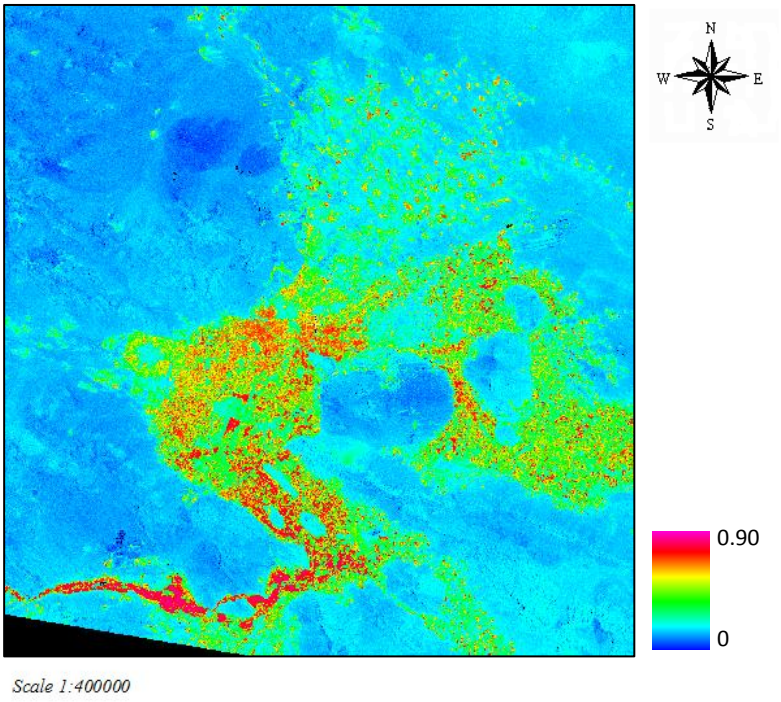

Figure 4. 25.TDVI map of the1985 image of Isfahan

In the next step TDVI is applied to the 2000 and 2009 images, as the most accurate vegetation index. Figure 4.26 shows the TDVI maps for the 2000 and 2009 images. Visual comparison of the 1985 TDVI map with the 2000 and 2009 TDVI maps indicates the changes in vegetation cover, especially considerable decrease in total area of dense vegetation from 1985 to 2000 and 2000 to 2009. Figure 4.26 shows that in the 2000-2009 interval, the biggest changes in vegetation cover occur in the natural and agricultural lands in the river basin at a close distance to main river branches, especially the south-west of the scene. Agricultural lands at the north-east of the city also show significant changes in vegetation density. Urban vegetation and parks in the centre of the city adjacent to the river path way are also impacted by severe changes in vegetation cover. `

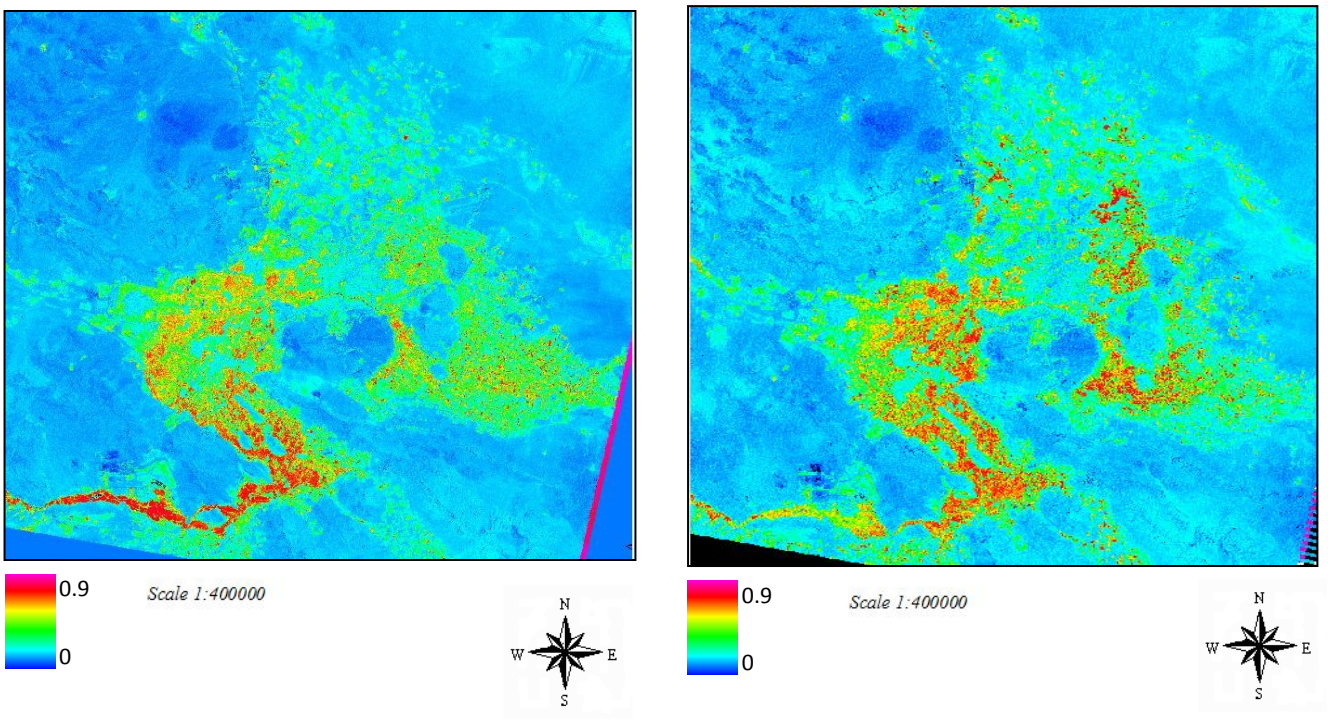

a b

Figure 4. 26. TDVI maps of Isfahan; a)2000 and b)2009

More focus on the city core can help provided more accurate visual interpretation. Figures 4.27 focuses on the main urban areas of the 1985 TDVI map. The results

of visual interpretation of the TDVI maps are in agreement with those of the PCA color composite maps. Moreover, the TDVI maps are more informative about the vegetation cover and vegetation status during the period of study. Black circles on this figure show small towns that have been expanded during the period of study. Circle 1 shows Najaf-Abad (figure 4.28), circle 2 is the town of Khomeyni-Shar (figure 4.29), and finally Circle 3 shows the town of Khorasgan at the east of Isfahan. Comparing the TDVI maps of these towns in 1985 with the 2000 and 2009 maps clearly shows the destruction of agricultural lands and diminishment of dense vegetation cover around the towns.

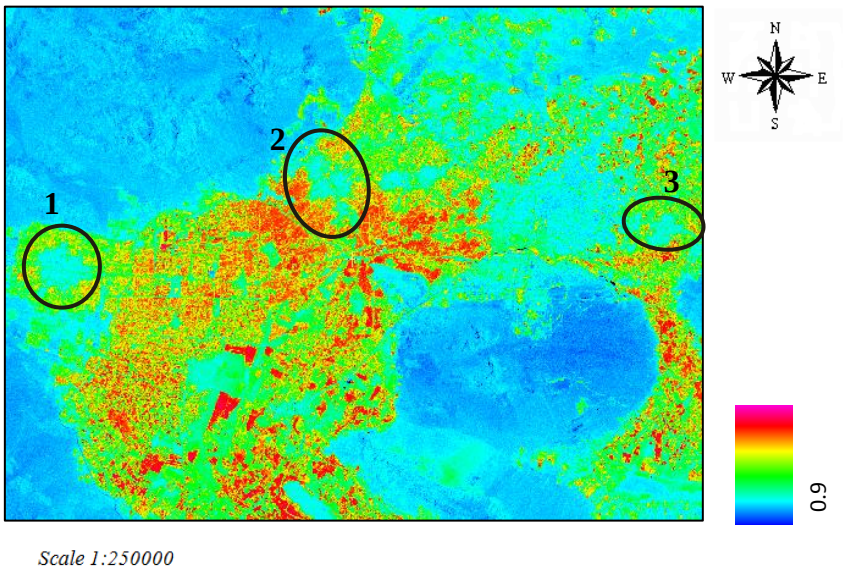

Figure 4. 27. A close up view of the city of Isfahan and adjacent towns on the 1985 TDVI map

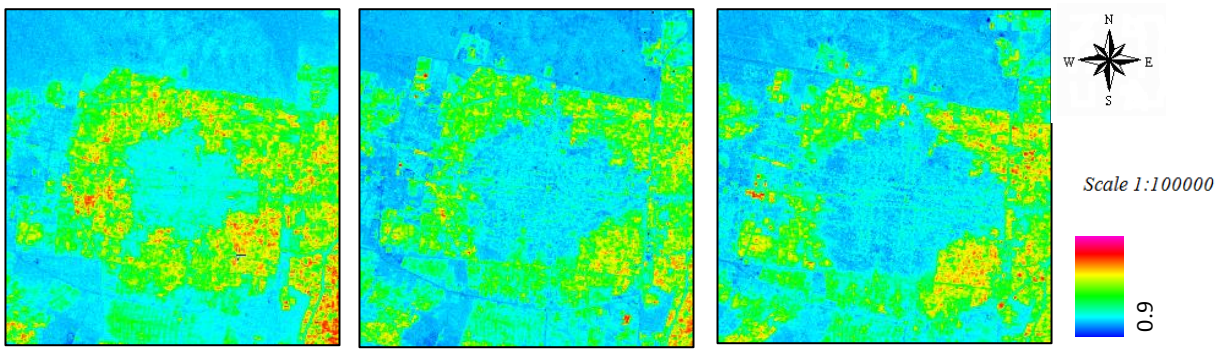

a b c

Figure 4. 28 .Urban expansion in Najaf-Abad, a)1985, b)2000, and c)2009

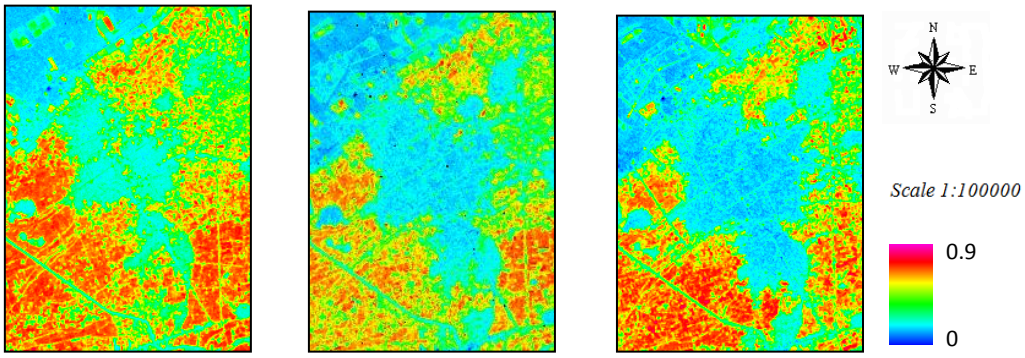

a b c

Figure 4. 29. Urban expansion in Khomeyni-Shahr, a)1985, b)2000, and c)2009

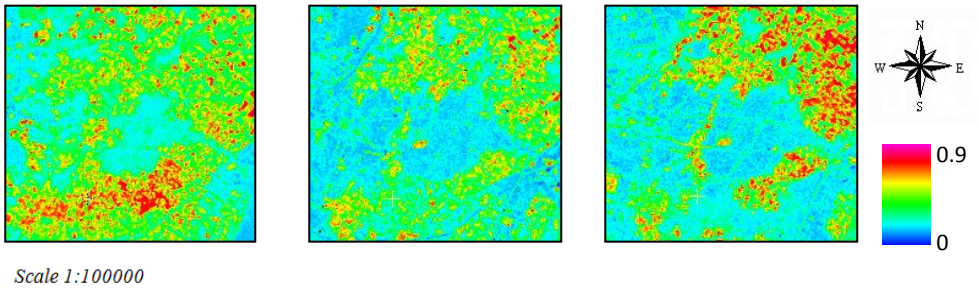

a b c

Figure 4. 30. Urban expansion in Khorasgan, a)1985, b)2000, and c)2009

To best visualize changes in land use and especially vegetation cover in the study area, differencing is implemented using PCI Geomatica EASI Modeling and

programing function. This is done by subtracting the TDVI 1985 from TDVI 2000 and TDVI 2009. Figure 4.31 shows $\Delta TDVI_{1985\text{-}2009}$. Black and dark blue areas are the areas with no or minimum changes during this time. Pixel analysis of this map shows that 52.82% of the total pixels show values of 0 and absolutely no changes, which is in agreement with the result obtained from the $\Delta PC1_{1985\text{-}2009}$ pixel analysis. Higher values in the dynamic range of the map indicate more considerable changes in vegetation density and biomass. These pixels are shown in green and greenish colors and small red and pink spots. The dynamic range of this map is 0-55, which is close to that of ΔPC1. However, ΔTDVI shows higher visual sensitivity to identifying and distinguishing vegetation sub-classes, compare to ΔPC1. According to figure 4.31, most of the changes in vegetation cover have happened in agricultural and natural lands in the river path. Large areas east and south-east of the city also show big changes. Some small changes can also be seen in the main city core, which could be due to increase in total built-up area or increase and decrease in the total area of urban gardens and parks.

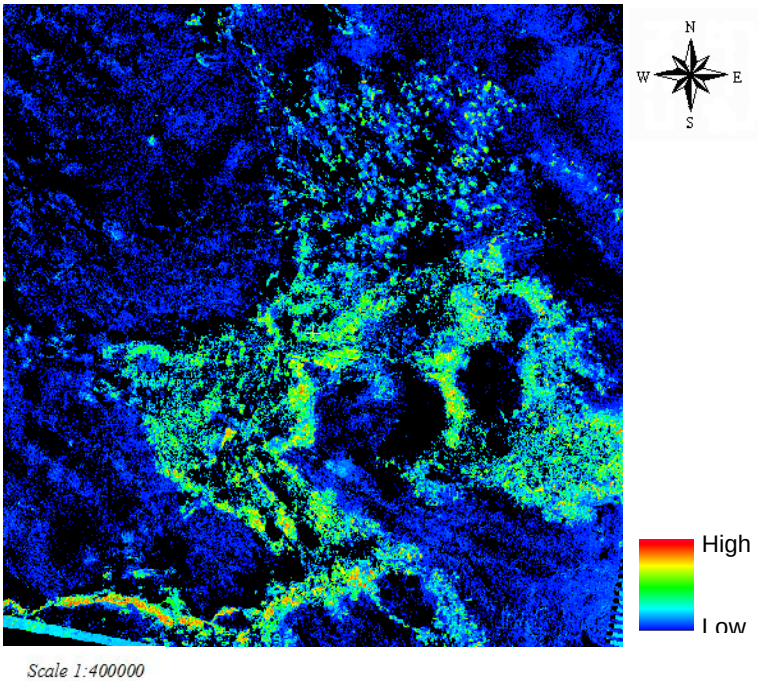

Figure 4. 31. The $\Delta TDVI_{1985\text{-}2009}$ map of Isfahan

4.3.3. Classification

Classification uses the spectral information of each image pixel to make a thematic map containing a mosaic of pixels representing different classes of land cover. Training sites are the homogenous sample representatives of known land cover types on the image, describe the spectral attributes of each feature of interest. In supervised classification training site selection is implemented by the analyst. The accuracy of training site selection is based on the knowledge and skills of the analyst and familiarity with the different land covers of the region. Furthermore, in this study the training site selection should be repeated for images acquired in different times, and the accuracy of training site selection for all three images might be different due to the analyst error. For the 1985 and 2000 TM images, ten land cover classes are identified; whereas, for the 2009 ETM+ image, twelve land cover classes are identified. These classes are presented in table 3.6.

Training site samples are created by drawing small polygons over multiple pixels located nearby that are likely to be in the information class that interests the analyst. However, point selection is also used to select training site sample pixels in some heterogeneous land covers such as urban areas.

There are different methods to insure that the training sites are accurate and representative of the land cover class. “Signature statistics” is a set of information provided by the PCI software for the purpose of testing the accuracy of the training sites. The number of sample pixels for each category is presented in signature statistics. These numbers are given in table 4.3 for the 1985, 2000, and 2009 image training sites. Furthermore, the “threshold” and the “bias” are also presented in the signature statistics. The software enables the analyst to enter these values. The threshold determines the maximum spectral distance within which pixels can occur while still being within the same category. The bias determines which category will be assigned to the overlapping pixels. A threshold of 3.0 and bias of 1.0 are selected for this study. The mean and standard deviation are other pieces of information provided in the signature statistics. The mean shows the position of a class in the spectral range, while the standard deviation

presents the variance of training site pixels reflectance for each class. The means and standard deviations of each class for each image are presented in appendix D

Table 4. 3. Number of pixels selected for each training class

	1985	2000	2009
Bright soil	225	383	185
Water	217	222	263
Road	233	142	330
Urban	274	336	267
Soil 1	469	378	277
Soil 2	180	172	194
Soil 3	339	359	190
Soil 4	-	-	137
Vegetation 1	141	305	271
Vegetation 2	194	161	185
Vegetation 3	95	211	208
Vegetation 4	-	-	270

Signature separability is another important measure to assess the accuracy of the training sites. Signature separability has real values between zero to two. A zero indicates complete overlap, while two indicates complete separation between two classes. The signature separabilities of the training sites selected to classify the 1985, 2000, and 2009 images are given in appendix D. For the 1985 image the average separability is 1.98 which is an excellent level and shows an acceptable level of accuracy and low confusion between the land cover classes. The separabilities for all classes are between 1.90-2.0, while there is only one class with poor separability of lower than this range. The poorest separability (1.749356) occurs between soil type 2 and soil type 3, which is due to the proximity of the reflectance of these two classes. This poor separability does not affect the clustering of the urban class for this image.

Moreover, for the 2000 image, the average separability is 1.96 and lower than that of the 1985 image, and some classes show poor separabilities. For this map the low level of separability (1.596124) shows that the urban class is not very well

separated from soil type 2. This poor separability caused some error in urban class clustering and led to the selection of some incorrect urban clusters in non-urban areas. This is due to the proximity of reflectance of the soil type 2 class and some roof materials. Furthermore, the water class is also poorly separated from the vegetation type 1 and 2 classes (1.877476 and 1.815764, respectively). This is due to the high moisture content of those vegetation types and the low level of stream water on certain parts of the river which occurs along with the development of alga and other aquatic plants at the bed of the river or water surface. Road and urban classes also show poor separability (1.803470). This is caused by the similarity of the materials used for the pavements and the roof covers.

As mentioned above, for the 2009 image, due to higher radiometric sensitivity and accuracy of the ETM+ sensor, the number of land cover classes are more than those of the 1985 and 2000 images. However, the average separability of this image is not significantly different from those of 1985 and 2000 images. The average seperability for the 2009 image training sites is 1.9745. Poor separability (1.4515) can be seen for urban class and soil type 1, which led to the identification of some false urban clusters. The water class and vegetation type 4 are also not well separated (1.794176) due to a high level of moisture content in this vegetation type and a high level of alga and aquatic plants in the river. Separability of soil type 1 and soil type 2 is also poor (1.850803), which causes confusion between these two soil types, but does not affect the urban class. However, for all three images the signature separabilities for most of the classes are in the acceptable range of 1.90-2.0, which demonstrate the high accuracy of training site selection.

Having achieved acceptable levels of signature separability for the training sites, the next step is to run the classification process based on the maximum likelihood classifier. This classifier outputs an output map in which no pixels are left unclassified (Ozbakir and Bannari, 2008). Figure 4.32 shows the output map of the study site for the 1985 image. Urban class, roads, river, different vegetation types, bright soil and darker soil tones can be clearly distinguished on the map. However, as the low signature separabilities also suggest, there is some confusion

between classes, especially in different soil tones. Nevertheless, the main purpose of the classification is to identify and distinguish urban area, and the confusion between soil tones does not affect it, so it is not considered significant. Figure 4.33 shows the classification map of the 2000 image. This map shows some urban clusters in non-construction areas which are due to similarity in reflectance of some urban materials and some soil tones. However, the expansion of the urban class, especially in the north and north-west of the city is shown perfectly on the map. Figure 4.34 shows the classification map of the 2009 image. This map shows more visual preciseness in the clusters. This is due to the high radiometric sensitivity and accuracy of the ETM+ sensor. Visual comparison between the 1985, the 2000, and the 2009 maps clearly displays the expansion of the urban class in this period. In the 2000 to 2009 period, more expansion in the north and north-west parts of the city can be observed, as well as the amalgamation of some small towns to the main city core in the west side of the city.

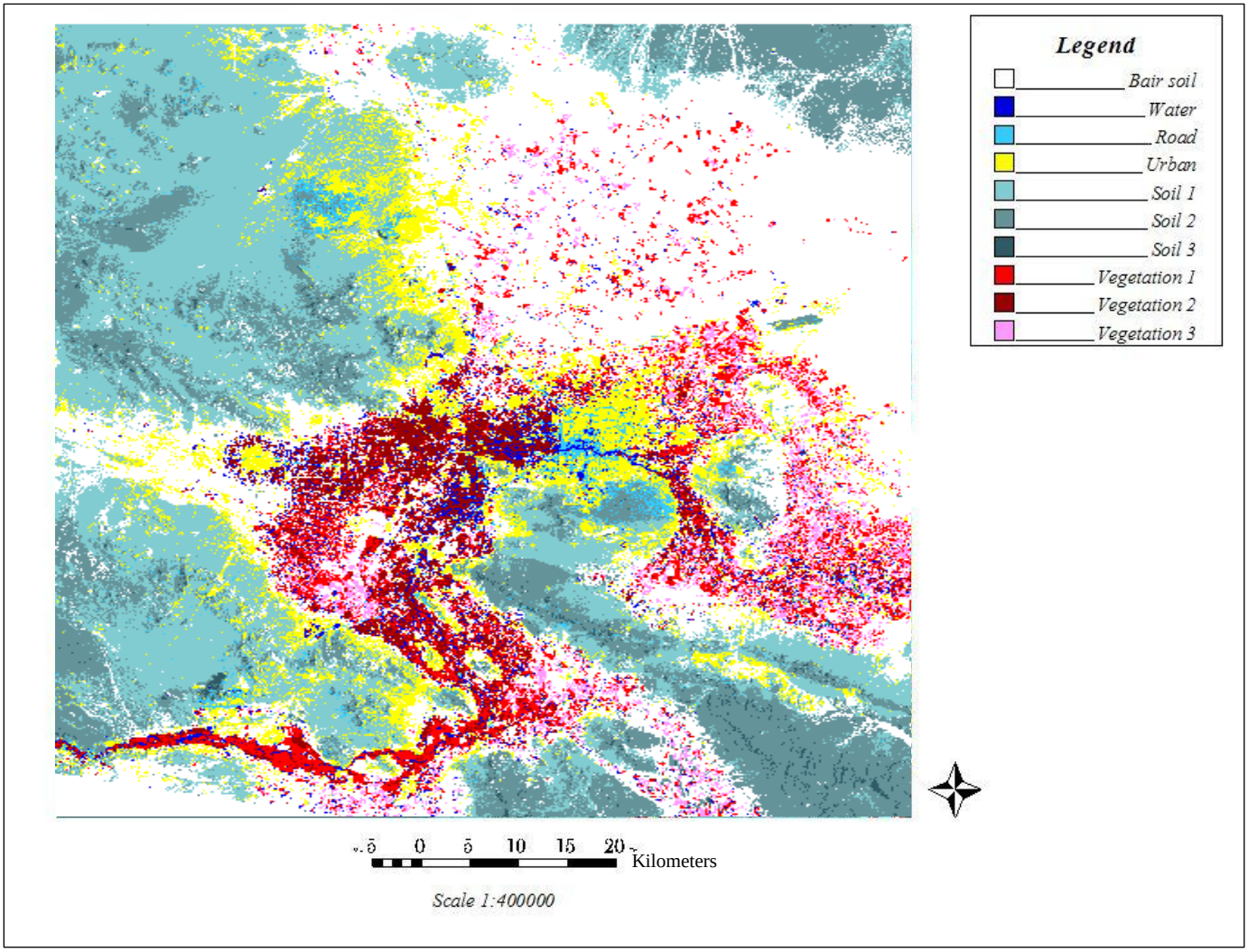

Figure 4. 32. The 1985 classification map of Isfahan

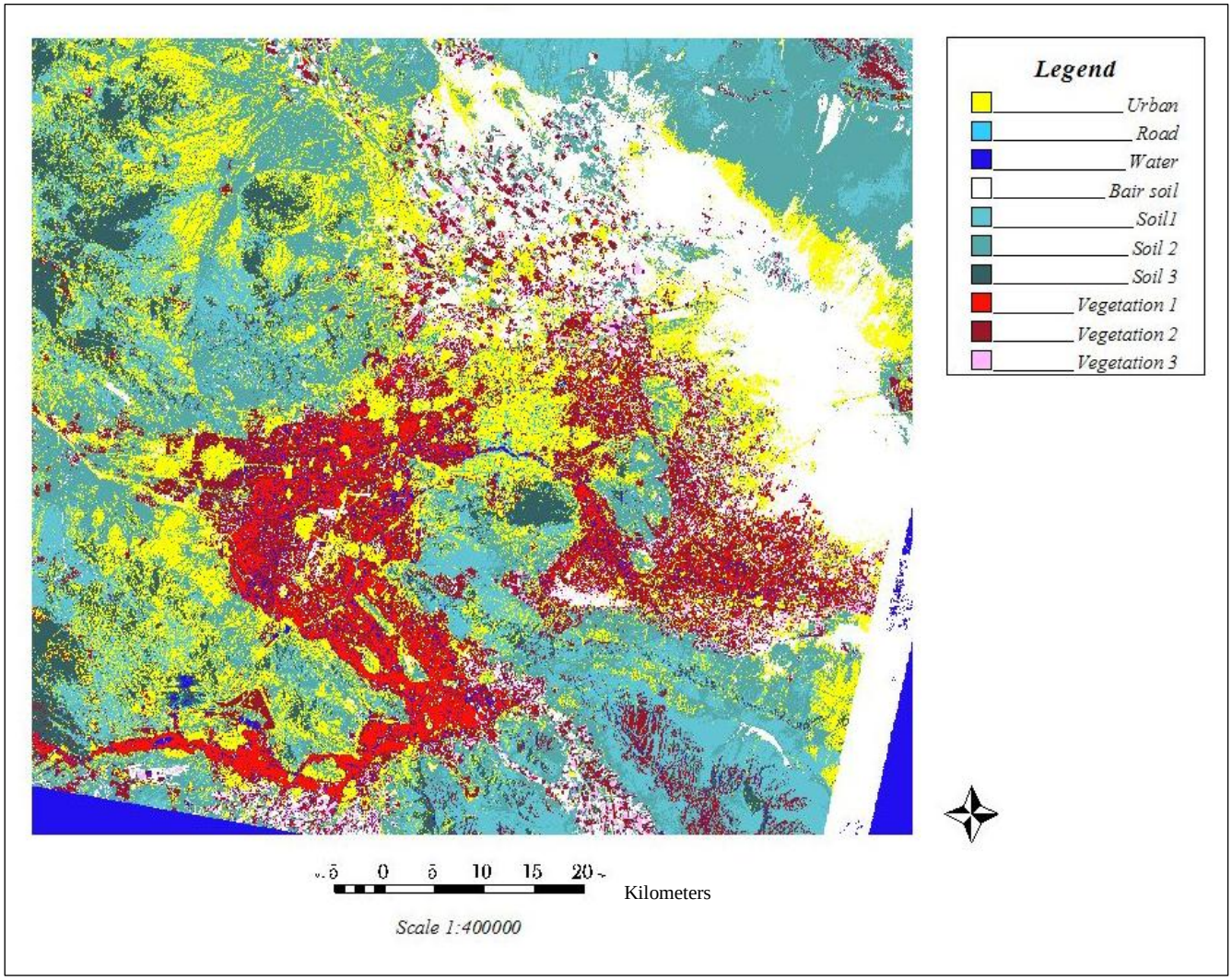

Figure 4. 33. The 2000 classification map of Isfahan

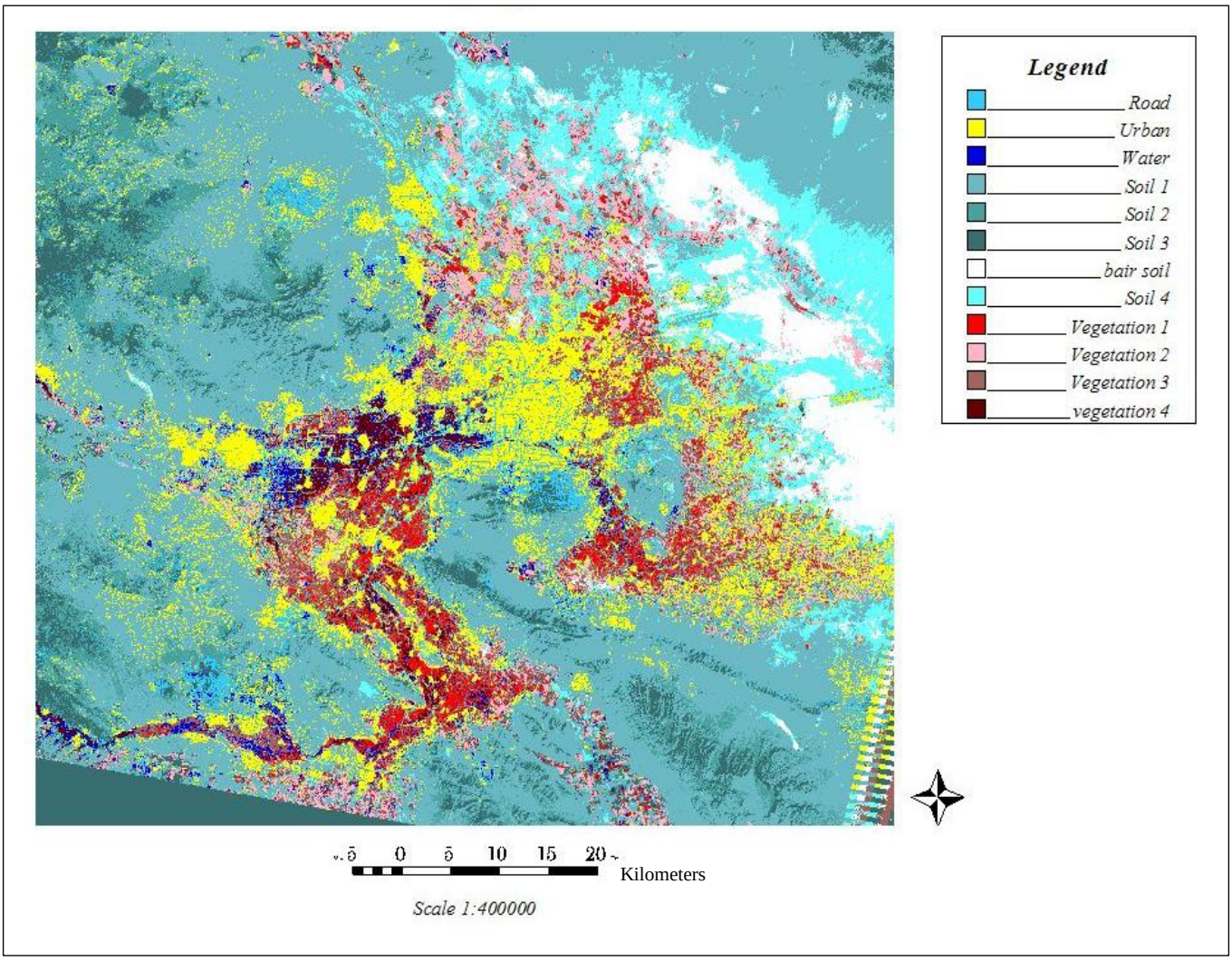

Figure 4. 34. The 2009 classification map of Isfahan

More focus on the city core can help provided more accurate visual interpretation. Figures 4.35, 4.36 and 4.37 give more focus on the classification map of the 1985, 2000 and 2009 images, respectively. Expansion of the north, north-east and north-west parts of the city, as well as emerging new townships in the far west and south-west of the main city core can be observed during this period. Moreover, during the 2000-2009 period, the new, already existing, urban hubs experienced huge growth and expansion. These results are in agreement with the results obtained from the analysis of the PCs, and confirm the two city growth trends that were explained in section 4.3.1. Black circles on figure 4.35 show small towns that have been expanded during the period of study. Circle number 1 is the town of Khomieni-Shahr. In the 1985 map, this town was thoroughly separated from the main city core. However, in 2000 and especially 2009, the expansion of the urban class west of the main urban core, caused this town to be attached to the city. More details can be seen in figure 4.38. Circle 2 in figure 4.35 is the town of Najaf-Abad, which is further away from the main city hub, but shows huge expansion in the 2000 and 2009 maps. More details about this city can be seen in figure 4.39. These maps show that the expansion of built up area in Najaf-Abad in the 1985-2000 period is much more than the 2000-2009 period. Circle 3 in figure 4.35 is the town of Khorasgan at the east of Isfahan, which was annexed to the main city core during the 1985-2009 period due to the expansion of both the Khorasgan town and the main city core. Figure 4.40 shows more details about the urban expansion in this town.

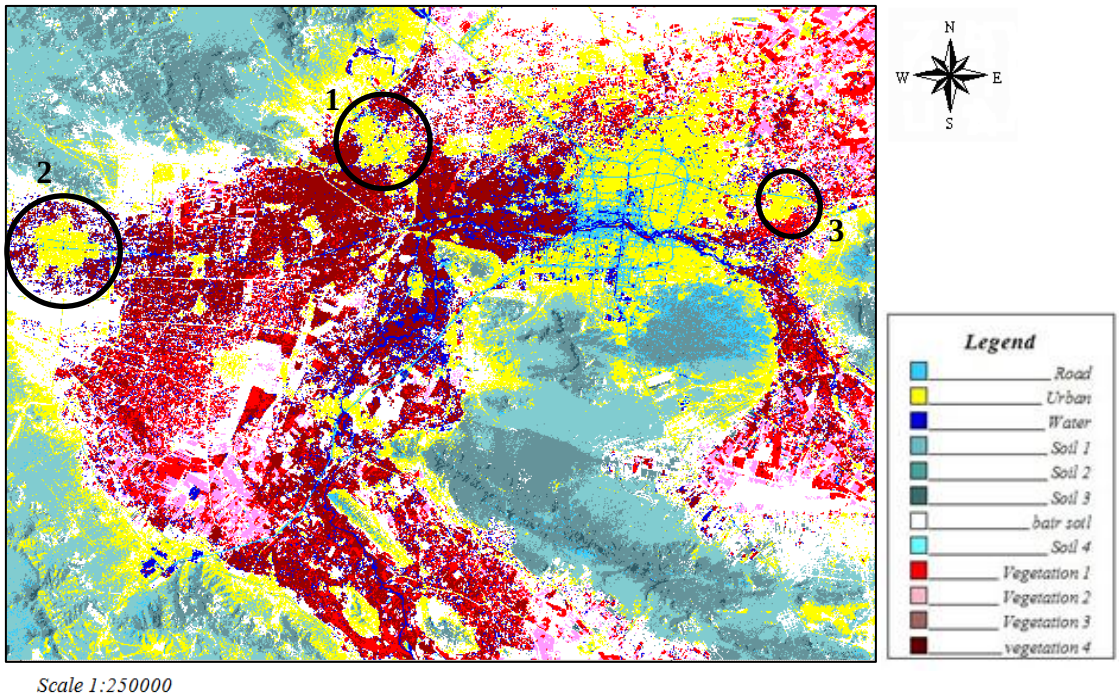

Figure 4. 35. A close up view of the city of Isfahan and adjacent towns on the 1985 classification map of Isfahan

.

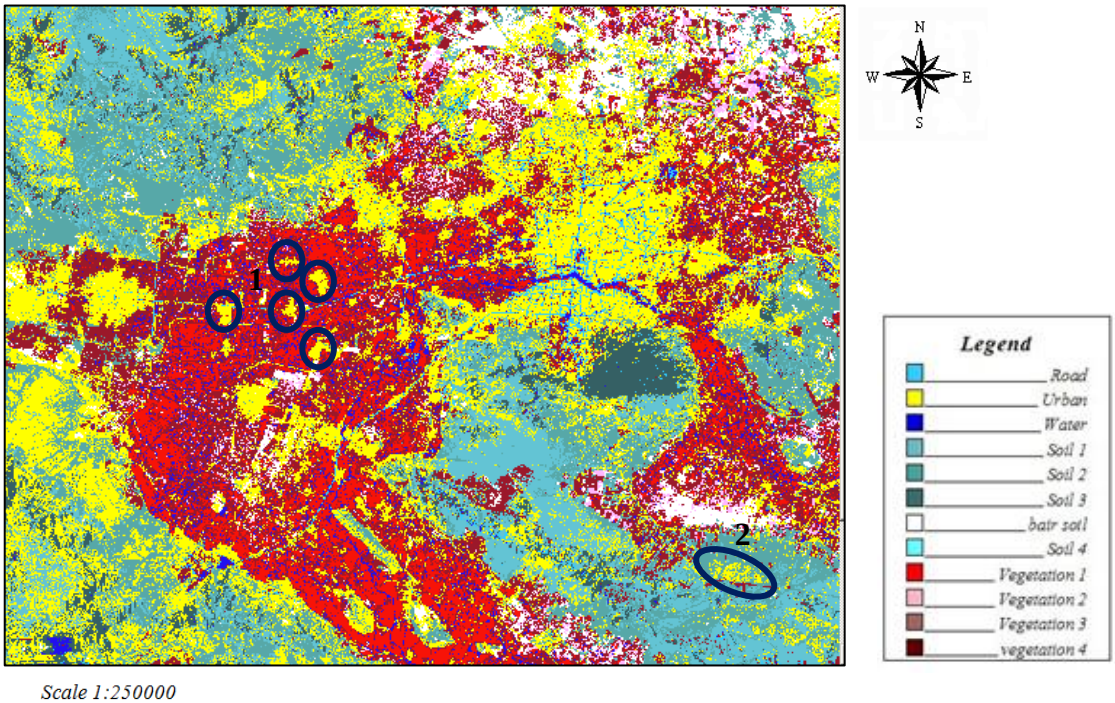

Figure 4. 36. A close up view of the city of Isfahan and adjacent towns on the 2000 classification map of Isfahan

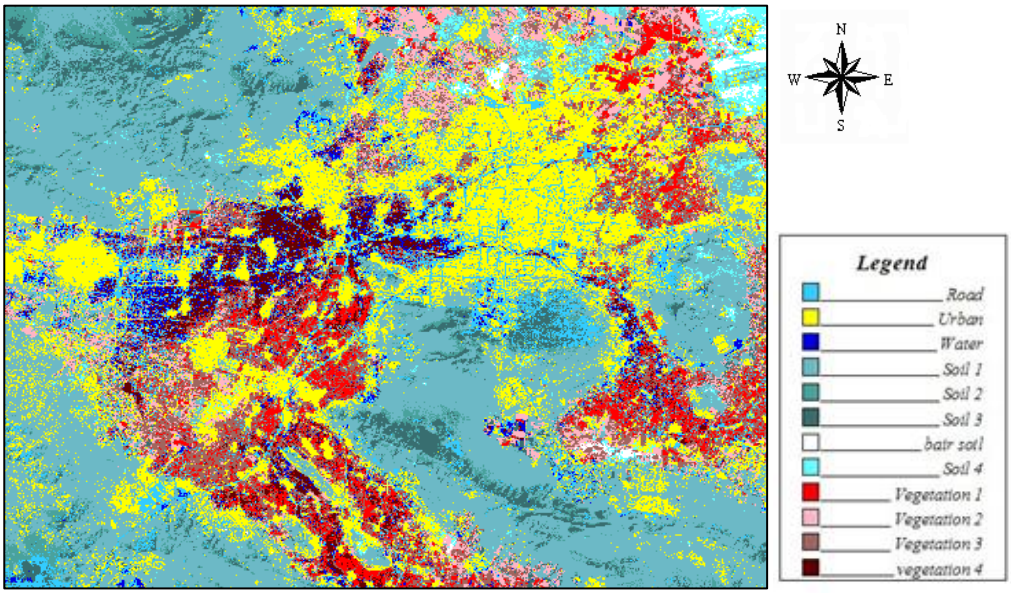

Figure 4. 37. A close up view of the city of Isfahan and adjacent towns on the 2009 classification map of Isfahan

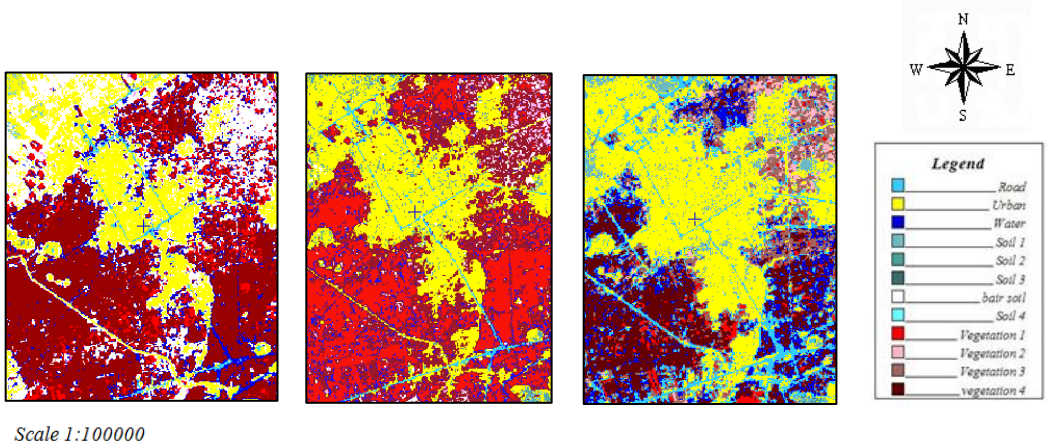

a b c

Figure 4. 38.Urban expansion in Khomeini-Shahr, a)1985, b)2000 and c)2009

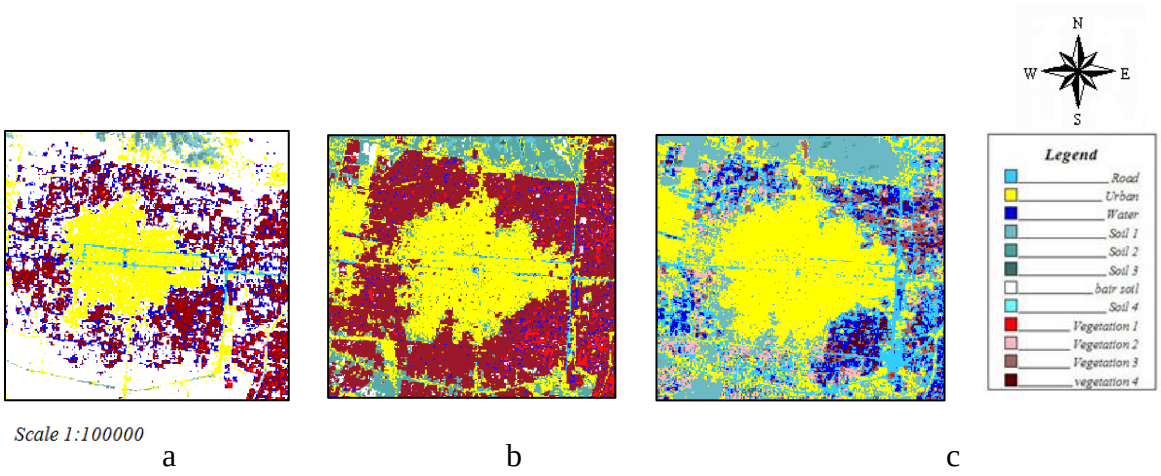

a b c

Figure 4. 39. Urban expansion in Najaf-Abad, a)1985, b)2000 and c)2009

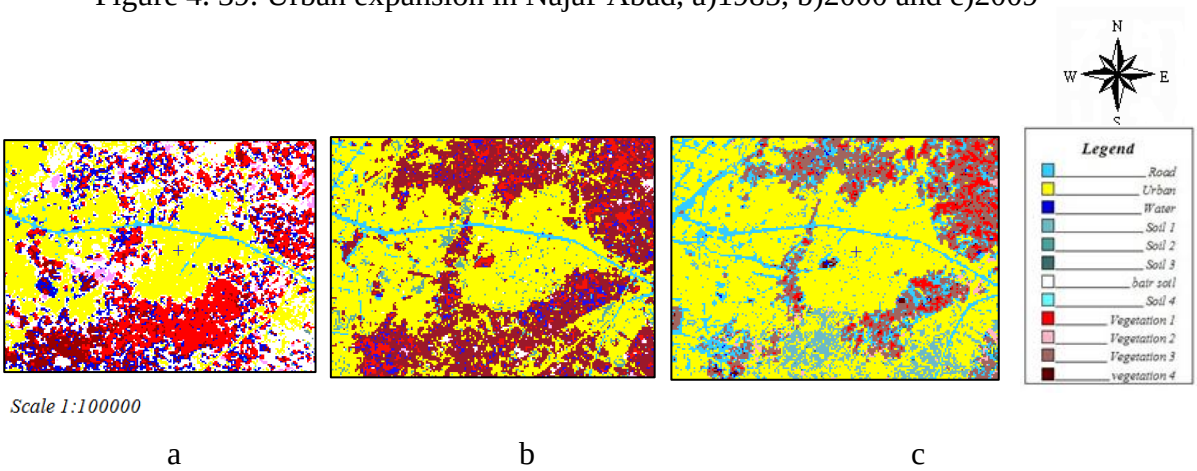

a b c

Figure 4. 40. Urban expansion in Khorasgan, a)1985, b)2000 and c)2009

Small towns shown by circles and number 1 in figure 4.36 are examples of new built up areas that didn't exist in 1985, or existed in the forms of small villages or rural settlements. These new towns show even more expansion in the 2009 map. The circle number 2 shows the new town of Baharestan which was first established in 1993 based on the New Town Strategy. This city is an example of a planned city and shows more development in the 2009 map.

Figure 4.41 shows the urban expansion in the main city core in more detail. As mentioned before, the urban growth is mainly in the north and north-west of the city, but the east and small areas of the south also show expansion during the period of study.

a

b

c

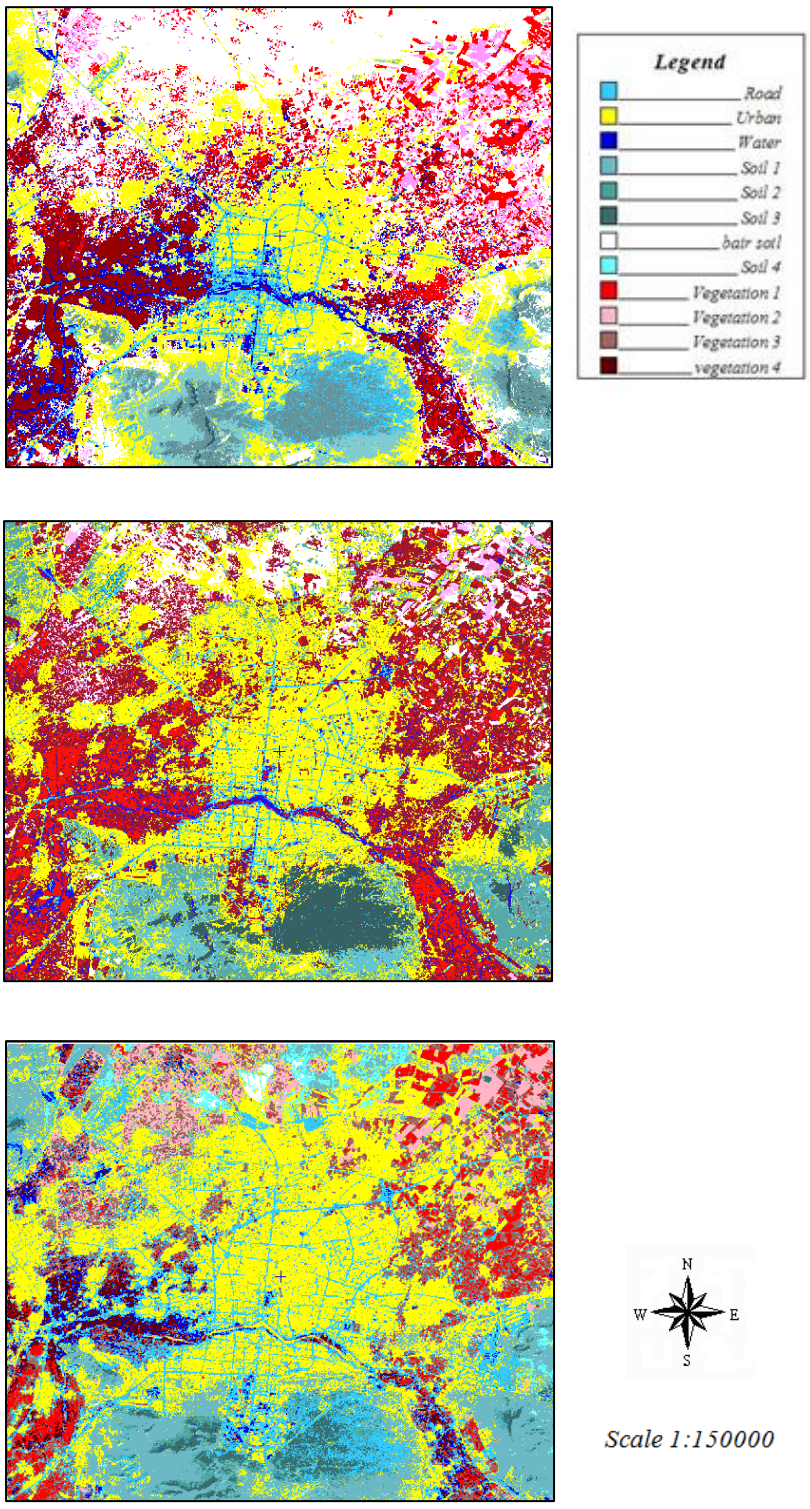

Figure 4. 41.Urban expansion in the main core of Isfahan, a)1985, b)2000 and c)2009

The accuracy of the classification can also be tested using the “confusion matrix”, to determine how well the classification has categorized a representative subset of pixels used in training site selection. The confusion matrix shows the probability of the classification to accept or reject a pixel. The error of commission and error of omission are also information that is provided by the confusion matrix. According to the classification reports, the probability of the pixels being assigned to the correct class for all three maps is 95%. The confusion matrices for the 1985, 2000 and 2009 classification maps are presented in appendix E. For the 1985 map the lowest probability is 92.89% for the bright soil class. The 7.11% of the pixels are assigned to the urban class, indicate the error commission. However, it also indicates the error of omission for the bright soil class, while this percentage of pixels should normally have been assigned to this class. The lowest accuracy for the 2000 map is 94.37% for the road class. The overall error of omission for this class is 5.63%, while 3.52%, 1.41% and 0.7% of the pixels that should have been assigned for this class are assigned to the water, urban, and soil type 3 classes, respectively. Thus, these percentages of pixels indicate the errors of commission for the correspondent classes. Furthermore, the highest error of commission is 5.19%, which is for the soil type 2 class, while this percentage of pixels should normally have been assigned to the urban class. Therefore, 5.19% indicates the error of omission for the urban class. The lowest accuracy in the confusion matrix of the 2009 map is 83.39% for the soil type 1 class, while this class shows the highest error of omission of 16.61%. This percentage of pixels should normally have been assigned to the urban class; therefore it indicates the error of commission for this class. Figure 4.34 shows the accuracy of each selected class presented in the confusion matrices of the 1985, 2000 and 2009 maps.

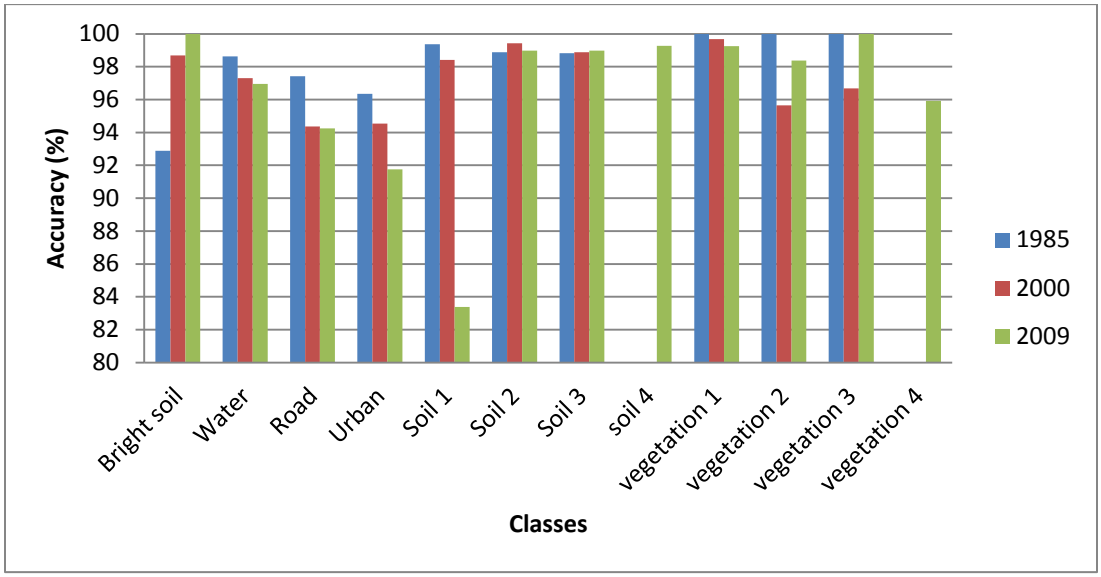

Figure 4. 42. The accuracy of the selected classes (%) for the 1985, 2000 and 2009 maps based on the confusion matrices

The overall accuracy is another measure of testing the accuracy of the classification process. The overall accuracy presents the percentage of pixels classified into the correct classes. Table 4.4 shows the overall accuracies for the 1985, 2000 and 2009 classification maps. The overall accuracy of the 1985 map is the highest amongst all three maps and is 98.14%, while the overall accuracy of the 2000 map is 97.59% and only 0.55% lower than that of the 1985 map. The overall accuracy of the 2009 map is 95.68, which is 2.46% and 1.91% lower than those of the 1985 and 2000 maps, respectively.

"Kappa coefficient" is another measure to assess the accuracy of the classification process. This statistic presents the difference between the actual agreement between the reference data and an automated classifier and the chance agreement between the reference data and a random classifier (Bannari *et al*., 1998). Kappa coefficient ranges between 0 and 1. The actual agreement is a value close to 1, while the chance agreement approaches 0. The Kappa coefficients for all three maps are presented in table 4.10. According to this table, this coefficient for the 1985 map is 0.97893, while it is 0.97290 and 0.95263 for the 2000 and 2009

maps, respectively. These values are very close to 1, thus are indicators of good classifications.

Table 4. 4. The overall accuracy and Kappa coefficient for the 1985, 2000 and 2009 classification maps

	Overall accuracy	Kappa coefficient
1985	98.14	0.97893
2000	97.59	0.97290
2009	95.68	0.95263

The pixel analysis of the three classified maps perfectly indicates the growth of urban class and diminishment of vegetation class. In the 1985 map, the total area of buildings, roads and urban infrastructure, is 41% of the total pixels, while this amount grows to 50.89% and 60.61% in the 2000 and 2009 maps, respectively. The opposite trend can be seen for vegetation class. The total area of all vegetation classes for the 1985 map is 39.9% of the total map, while this amount declines to 31.22% and 21.22% for the 2000 and 2009 maps, respectively. The area of the water class also declines by time. Water class occupies 10.61% of the total area of the 1985 map, while it declines to 5.08% and 4.59% for 2000 and 2009 maps, respectively. The results are in agreement with the pixel analysis results of the PCA and TDVI.

4.4. Conclusion

The semi-empirical line model and the pseudo-invariant targets selected in this study performed accurately in radiometric calibration of the 1985 and 2000 TM and 2009 ETM+ images. After the pre-processing step, the processing methods were applied successfully to the images. First, the principal component analysis was calculated. The first three components were found to be responsible for more than 99% of the variances and were able to successfully distinguish the land use classes. $\Delta PC_{i\ t1\text{-}t2}$ was successful in showing changes in study site over time. 10

selected vegetation indices, then were successfully applied to the 1985 image. Visual interpretation and pixel analysis of these indices showed that TDVI performs better than other indices in mapping vegetation in urban areas. TDVI was calculated for the 2000 and 2009 images, and $\Delta TDVI_{t1-t2}$ calculated successfully to detect the changes in land use over time. Classification was the final processing method that applied in this study. Training sites were selected with acceptable accuracies, and a maximum likelihood classifier was run successfully on all three images. Confusion matrix, overall accuracy and Kappa coefficient approved the accuracy of the classification procedure. Visual interpretation of the classified maps shows the overall changes in the study site over the period of study. Chapter 5 will present the conclusions of this study and will list recommendations for future works.

Chapter 5: Conclusions and Recommendations

5.1. Introduction

This chapter presents the conclusions drawn from the land use and land cover change detection research carried out in this thesis using multitemporal Landsat TM and ETM+ images. Recommendations for future researches are also stated at the end of this chapter.

5.2. Summary and Contributions

In this study, three Landsat images acquired in 1985, 2000 and 2009 were used for the land use and land cover change detection of the city of Isfahan, Iran, over a period of 25 years. The sensor radiometric calibration was carried out to normalize the reflectance of each pixel, based on the equivalent pixel in the image used as the reference scene. The variation of coefficient suggested that the 1985 image was least affected by the atmospheric effects, and was thus most suitable for being selected as the reference scene. Sample pixels of the pseudo-invariant targets were selected for the calibration purpose. A semi-empirical line model was used to relate the spectral bands in the reference scene to their homologous bands in the 2000 and 2009 images. The slope and intercept of the semi-empirical lines were the correction coefficients used to normalize the 2000 and 2009 images based on the 198 image. The presence of R^2 higher than 0.87 for all linear regressions shows the high accuracy of this method in sensor radiometric calibration.

After the pre-processing, three processing techniques were implemented on the images. First, PCA was calculated for the images. PC1 was found to be responsible for the most variances and used in differencing analyses. $\Delta PC1_{t1-t2}$ was successfully calculated and showed the total changes in the study area. The pixel analysis of the $\Delta PC1_{t1-t2}$ demonstrated that approximately 50% of the total pixels showed no changes over time. Second, selected vegetation indices in table 3.5 were calculated for the 1985 images. The accuracy assessment showed that

the TDVI had the highest dynamic range value and was thus perfect for showing classes and sub-classes of vegetation in urban areas. Thus, this index was selected to be calculated for the 2000 and 2009 images. $\Delta TDVI_{t1-t2}$ was successfully calculated to show the total change in the vegetation cover in the study site. The results of pixel analysis of the $\Delta TDVI_{t1-t2}$ showed that approximately 50% of the total pixels remained unchanged over the period of study. This result was in agreement with those of $\Delta PC1_{t1-t2.}$ Third, maximum likelihood supervised classification was successfully calculated for the images. The overall accuracy of the classification procedure for all three images was higher than 95% with the Kappa coefficient being higher than 95. The expansion of urban class was clearly detectable through the comparison of the classified maps.

The analysis showed that the city has been expanded in different dimensions over the period of study. The main city core had grown mostly in north, north-east, and south west parts. New small city hubs had emerged for the first time during the 1985-2000 time period. Furthermore, some small villages expanded during this time and converted from rural areas into urban hubs. However, during the 2000-2009 period the new city hubs continued to expand and in some cases amalgamate to the main city core. In the process of city expansion, large areas of natural and agricultural lands became built up.

5.3. Recommendations for future research

Various issues must be considered in multitemporal studies. The change in land cover classes of various data imageries acquired from the same scene but in different seasons might be a result of not only manmade changes, but also the difference in plant growth stage and the effects of meteorological factors. The images which were used in this study were acquired on August 2, July 26, and September 5. The first and the second images were acquired within a one week interval but in different years. Therefore, no major difference in the growth season was to be expected. However, the third image is acquired more than a month later and not exactly in the same growth stage. This time of the year is the harvest season for some crop types. Some very dense agricultural fields with high

chlorophyll content in late July or early August might have been turned into bare soils or fields with dried crop residue in early September. The compatibility of the seasons which the data are taken in is very important and should be taken into consideration for future multitemporal researches.

Total annual precipitation was another limiting factor in this study. The study site was located in an arid and semi-arid environment. Hence, the annual precipitation was very important for the vegetation state. In this region the mean annual precipitation was 122.8 millimetres. It was 167.5, 88.1, and 215.7 millimetres for the 1985, 2000 and 2009 years, respectively (Isfahan Meteorology Center, 2011). While in the 1985 and 2009, the annual precipitation is above the average, in 2000 the annual precipitation was approximately 35 millimetres below the mean. In fact, the low precipitation affected the vegetation cover and the health state of the agriculture crops that year and caused some bias in the final results of the analysis.

The proximity of reflectance of different bare soil sub-classes with urban class wais another limitation of this study when running the maximum likelihood supervised classification method. This proximity led to low separability and some confusion between these classes and caused some urban clusters to be identified in areas were not actually built up. Previous knowledge of the area and ground truth and/or land use maps was necessary to avoid false interpretation of the classification map.

In this research, 10 vegetation indices were successfully applied for the study scene. Amongst these indices TDVI was the most recently developed one. Previously, this index had been shown to have high accuracy and sensitivity for mapping vegetation on Montreal Island compared to NDVI and SAVI (Ozbakir and Bannari 2007). Moreover, in this research this index also performed accurately for mapping low density vegetation in arid and semi-arid environments and outperformed other vegetation indices. In fact, TDVI makes considerable improvement in mapping vegetation classes and sub-classes and can be applied in future researches of different environments.

To sum up, this thesis examined the use of remote sensing data and techniques in urban land use and land cover change detection. The results of this research showed the accuracy of the remote sensing techniques which were applied to the data. Future work for the applicability of these methods in various environments is strongly recommended.

Chapter 6: References cited

Abo-el-Ghag M., Shalaby A. and Tateishi, 2004, Agricultural land monitoring in the Egyptian Nile Delta using Landsat data, *International Journal of Environmental Studies,* Vol. 61, No. 6, pp. 651–657

Aguilar A.G., 1999, Mexico City Growth and Regional Dispersal: the Expansion of Largest Cities and New Spatial Forms, *Habitat International*, Vol. 23, No. 3, pp. 391-412

Al-Awadhi T., 2007, Monitoring and modeling urban expansion using GIS and RS: case study from Muscat Oman, *Urban Remote sensing Joint Event*, 1-4244-0712, pp. 1-5

Anys H., He D.C., Bijaber N., and Bannari A., 2002, GIS and high-resolution SPOT imagery for evaluating the impact of urbanisation on agricultural lands, *Geocarto International* Vol. 17, NO 3, pp. 35-43

Asrar, G., Fuchs, M., Kanemasu, E. T., and Hatiield, J. L. (1984), Estimating absorbed photosynthetic radiation and leaf area in3o8 dex from spectral reflectance in wheat, Agron. 1. 76:300-306.

Atash F. and Shirazi Beheshti Y. S., 1998, New Towns and their Practical Challenges: The Experience of Poulad Shahr in Iran, *Habitat International*, Vol. 22, No. 1, pp. 1-13

Bakr N., Weindorf D.C., Bahnassy M.H., Marei S.M., El-Badawi M.M., 2010, Monitoring land cover changes in a newly reclaimed area of Egypt using multi-temporal Landsat data, *Applied Geography* Vol 30, pp. 592–605

Bannari A., Morin D., Bonn F. and Huete A. R., 1995, A review of vegetation indices, *Remote Sensing Reviews* Vol 13, pp. 95-120

Bannari A., Morin D., He D.C., 1998, Analysis of the contribution of two vegetation index to classification accuracy for heterogeneous areas, *Journal Canadian de Teledetection*, Vol. 24, No. 3, pp. 233-239

Bannari, A., Haboudane, D. et Bonn, F. (1999) Potentiel des mesures multispectrales pour la distinction entre les résidus de cultures et les sols nus sous-jacents. P. 359-366, in ERIM (ed.) Fourth International Airborne *Remote Sensing Conference and Exhibition/21st Canadian Symposium on Remote Sensing*, Ottawa, Ontario, Canada, 21-24 vol. II, ERIM International Inc., Ann Arbor: 907

Bannari, A., Asalhi H. and Teillet P.M., 2002, Transformed difference vegetation index (TDVI) forvegetation cover mapping, *International Goscience and Remote Sensing Symposium*, Toronto, Ontario, Candada, Proceeding on CD-Rom, Paper 12A35-1508

Bannari, A., Omari, K., Fedosejev, G. and Teillet, P.M. (2005) Using Getis Statistic for the Uniformity Characterization of Land Test Sites Used for Radiometric Calibration of Earth Observation Sensors, *IEEE-Transactions on Geoscience and Remote Sensing*, Vol. 43, No. 12, pp. 2918-2926.

Bannari A., Ozbakir A., and Langlois A., 2007, Spatial Distribution Mapping of Vegetation Cover in Urban Environment Using TDVI for Quality of Life Monitoring, *International Geosciences and Remote Sensing Symposium*, 1-4244-1212, pp. 679-682

Baret, F., Guyot, G. and Major, D. J. 1989b. Crop biomass evaluation using radiometric measurements. *Photogrammetria (PRS)*, Vol. 43, pp. 241–256.

Baret, F. and Guyot, G. 1991. Potentials and limits of vegetation indices for LAI and APAR assessment. *Remote Sensing of Environment*, Vol. 35, pp. 161–173.

Bayarsaikhan U., Boldgiv B., Kim K., Park K., Lee D., 2009, Change detection and classification of land cover at Hustai National Park in Mongolia, *International Journal of Applied Earth Observation and Geoinformation*, Vol. 11, pp. 273–280

Belaid M.A., 2003, Urban-rural land use change detection and analysis using GIS and RS techniques, *Geografic information for planning*, TS8

Binsell R., 1967, Dwelling Unit Estimation from Aerial Photography, Remote Sensing Laboratory, Department of Geography, North Western University, Evanston

Brockerhoff M., 1999, Urban Growth in Developing Countries: A review of projections and predictions, *Population and Development Review*, Vol. 25, No. 4, pp. 757–778

Byrne G.F., Crapper P.F., and Mayo K.K., 1980, Monitoring land-cover change by principal component analysis of multitemporal Landsat data, *Remote Sensing of Environment* Vol 10, pp. 175-184

Canada Centre of Remote Sensing, "Glossary of Remote Sensing Terms", 2005, 14 August 2010, http://www.ccrs.nrcan.gc.ca/glossary/index_e.php?id=654

Chander G., Markham B.L., and Helder D., 2009, Summary of current radiometric calibration coefficients for Landsat MSS, TM, ETM+, and ALI Sensors, *Remote Sensing of Environment,* Vol 113, pp. 893-903

Chander G., *et al.*, 2010, Monitoring on orbit calibration stability of the Terra MODIS and Landsat 7 ETM+ sensor using Pseudo-invariant test sites, *Remote Sensing of Environment,* Vol 114, pp. 925-939

Clevers J.P.W., 1986, The application of a vegetation index in correcting the infrared reflectance for soil back ground, *International Archive of Photogrammetry and Remote Sensing*, Balkema, Rotterdam, Boston, Vol. 26, No. 1, pp. 221-226

Construction Company of Iranian New Towns, 2004, Statistical Bureau, Tehran

Cohen B., 2004, Urban Growth in Developing Countries: A Review of Current Trends and a Caution Regarding Existing Forecasts, *World Development*, Vol. 32, No. 1, pp. 23–51

Collins J.B and Woodcock C.E, An Assessment of Several Linear Change Detection Techniques for Mapping Forest Mortality Using Multitemporal Landsat TM Data, 1996, *Remote Sensing of Environment*, Vol 56, pp. 66-77

Coppin P., Jonckeere I., Nackaerts K,. Ackaerts, Muys B., 2004, Digital change detection methods in ecosystem monitoring: a review, *International Journal of Remote Sensing*, Vol. 25, No. 9, pp. 1565–1596

Denis E., 1996, Urban Planning and Growth in Cairo, *Middle East Report*, No. 202, *Cairo: Power, Poverty and Urban Survival*, pp. 7-12

Deng J.S., Wang K., Deng Y. H., and QI G. J., 2008, PCA-based land-use change detection and analysis using multitemporal and multisensor satellite data, *International Journal of Remote Sensing*, Vol. 29, No. 16, pp. 4823–4838

Döner, F. 2011, Using landsat data to determine land use/land cover changes in gümüş hane, Turkey, *Scientific Research and Essays*, Vol. 6, No. 6, pp. 1249-1255

Erdas Manual, 2008, Change Detection White Paper, 15 September 2010, http://www.erdas.com/LinkClick.aspx?fileticket=E%2B4l4IaGsng%3D&tabid=132&mid=540

Farrand W.H., Singer R.B., and Merrenyi E., 1994, Retrieval of apparent surface reflectance form AVIRIS data-a comparison of empirical line, radiative-transfer and spectral mixture methods, *Remote Sensing of Environment*, Vol. 47, pp. 2291-2297

Flippi, Codaccioni, O., Clobert J., and Julliard R. 2009, Urbanisation effects on the functional diversity of avian, *Acta Oecologica*, Vol 35, pp. 705-710

Find Latitude and Longitude, 2010, www.findlatitudeandlonitude.com

Foley J.A., DeFries R.,Asner G.P., Barford C., Bonan G., Carpenter S., Chapin F.S., Coe M., Daily G., Gibbs H., Helkowski J., Holloway T., Howard E., Kucharik C., Monfreda C., Patz J., Prentice I., Ramankutty N. and Snyder P., 2005, Global consequences of land use, *Science* Vol **309,** pp. 570–574

Freemantle J.R., Pu R., and Miller J.R. 1992, Calibration of imaging spectrometer data to reflectance using pseudo-invariant features, *Proceedings of the 15th Canadian Symposium on Remote Sensing*, pp. 452-457,

Fung, T., and Ledrew, E., 1987, The application of principal component analysis to change detection. *Photogrammetric Engineering and Remote Sensing*, Vol. 53, pp. 1649–1658

Gilbert A., 1993, Third World Cities: The Changing National Settlement System, *Urban Studies*, Vol. 30, No. 4/5, pp. 721-740

Goodchild M.F., 1992, Geographical data modeling, *Computers and Geosciences*, Vol. 18, pp. 401-408

Government of Iran Information Website, "Social, Economical and Cultural situation on Isfahan Province in years 2006-2009", 1 September 2010, http://www.dolat.ir/NSite/FullStory/?id=181922

Gong, P., 1993, Change detection using principal component analysis and fuzzy set theory, *Canadian Journal of Remote Sensing*, Vol. 19, pp. 22–29.

Green N.E. and Monier R.B., 1959, Aerial Photographic Interpretation and Social Structure of the City, Photogrammetric Engineerign, Vol 23, pp. 89-96

Green N.E., 1957, Aerial Photographic Interpretation and Social Structure of the City, *Photogrammetric Engineering*, Vol 23, pp. 89-96

Griffiths, G. H., 1988, Monitoring urban change from Landsat TM and SPOT satellite imagery by image diOEerencing. Proceedings of IGARSS '88 Symposium, Edinburgh (Piscataway, NJ: IEEE), pp. 493–497.

Griffiths P., Hoster P., Grubner O. Linden S., 2009, Mapping megacity growth with multi sensor data, *Remote sensing of Environment,* Vol 114, pp. 426-439

Grimm N., Faeth S., Golubiewski N., Redman C., Wu J., Bai X. and Briggs J., 2008, Global change and the ecology of cities, *Science* Vol **319,** pp. 756–760

Hadeel A. S., Jabbar M. T., Xiaoling C., 2011, Remote Sensing and GIS Application in the Detection of Environmental Degradation Indicators, *Geo-spatial Information Science,* Vol. 14, No.1, pp. 39-47

Hadfield S.M., 1963, An Evaluation of Land Use and Dwelling Unit Data Derived from Aerial Photography, Chcago Area Transportation Study, Chicago, USA

Hadjimitsis D.G., Clayton C.R.I., Retalis A., 2009, The use of selected pseudo-invariant targets for the application of atmospheric correction in multi-temporal studies using satellite remotely sensed imagery, *International Journal of Applied Earth Observation and Geoinformation*, Vol. 11, pp. 192–200

Hayes D.H and Sader S.A. 2001, Comparison of ChangeDetection Techniques for Monitoring Tropical Forest Clearing and Vegetation Regrowth in a Time Series, *Photogrammetric Engineering and Remote Sensing*, Vol. 67. No. 1, pp. 1067-1075

Hong Z., Xuanbing Z. and Ning S., 2009, Study on Land Use Cover Change (LUCC) based on remote sensing and GIS, *International Symposium on Spatial Analysis, Spatial-Temporal Data Modeling, and Data Mining*

Hoshino S., Kosaka N, 2005, Analysis of salt-damaged paddy fieldusing SPOT5 satellite images in Yamagata Prefecture, IGARSS, in press.

Howarth, P. J., and Boasson, E., 1983, Landsat digital enhancements for change detection in urban environments. *Remote Sensing of the Environment*, Vol. 13, pp. 149–160.

Huete A.R., Liu H. Q., Batchily K., and Leeuwen W.V., 1997, A Comparison of Vegetation Indices over a Global Set of TM Images for EOS-MODIS, *Remote Sensing of Environment*, Vol. 59, pp. 440-451

Ihse M., 1995, Swedish agricultural landscapes - patterns and changes during the last 50 years, studied by aerial photos, *Landscape and Urban Planning* Vol. 3, No. 1, pp. 2 l-37

Isfahan Province Portal, 2007, 12 September 2010, http://www.isfahanportal.ir/framework.jsp?SID=2345

Iran Meteorology Organization (IMO), 2010, http://www.weather.ir/farsi/statistics/TMAX.pdf

Jaiswal R.K., Saxena R., Mukherjee S., 1999, Application of remote sensing for land use/ land cover change detection, *Journal of the Indian society of Remote Sensing* Vol 27, No 2, pp. 123-128

Jackson, R. D., Pinter, P. J., Paul, J., Reginato, R.J., Robert, J. and Idso, S. B., 1980, Hand-held radiometry. Agricultural Reviews and Manuals ARM-W-19, Oakland, California: U.S. Department of Agriculture, Science and Education Administration

Jenson, J.R., 1986. Introductory Digital Image Processing, Prentice Hall, New Jersey

Jenson J.R., Im J., Hardin P., and Jensen R.R., 2009, The SAGE Handbook of Remote Sensing, SAGE Publication Inc. Chapter 19

Jolliffe I. T., Principal Component Analysis, 2002, *Springer*

Joshi M.A., 2006., Digital Image Processing: An algorithmic approach, Prentice Hall of India, New Delhi, India

Kadmon R. and Harari-Kremer R., 1999, Studying Long-Term Vegetation Dynamics Using Digital Processing of Historical Aerial Photographs, *Remote Sensing of Environment,* Vol. 68, pp. 164–176

Knorn J., Rabe A., Radeloff V.C., Kuemmerle T., Kozak J. Hostert P., 2009, Land cover mapping pf large areas using chain classification of neighbouring Landsat satellite images, *Remote Sensing of environment,* Vol 113, pp. 957-964

Keuchel J., Naumann S., Heiler M., Siegmund A., 2003, Automatic land cover analysis for Tenerife by supervised classification using remotely sensed data, *Remote Sensing of Environment*, Vol. 86, No. 4, pp. 530-541

Lamhin E.F. and Ehrlich D., 1997, Land-cover Changes in Sub-Saharan Africa (1982-1991): Application of a Change Index Based on Remotely Sensed Surface Temperature and Vegetation Indices at a Continental Scale, *Remote Sensing of Environment*, Vol 61, pp. 181-200

Lillesand T. and Kifer R.W., 1994, Remote Sensing and Image Interpretation, *John Wiley and Sons, INC,* Third Edition, Chapter 7, pp. 573-574

Lodwick D., 1979, Measuring ecological changes in multitemporal Landsat data using principal components. *Proceedings of the 13th International Symposium on Remote Sensing of Enuironment held in Ann Arbor in 1979* (Ann Arbor, Michigan: Environmental Research Institute of Michigan), pp. 1-1 1.

Lu D., Mausel P., Brondi Zio E. and Moran E., 2004, Change detection techniques, *International Journal of Remote sensing*, Vol. 25, No. 12, pp. 2365–2407

Lunetta R. S., Knight J. F., Ediriwickrema J., J. G. Lyon, and L. D. Worthy, 2006, Land-cover change detection using multi-temporal MODIS NDVI data, *Remote Sensing of Environment,* Vol. 105, pp. 142-154

Luong, P.T., 1993. The detection of land use/ land cover changes using remote sensing and GIS in Vietnam, *Asian Pacific Remote Sensing Journal*, Vol. 5, No. 2, pp. 63-66

Lutolf M., Guisan A., Kienast F., 2009, History Matters: Relating Land-Use Change to Butterfly Species Occurrence, *Environmental Management* Vol 43, pp. 436–446

Lyon G., Youan D., Lunetta R.S., Elvidge C.D., 1998, A change detetion experiment using vegetation indices, *Photogrammetric Engineering and Remote Sensing* Vol 64, No 2, pp. 143-150

Major D. J., Baret F., and Guyot G., 1990, A ratio vegetation index adjusted for soil brightness, *International Journal of Remote Sensing* Vol 11, No 5, pp 727-740

Maktav, F.S. Erbek and C. Jurgens, 2005. Remote sensing of urban areas, *International Journal of Remote Sensing* Vol 26, pp. 655–659

Mas J.F., 1999, Monitoring Land-cover Changes: A Comparison of Change Detection Techniques, *International. Journal of Remote Sensing*, Vol. 20, No. 1, pp.139-152

Masket J. G., Lindsay F. E. and Goward S. N., 2000, Dynamics of urban growth in the Washington DC metropolitan area, 1973–1996, from Landsat observations, *International Journal of Remote Sensing*, Vol. 21, No. 18, pp. 3473–3486

Mason C.F., 2006, Avian species richness and numbers in the built environment, can new housing developments be good for birds?, *Biodiversity Conservation*, Vol 15**,** pp. 2365–2378

Mast J. N., Veblen T.T., Hodgson M.E., 1997, Tree invasion within a pine/grassland ecotone: an approach with historic aerial photography and GIS modeling, *Forest Ecology and Management* Vol. 93, pp. 181-194

Meteorology Administration of Isfahan Province, 2008, www.esfahanmet.ir

Miller R. B., Small C., 2003, Cities from space: potential applications of remote sensing in urban environment research and policy, *Environment and Science and Policy* Vol 6, pp. 129-137

Moran M.S., Bryant R., Thome K., Nouvellon Y., Gonzalez-Dugo M.P., Qi J., and Clarke T.R., 2001, A refined empirical line approach for reflectance factor retrival from Landsat-5 TM and Landsat-7 ETM+, *Remote Sensing of Environment*, Vol. 78, pp. 71-82

Mumbower L. And Donghue J., 1967, Urban Poverty Study, *Photogrammetric Engineering*, Vol 33, pp 610-618

NASA website, Landsat 5, 28 August 2010, http://landsat.gsfc.nasa.gov/about/landsat5.html

NASA website, Landsat 7,28 August 2010, http://landsat.gsfc.nasa.gov/about/landsat7.html

Short N. M., "Principal Component Analysis", Remote Sensing Tutorial, 28 August 2010, http://rst.gsfc.nasa.gov/Sect1/Sect1_14.html

Natural Resource Administration of Isfahan Province, 2010, http://www.isfahan.frw.org.ir/frmArticle_fa-IR.aspx?ID=3562&CategoryID=812

Nicoloyanni, E., 1990, A diachronic change index applied to two Landsat MSS images of Athens, Greece. *International Journal of Remote Sensing*, Vol. 11, pp. 1617–1623.

Odunuga S., Oyebande L., 2007, Change detection and hydrological implications in the Lower Ogun flood plain, SW Nigeria, *Remote Sensing for Environmental Monitoring and Change detection* Vol. 316, pp. 91-99

Omran, A. R., & Roudi, F., 1993, The Middle East population puzzle. *Population Bulletin*, 48(1).

O'Meara, M., 1999. Reinventing Cities for People and the Planet. (Worldwatch Institute paper 147) Worldwatch, Washington D.C.

Ozbakir A. and Bannari A, 2008, Performance of TDVI in urban land use land cover classification for quality of place measurement, *The International Archives of the Photogrammetry, Remote Sensing and Spatial Information Science,* Vol. 37, Part B7.

Palandro D., Andrefoune S., Dustant. P. and Muller-Karger F. E., Change detection in coral reef communities using Ikonos satellite sensor imagery and historic aerial photographs, *International Journal of Remote Sensing*, Vol. 24, No. 4, pp. 873–878

Petit C., Scudder T., Lambian E., 2001 Gualification processes of land cover change by remote sensing: resettlement and rapid land cover change in south-eastern Zambia, *International Journal of Remote Sensing* Vol 22, No 17, pp. 3435-3456

Phinn S., Stanford M., Scarth P., Murry A.T., Shyy P.T., 2002, Monitoring the composition of urban environment based on the vegetation-impervious surface-soil (VIS) model by subpixel analysis techniques, *International Journal of Remote Sensing* Vol 23, No 20, pp. 4131-4153

Pu R., Gong P., Tian Y., Miao X., Carruthers R., and Anderson G.L., 2008, Using classification and NDVI differencing methods for monitoring sparse vegetation coverage: a case study of saltcedar in Nevada, USA, International Journal of Remote Sensing, Vol. 29, No. 14, pp. 3987–4011

Qi, J., Chehbouni A., Huete A. R., Kerr Y. H, and Sorooshian S., 1994, A Modified Soil Adjusted Vegetation Index, *Remote Sensing of Environment*, Vol 48, pp 119-126

Rajeshwari K. 2006, Management of the urban environment using remote sensing and geographic information systems, *Journal of Human Ecology,* Vol 20. No 4, pp. 269-277

Ramirez-Garcia, P., Lopez-Blanco, J. and Ocana, D., 1998, Mangrove vegetation assessment in the Santiago river mouth, Mexico, by means of supervised classification using Landsat TM imagery, *Forest Ecology and Management*, Vol. 105, pp. 217–229.

Rastmanesh F., Moore F., Kharati-kopaei M., Behrooz M., 2010, Monitoring deterioration of vegetation cover in the vicinity of smelting industry, using statistical methods and TM and ETM+ imageries, Sarcheshmeh copper complex, Central Iran, *Environment Monitoring and Assessment,* Vol 163, pp. 397–410

Richardson, A.J. and Wiegand, C.L., 1977. Distinguishing vegetation from soil background information. *Photogramm. Eng. Remote Sensing*

Rondinell D. A., 1983, Dynamics of Growth of Secondary Cities in Developing Countries, *Geographical Review,* Vol. 73, No. 1, pp. 42-57

Rogan J. and Yool S.R., 2001, Mapping fire-induced vegetation depletion in Peloncillo Mountain, Arizona and New Mexico, *International Journal of Remote Sensing,* Vol 22, No 16, pp. 3101-3121

Macleod R.D and Congalton R.G, 1998, A Quantitative Comparison of Change-Detection Algorithms for Monitoring Eelgrass from Remotely Sensed Data, *Photogrammetric Engineering & Remote Sensing*, Vol. 64, No. 3, pp. 207-216

Rouse J. W., Haas, R. S., Schell, J. A., and Deering, D. W., 1973, Monitoring vegetation systems in the Great Plains with ERTS. Proceedings, 3rd ERT S Symposium, 1, 48–62.

Roy D.P. *et al*., 2010, Web-enable Landsat data (WELD): Landsat ETM+ composited mosaic of the conterminous United states, *Remote Sensing of Environment*, Vol 114, pp. 35-49

Schott J.R., Salvaggio C., and Volchok W., 1988, Radiometric Scene Normalization Using Pseudo-invariant Features, *Remote Snsing of Environment*, Vol 26, pp. 1-16

Schmidt S., 2011, Sprawl Without Growth in Eastern Germany, *Urban Geography*, Vol. 32, No. 1, pp. 105–128

Schroeder T.A., Cohen W.B., Song C., Canty M., and Yang Z., 2006, Radiometric correction of multi-temporal Landsat data for characterization of early successional forest patterns in western Oregon, *Remote Sensing of Environment*, Vol. 103, pp. 10-26

Serra P., Ponis X., Sauri D., 2003, Post-classification change detection with data from different sensors: some accuracy consideration, *International Journal of Remote Sensing* Vol 24, No 16, pp. 3311-3340

Seto K.C., Woodcock C.E., Song C., Huang X., Lus J., Kaufamann R.K., 2002, Monitoirng land use change in Pearl River Delta using Landsat TM, *International Journal of Remote Sensing* Vol 23, No 10, pp. 1985-2004

Singh A., 1989, Review Article, Digital change detection techniques using remotely-sensed data *International Journal of Remote Sensing* Vol 10, No 6, pp. 989-1003

Smaou A., Georgiadis Ch., and Patias P., 2008, Land cover Change in Three Selected Areas under Direct Influence of the "Egnatia" Highway in Greece, *Remote Sensing and Spatial Information Sciences*, Vol 37, Part B6b

Solhi M., Shariatmadari H., Hajabbasi M.A., 2005, Lead and Zinc Extraction Potential of Two Common Crop Plants, Heliantus Annaus and Brasica Nacus, *Water, Air and Soil Pollution*, Vol 167, pp. 59-71

Song C., Woodcock C.E., Seto K.C., Lenney M.P., Macomber S.A, 2001, Classification and change detection using Landsat TM Data: When and how to correct atmospheric effects?, *Remote Sensing of Environment* 75 (2009) 230-244

Stewart D. J., 2002, Middle East Urban Studies II: Growth Environment, and Economic Development, *Urban Geography*, Vol. 23, No. 4, pp. 388–394

Sunar F., 1998, An analysis of changes in a multi-date data set: a case study in the Ikitelli area, Istanbul, Turkey, *International Journal of Remote Sensing*, Vol. 19, pp. 225–235.

Taillet P.M, Barker J.L., Markham B.L., Irish R.R., Fedosejevs G., Storey J.c., 2001, Radiometric cross calibration of Landsat-7 ETM+ and Landsat-5 TM sensors based on tandem data sets, *Remote Sensing of Environment*, Vol. 78, pp. 39-54

Thapa R.B., Murayama Y., 2011, Urban growth modeling of Kathmandu metropolitan region, Nepal, *Computers, Environment and Urban Systems* Vol. 35 pp. 25–34

Turner BL, Meyer WB, Skole D. 1994. Global land-use/land-cover change: Towards an integrated study. *Ambio,* Vol. 23, pp. 91–95.

Turner MG. 1987. Spatial simulation of landscape changes in Georgia: A comparison of 3 transition models. *Landscape Ecology*, Vol. 1, pp. 29–36.

US Geological Survey, 2010, http://glovis.usgs.gov/

Walter V., 2004, Object-based classification of remote sensing data for change detection, *Journal of Photogrammetry & Remote Sensing*, Vol. 58, pp. 225– 238

Wang H. and Ellis E. C., 2005, Spatial accuracy of orthorectified IKONOS imagery and historical aerial photographs across five sites in China, *International Journal of Remote Sensing*, Vol. 26, No. 9, pp. 1893–1911

Willhauck G., 2000, Comparison of object oriented classification techniques and standard image analysis for the use of change detection between SPOT multispectral satellite images and aerial photos, *International Archives of Photogrammetry and Remote Sensing*, Vol. 33, Part B3

Williams D.C. and Lyon J.G., 1997, Historical aerial photographs and a geographic information system (GIS) to determine effects of long-term water level

fluctuations on wetlands along the St. Marys River, Michigan, USA, *Aquatic Botany*, Vol. 58, pp. 363-378

Winterbottom S. J. And Gilvear D. J., 1997, Quantification of Channel Bed Morphology in Gravel-Bed Rivers Using Airborne Multispectral Imagery and Aerial Photography, *Regulated Rivers: Research and Management*, Vol. 13, pp. 489-499

World Health Organization (WHO), Tutorial on Geometric Correction, 2010, http://apps.who.int/gisresource/sections/documents/html/files/Tutorial%20on%20Geometric%20correction.pdf

Ziari, K. and Gharakhlou, M., 2009, A Study of Iranian New Towns During Pre– and Post Revolution, *International Journal of Remote Sensing*, Vol. 3, No. 1, pp. 143-154

APPENDICES

Appendix A: Semi-empirical line models

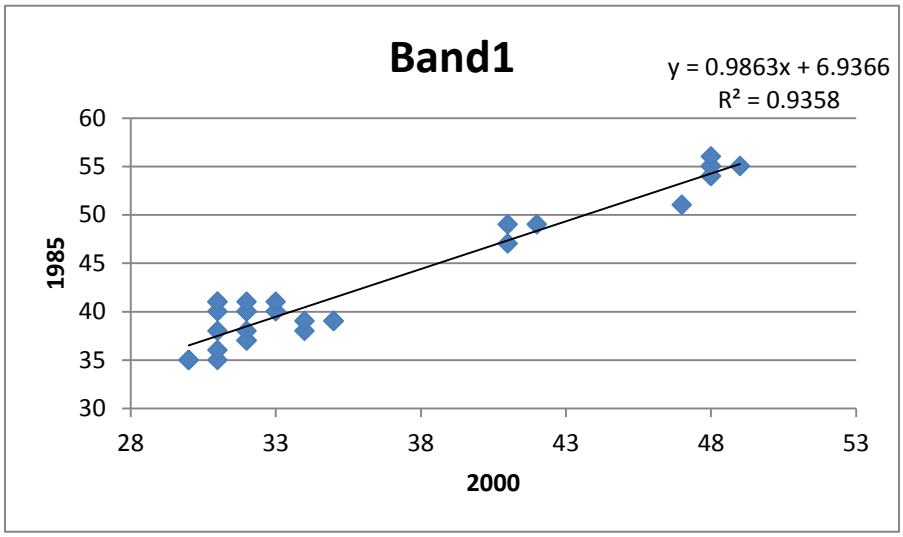

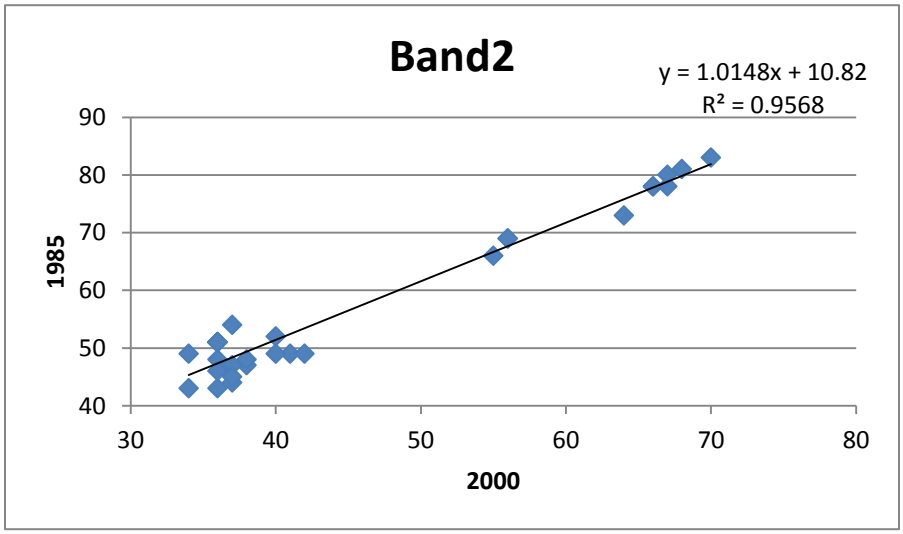

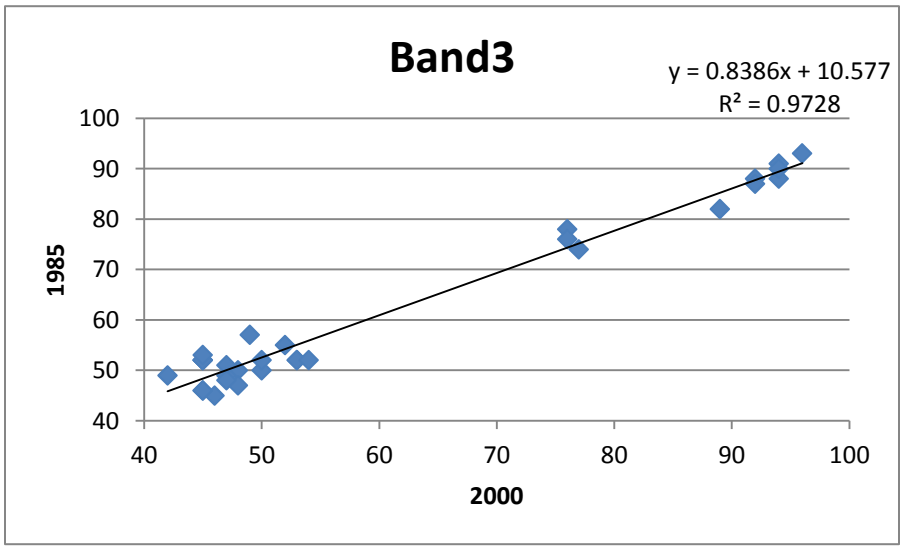

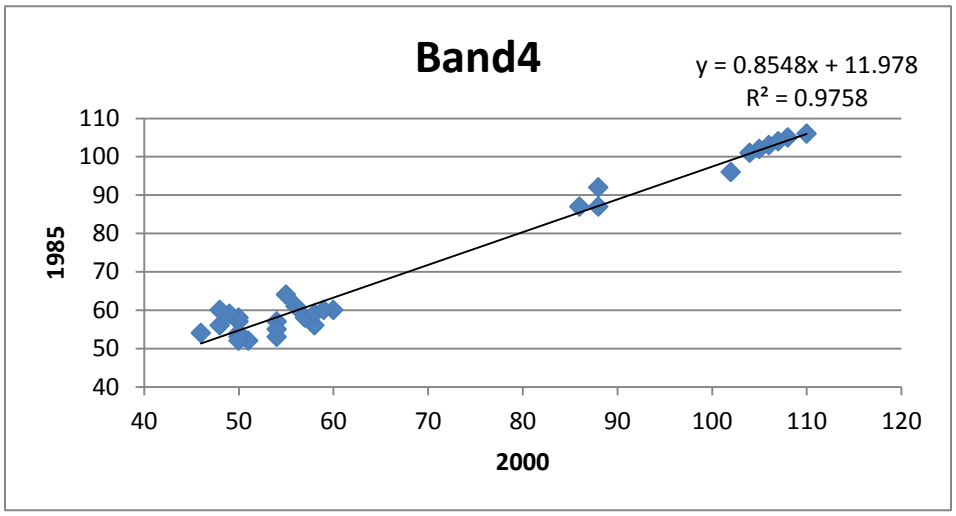
Band4
y = 0.8548x + 11.978
R² = 0.9758
1985
2000
110
100
90
80
70
60
50
40
40
50
60
70
80
90
100
110
120

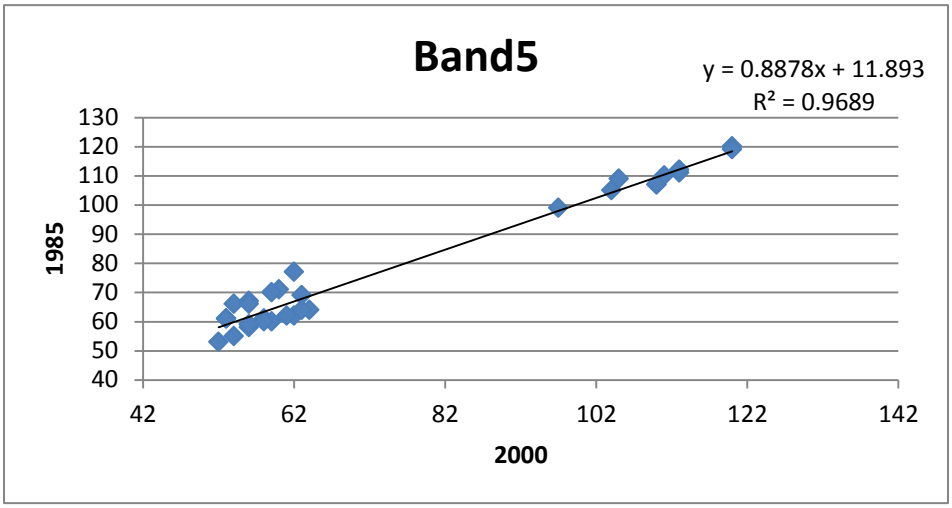
Band5
y = 0.8878x + 11.893
R² = 0.9689
1985
2000
130
120
110
100
90
80
70
60
50
40
42
62
82
102
122
142

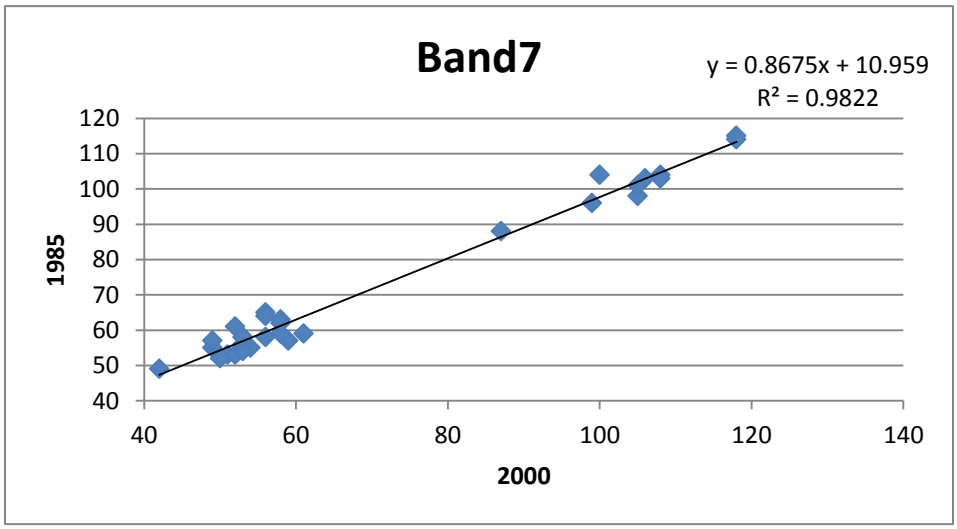
Band7
y = 0.8675x + 10.959
R² = 0.9822
1985
2000
120
110
100
90
80
70
60
50
40
40
60
80
100
120
140

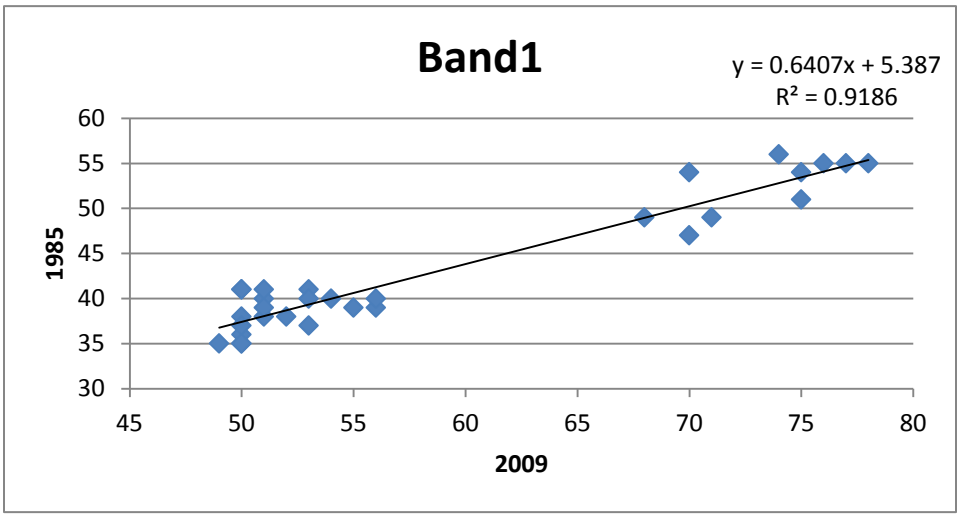
Band1
y = 0.6407x + 5.387
R² = 0.9186
1985
2009
60
55
50
45
40
35
30
45
50
55
60
65
70
75
80

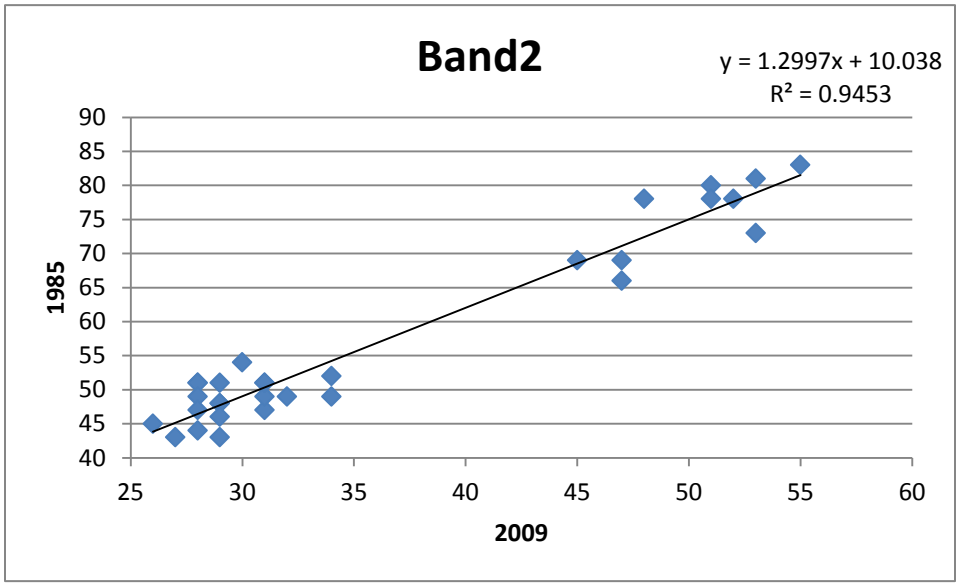
Band2
y = 1.2997x + 10.038
R² = 0.9453
1985
2009
90
85
80
75
70
65
60
55
50
45
40
25
30
35
40
45
50
55
60

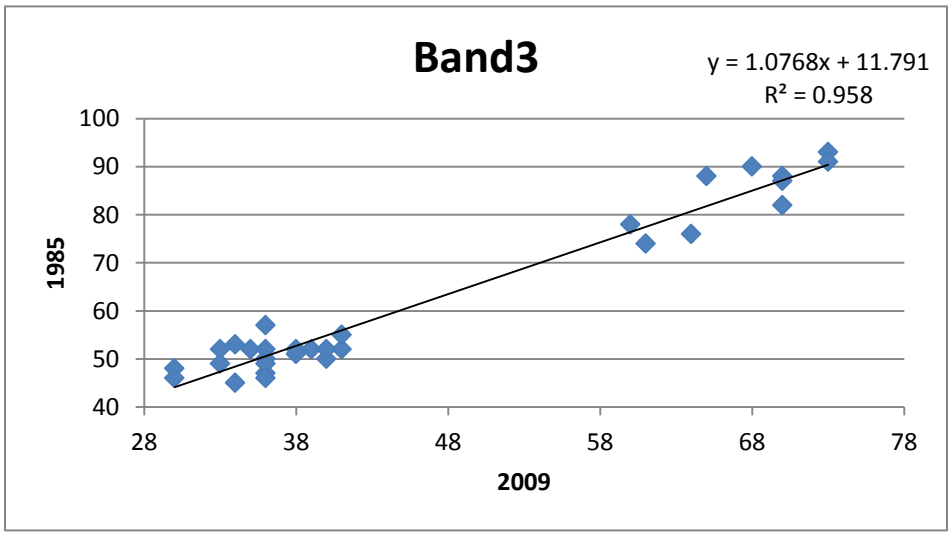
Band3
y = 1.0768x + 11.791
R² = 0.958
1985
2009
100
90
80
70
60
50
40
28
38
48
58
68
78

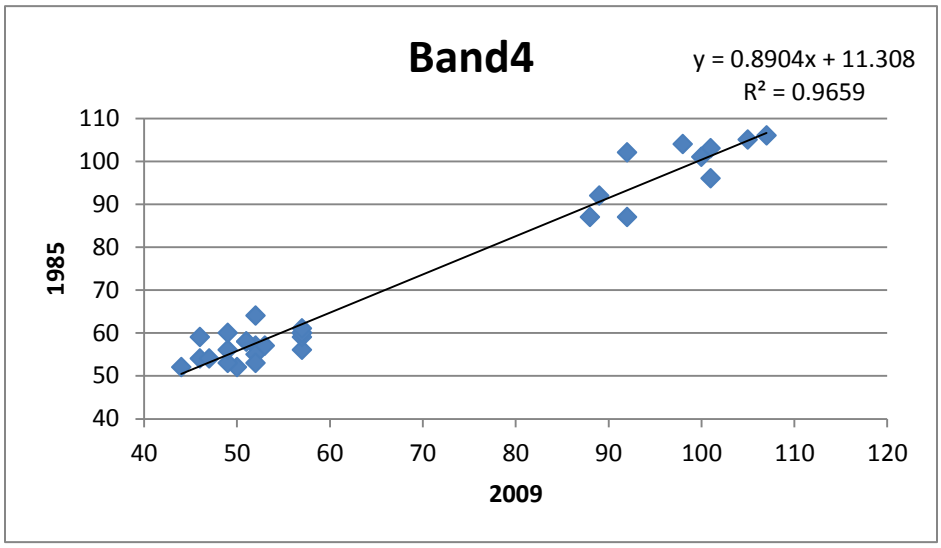
Band4
y = 0.8904x + 11.308
R² = 0.9659
1985
2009
110
100
90
80
70
60
50
40
40
50
60
70
80
90
100
110
120

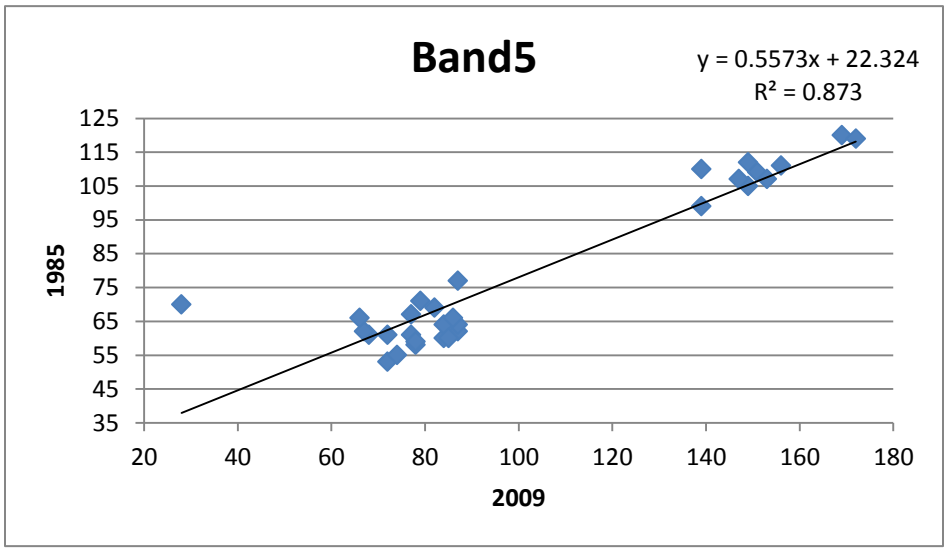
Band5
y = 0.5573x + 22.324
R² = 0.873
1985
2009
125
115
105
95
85
75
65
55
45
35
20
40
60
80
100
120
140
160
180

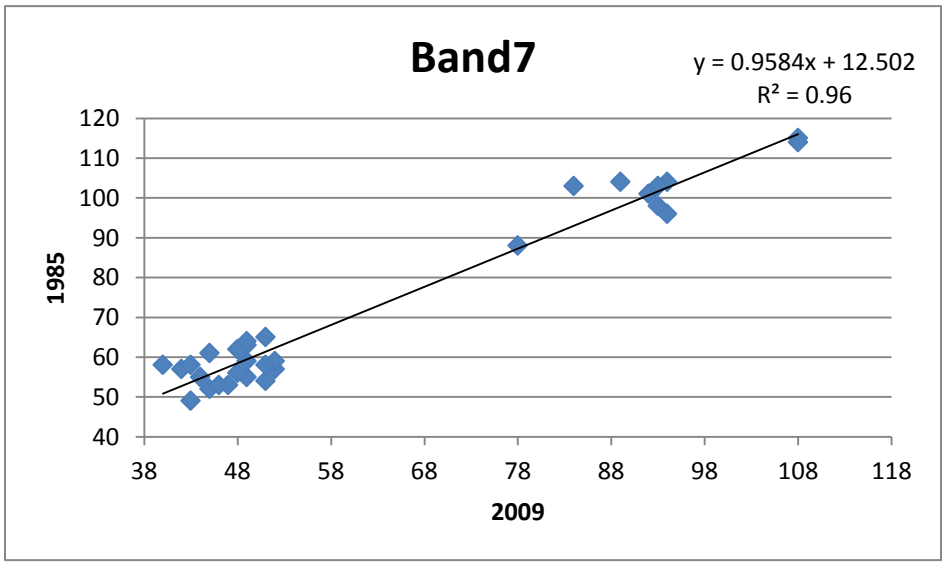
Band7
y = 0.9584x + 12.502
R² = 0.96
1985
2009
120
110
100
90
80
70
60
50
40
38
48
58
68
78
88
98
108
118

Appendix B: PC4, PC5 and PC7 for the 1985 image

PC1

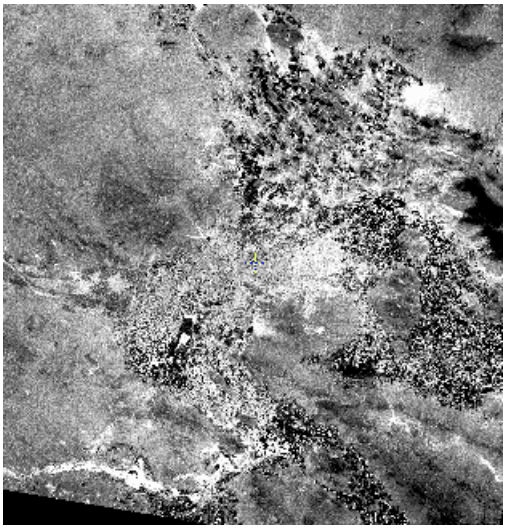

PC2

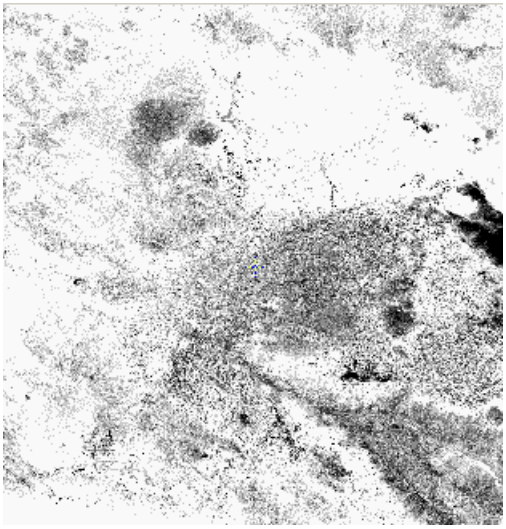

PC3

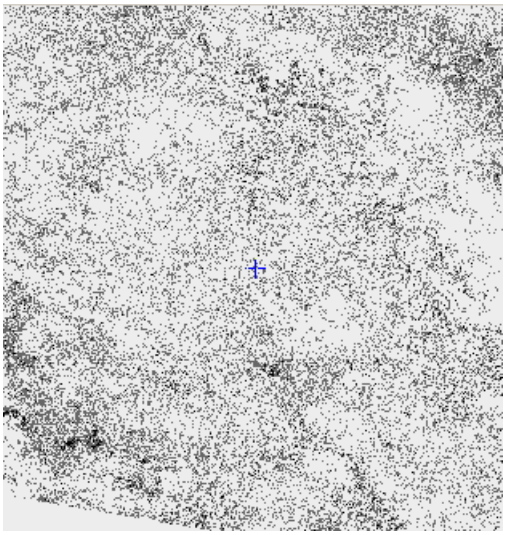

Appendix B Continue: PC4, PC5 and PC7 for the 2000 image

PC1

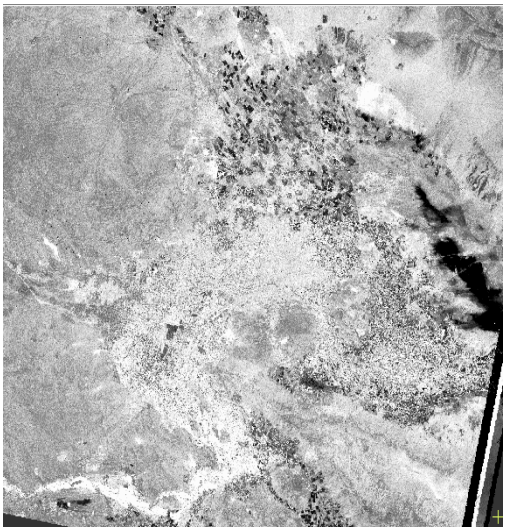

PC2

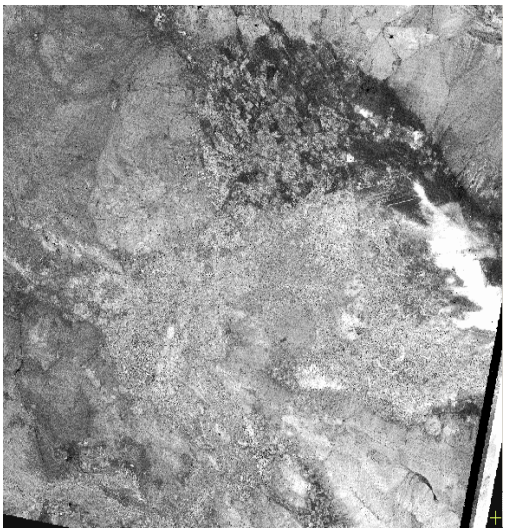

PC3

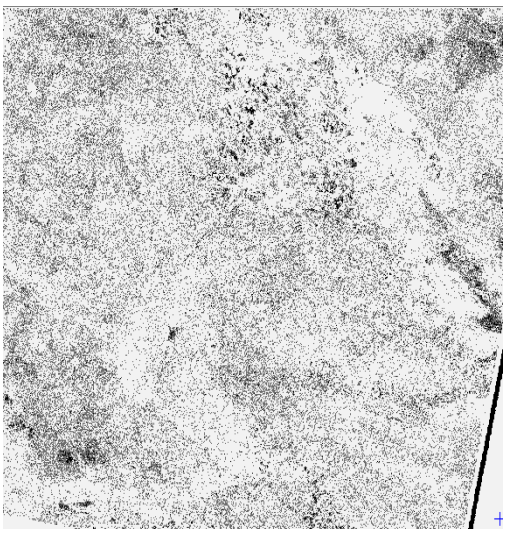

Appendix B Continue: PC4, PC5 and PC7 for the 2009 image

PC1

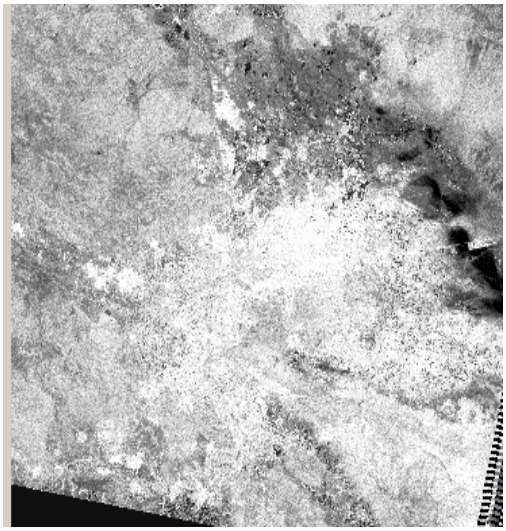

PC2

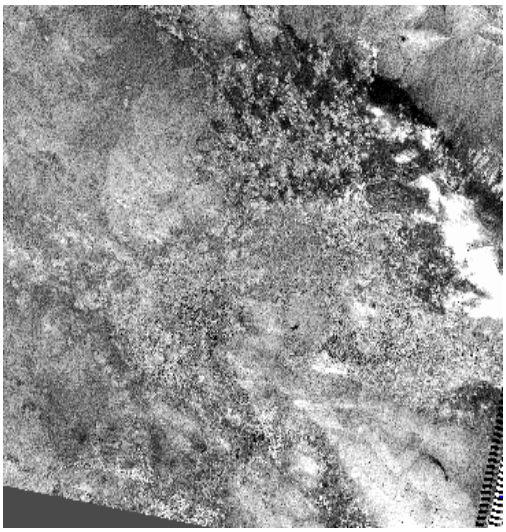

PC3

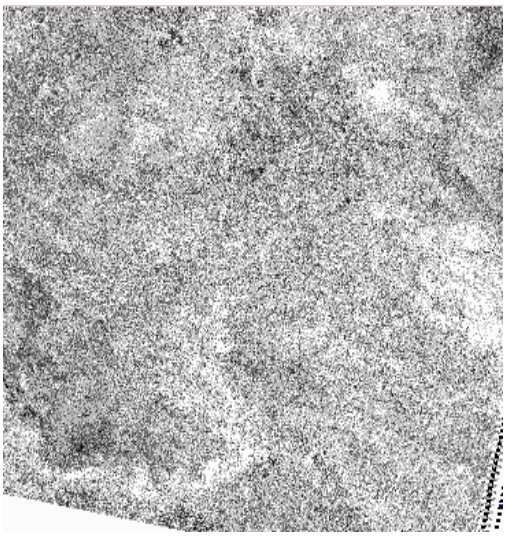

Appendix C: $\Delta PC2_{t1\text{-}t2}$ and $\Delta PC3_{t1\text{-}t2}$

$\Delta PC2_{1985\text{-}2000}$

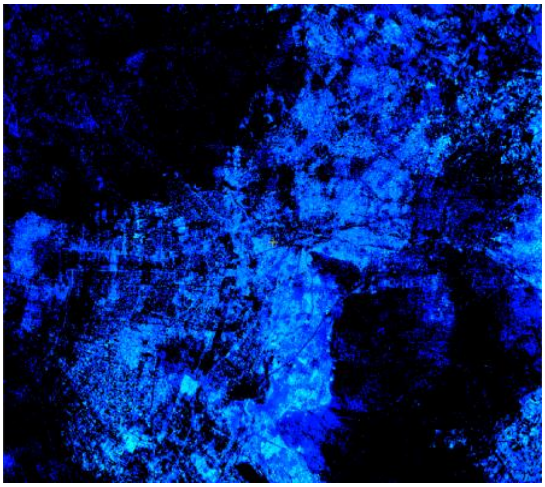

$\Delta PC3_{1985\text{-}2000}$

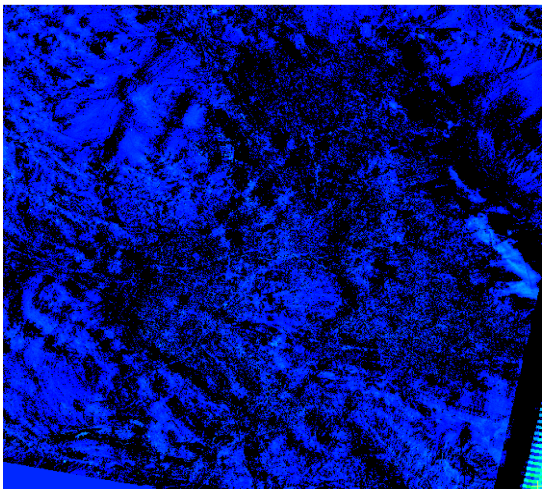

$\Delta PC2_{2000\text{-}2009}$

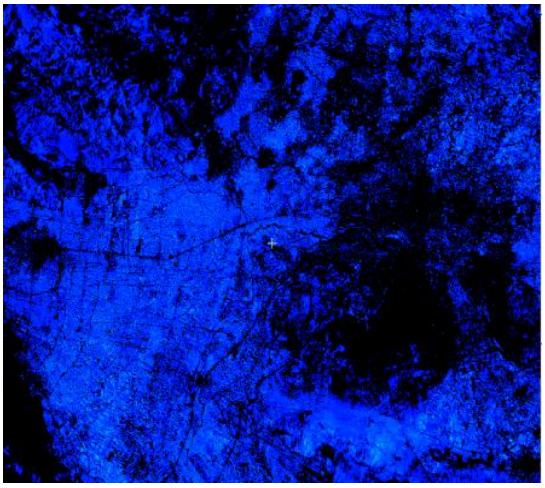

$\Delta PC3_{2000\text{-}2009}$

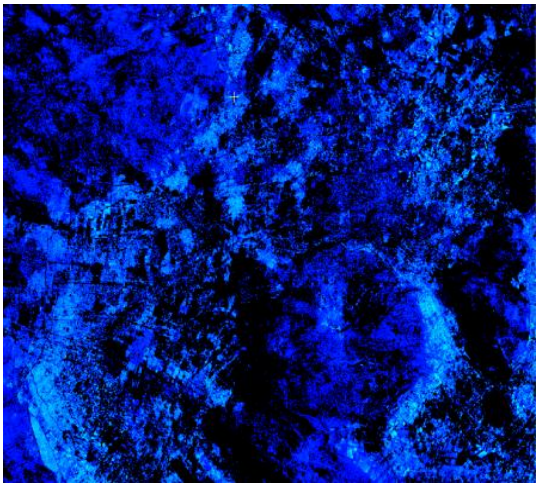

Appendix D: Signature Separabilities

Name 1985	Bright soil	Water	Road	Urban	Soil 1	Soil 2	Soil 3	Vegetation 1	Vegetation 2
Water	1.999984								
Road	1.997477	1.991963							
Urban	1.926450	1.999992	1.906648						
Soil 1	1.997764	2.000000	1.989018	1.984467					
Soil 2	1.998798	1.991127	1.974897	1.998968	1.956214				
Soil 3	1.999961	1.991678	1.989964	1.999845	1.997429	1.749356			
Vegetation 1	2.000000	1.999785	2.000000	2.000000	2.000000	2.000000	2.000000		
Vegetation 2	2.000000	1.955495	2.000000	2.000000	2.000000	2.000000	2.000000	1.992233	
Vegetation 3	1.944512	2.000000	2.000000	2.000000	2.000000	2.000000	2.000000	2.000000	2.000000

Name 2000	Urban	Road	Water	Bright soil	Soil 1	Soil 2	Soil 3	Vegetation 1	Vegetation 2
Road	1.803470								
Water	1.996191	1.798342							
Bright Soil	1.998681	2.000000	2.000000						
Soil 1	1.968673	1.999616	1.999998	1.999963					
Soil 2	1.596124	1.999999	2.000000	1.998593	1.996093				
Soil 3	1.9550307	1.911929	1.962332	2.000000	1.992548	1.999560			
Vegetation 1	1.999998	1.998862	1.877476	2.000000	2.000000	2.000000	1.999974		
Vegetation 2	1.992346	1.978230	1.815764	1.999854	1.997763	1.999573	1.997647	1.964693	
Vegetation 3	2.000000	2.000000	1.999861	1.987817	2.000000	2.000000	2.000000	1.999997	1.902348

Appendix D continue : Signature Separabilities

Name 2009	Urban	Water	Soil 1	Soil 2	Soil 3	Bright Soil	Soil 4	Vegetation 1	Vegetation 2	Vegetation 3
Urban										
Water	1.999961									
Soil 1	1.451593	1.999993								
Soil 2	1.975227	1.999995	1.850803							
Soil 3	1.996074	1.945709	1.984897	1.905412						
Bright Soil	2.000000	2.000000	1.999841	2.000000	2.000000					
Soil 4	1.999796	2.000000	1.999966	2.000000	2.000000	1.998202				
Vegetation 1	2.000000	1.998986	2.000000	2.000000	2.000000	2.000000	2.000000			
Vegetation 2	1.999984	1.999996	1.999966	1.999996	1.999977	1.999969	1.999988	2.000000		
Vegetation 3	1.99999	1.982111	2.000000	2.000000	2.000000	2.000000	2.000000	1.981273	1.969800	
Vegetation 4	2.000000	1.794176	2.000000	2.000000	2.000000	2.000000	2.000000	1.998626	2.000000	1.987589

Appendix E: Confusion Matrices

Name 1985	Code	Pixels	1	2	3	4	5	6	7	8	9	10
Bright soil	1	255	92.89	0.00	0.00	7.11	0.00	0.00	0.00	0.00	0.00	0.00
Water	2	217	0.00	98.62	0.92	0.00	0.00	0.00	0.46	0.00	0.00	0.00
Road	3	233	0.00	0.00	97.42	1.72	0.43	0.43	0.00	0.00	0.00	0.00
Urban	4	274	2.92	0.00	0.36	96.35	0.36	0.00	0.00	0.00	0.00	0.00
Soil 1	5	469	0.00	0.00	0.00	0.00	99.36	0.64	0.00	0.00	0.00	0.00
Soil 2	6	180	0.00	0.00	0.56	0.00	0.00	98.89	0.56	0.00	0.00	0.00
Soil 3	7	339	0.00	0.00	0.00	0.00	0.00	1.18	98.82	0.00	0.00	0.00
vegetation 1	8	141	0.00	0.00	0.00	0.00	0.00	0.00	0.00	100	0.00	0.00
vegetation 2	9	194	0.00	0.00	0.00	0.00	0.00	0.00	0.00	0.00	100	0.00
vegetation 3	10	95	0.00	0.00	0.00	0.00	0.00	0.00	0.00	0.00	0.00	100

Name 2000	Code	Pixels	1	2	3	4	5	6	7	8	9	10
Urban	1	366	94.54	0.27	0.00	0.00	0.00	5.19	0.00	0.00	0.00	0.00
Road	2	142	1.41	94.37	3.52	0.00	0.00	0.00	0.7	0.00	0.00	0.00
Water	3	222	0.00	1.35	97.3	0.00	0.00	0.00	0.00	0.9	0.45	0.00
Bright soil	4	383	0.52	0.00	0.00	98.69	0.00	0.00	0.00	0.00	0.00	0.78
Soil 1	5	378	1.59	0.00	0.00	0.00	98.41	0.00	0.00	0.00	0.00	0.00
Soil 2	6	172	0.58	0.00	0.00	0.00	0.00	99.42	0.00	0.00	0.00	0.00
Soil 3	7	359	0.00	0.56	0.56	0.00	0.00	0.00	98.89	0.00	0.00	0.00
Vegetation 1	8	305	0.00	0.00	0.33	0.00	0.00	0.00	0.00	99.67	0.00	0.00
Vegetation 2	9	161	0.00	0.00	2.48	0.00	0.00	0.00	0.00	0.62	95.65	1.24
Vegetation 3	10	211	0.00	0.00	0.00	0.00	0.00	0.00	0.00	0.00	3.32	96.68

Appendix E continue: Confusion Matrices

Name 2009	Code	Pixels	1	2	3	4	5	6	7	8	9	10	11	12
Road	1	330	94.24	1.52	1.82	1.52	0.61	0.1	0.00	0.00	0.00	0.00	0.00	0.00
Urban	2	267	0.37	91.76	0.00	7.12	0.00	0.00	0.00	0.00	0.00	0.00	0.75	0.00
Water	3	263	1.9	0.00	96.96	0.00	0.00	0.00	0.00	0.00	0.00	0.00	0.00	1.14
Soil 1	4	277	0.00	16.61	0.00	83.39	0.00	0.00	0.00	0.00	0.00	0.00	0.00	0.00
Soil 2	5	194	0.52	0.00	0.00	0.52	98.97	0.00	0.00	0.00	0.00	0.00	0.00	0.00
Soil 3	6	190	2.63	0.00	0.53	0.00	0.00	98.97	0.00	0.00	0.00	0.00	0.00	0.00
Bright soil	7	185	0.00	0.00	0.00	0.00	0.00	0.00	100	0.00	0.00	0.00	0.00	0.00
Soil 4	8	137	0.00	0.00	0.00	0.37	0.00	0.00	0.00	99.27	0.00	0.00	0.00	0.00
Vegetation 1	9	271	0.00	0.00	0.00	0.00	0.00	0.00	0.00	0.00	99.26	0.00	0.74	0.00
Vegetation 2	10	185	0.00	0.00	0.00	0.00	0.00	0.00	0.00	0.00	0.00	98.38	1.62	0.00
Vegetation 3	11	208	0.00	0.00	0.00	0.00	0.00	0.00	0.00	0.00	0.00	0.00	100	0.00
vegetation 4	12	270	0.37	0.00	2.96	0.00	0.00	0.00	0.00	0.00	0.00	0.00	0.74	95.93

Appendix F: Signature Statistic Results

1985	Band 1		Band 2		Band 3		Band 4		Band 5		Band 7	
	Mean	SD	Mean	SD	Mean	SD	Mean	SD	Mean	SD	Mean	SD
Water	28.32719	2.26552	31.05069	3.30231	25.97235	3.35588	58.83369	2.16831	29.29954	6.46634	21.47465	5.63568
Road	37.15021	1.4791	43.88841	2.29676	42.79399	2.63039	52.77682	3.24427	53.63948	4.82381	48.82403	4.57451
Urban	43.62774	1.79418	55.91971	2.96588	57.51095	3.59768	70.24818	4.44148	72.98905	5.17044	66.65328	4.72378
Bright Soil	52.68	4.69655	74.78222	7.68558	84.04	9.03687	101.4978	10.64378	104.8222	10.88952	66.65328	4.72378
Soil 1	38.31343	0.82721	49.05544	1.32594	52.01279	1.73016	58.83369	2.16831	64.14286	4.84414	58.71642	4.13402
Soil 2	34.36667	1.68292	42.02222	3.16922	43.53333	4.71216	50.83889	8.26113	63.04444	15.96622	57.53889	14.49727
Soil3	27.14454	2.63061	29.50147	4.10293	28.35988	4.67722	30.99115	5.8519	38.23304	10.42187	33.50442	9.31848
Vegetation 1	26.4539	2.70664	30.48936	4.48103	24.66667	4.79164	101.6738	6.38759	45.96454	6.75447	25.63121	5.1974
Vegetation 2	24.61856	1.5889	27.15979	2.47674	22.55155	2.81746	70.37113	3.06062	38.59278	4.91098	22.78351	4.17461
Vegetation 3	38.96842	1.56577	54.01053	2.6695	63.4	3.21968	92.49474	4.22741	85.11579	3.48489	55.76842	2.88171
2000	Band 1		Band 2		Band 3		Band 4		Band 5		Band 7	
	Mean	SD	Mean	SD	Mean	SD	Mean	SD	Mean	SD	Mean	SD
Water	27.82432	1.89374	33.07207	2.73520	29.16667	3.74457	42.27928	11.01037	34.25676	11.42708	27.05405	7.90294
Road	33.53521	1.66430	39.26761	2.20727	37.53521	2.68712	49.53521	3.15707	48.13380	5.11588	42.73239	5.32191
Urban	41.79508	2.72392	53.40164	4.58614	55.11749	5.69871	65.76230	6.44063	69.56557	8.08931	64.04645	7.56361
Bright Soil	56.80679	10.3656	79.84073	13.23451	89.73107	12.6203	105.55875	11.04588	108.87467	6.80845	83.26632	12.75690
Soil 1	38.92063	0.75876	50.35450	1.18467	54.45767	1.84005	63.27513	2.66438	81.97884	6.06007	75.49471	5.97448
Soil 2	42.94186	1.04941	56.54651	1.08002	60.91279	2.08217	70.19186	3.26955	82.65116	8.65457	75.16860	7.66376
Soil3	34.02507	1.68953	41.16156	2.71005	41.24791	3.27263	44.67131	4.15615	45.40111	5.69715	41.06128	5.09319
Vegetation 1	26.95082	1.51090	33.19672	2.22371	28.30164	2.90407	90.14426	13.84453	50.23279	4.34363	30.95410	3.28002
Vegetation 2	33.75155	2.11481	43.55280	3.13842	44.20497	4.18385	68.89441	10.22031	68.89441	10.22031	52.90062	8.16766
Vegetation 3	36.77251	1.12085	50.18483	1.87499	57.51185	3.25585	86.91943	3.23900	83.30332	4.73996	58.20379	3.36573
2009	Band 1		Band 2		Band 3		Band 4		Band 5		Band 7	
	Mean	SD	Mean	SD	Mean	SD	Mean	SD	Mean	SD	Mean	SD
Water	27.20532	1.36901	31.45627	2.49047	29.62357	3.10754	53.27757	10.19482	46.38403	6.36298	30.63878	4.92247
Road	34.85758	2.12225	40.45758	3.46056	40.45758	4.11491	53.66061	4.99878	56.60909	4.63405	45.64242	5.39916
Urban	44.25468	2.56648	56.37079	3.71064	57.68165	4.08521	67.70037	4.46628	74.94382	4.78456	67.4794	5.57302
Bright Soil	58.97297	3.1596	87.12432	4.74093	97.23243	4.68523	112.4541	4.93518	110.627	8.08979	87.7027	24.97638
Soil 1	42.31408	2.00871	56.01805	3.82133	59.98917	5.34005	69.06859	6.3501	83.75812	8.98551	76.82671	9.2138
Soil 2	36.80412	0.98063	46.8866	1.42059	50.54639	2.12021	58.37113	3.59931	71.52577	9.00469	62.18557	9.29064
Soil3	30.39474	2.19496	36.16316	4.36731	38.28421	5.50342	45.57895	7.79552	61.51053	9.77685	52.12632	10.48934
Soil 4	48.48905	1.53365	68.83942	1.63553	76.83212	1.75328	87.9781	2.02707	98.41606	3.62804	89.76642	4.82733
Vegetation 1	29.8524	1.72254	35.87454	2.75154	31.80074	3.01976	106.4539	4.96674	60.52399	3.98317	36.7048	4.0195
Vegetation 2	40.88108	2.0787	57.12973	3.67378	66.27027	4.41893	93.72432	5.21999	92.01081	5.18625	69.99459	4.70824
Vegetation 3	34.77404	2.02909	43.73077	3.2647	44.41827	4.5745	85.69712	4.09732	72.25	4.60821	50.19712	4.91608
Vegetation 4	27.44815	1.01612	31.57407	1.83789	28.65556	2.15077	76.47778	3.23142	53.14444	2.49397	32.17778	2.94484